

AUG 20 1957  
16682

Copy 238  
RM E57E06

NACA RM E57E06

TECH LIBRARY KAFB, NM  
0149938



# RESEARCH MEMORANDUM

JET EFFECTS ON BASE PRESSURES OF CONICAL AFTERBODIES

AT MACH 1.91 AND 3.12

By L. Eugene Baughman and Fred D. Kochendorfer

Lewis Flight Propulsion Laboratory  
Cleveland, Ohio

Classification cancelled (or changed to Unclassified)  
By Area Tech Rep Announcement # 29  
By 29 Sept 68  
JK  
GRADE OF OFFICER (or changed to) \_\_\_\_\_  
DATE 7 Aug 68  
CLASSIFIED DOCUMENT

**NATIONAL ADVISORY COMMITTEE  
FOR AERONAUTICS**

WASHINGTON  
August 12, 1957

**CONFIDENTIAL**

7018



## TABLE OF CONTENTS

	Page
SUMMARY . . . . .	1
INTRODUCTION . . . . .	1
SYMBOLS . . . . .	2
MODELS . . . . .	4
Basic Models . . . . .	4
Rocket Model . . . . .	4
Tail Interference Model . . . . .	5
Air Supply . . . . .	5
Tunnel Installation . . . . .	6
Support struts . . . . .	6
Effect of struts on flow . . . . .	6
Boundary Layer . . . . .	6
DATA REDUCTION . . . . .	7
INTRODUCTORY CONCEPTS . . . . .	7
Flow Geometry . . . . .	7
Wake Pressure Rise Ratio . . . . .	8
Theoretical Flow Model . . . . .	9
Role of Variables . . . . .	11
BOATTAIL AND WAKE PRESSURES . . . . .	12
Boattail . . . . .	13
Wake . . . . .	13
RESULTS AND DISCUSSION . . . . .	13
Effect of Jet Pressure Ratio . . . . .	13
Effect of Base-to-Jet Diameter Ratio . . . . .	15
Effect of Body-to-Jet Diameter Ratio . . . . .	16
Effect of Boattail Angle . . . . .	17
Effect of Nozzle Angle . . . . .	17
Effect of Jet Mach Number . . . . .	18
Effect of Free-Stream Mach Number . . . . .	19
Effect of Fluid Properties . . . . .	20
Effect of Jet Temperature . . . . .	21
Effect of Tail Interference . . . . .	21
WAKE PRESSURE RISE RATIO . . . . .	22
PREDICTION OF BASE-PRESSURE COEFFICIENT . . . . .	23

SUMMARY OF RESULTS . . . . .	Page 24
APPENDIXES	
A - CALCULATION OF THEORETICAL WAKE PRESSURE RISE RATIO . . . . .	26
B - CALCULATION OF EXPERIMENTAL PRESSURE RISE RATIO $p_w/p_D$ . . . . .	29
REFERENCES . . . . .	30
BIBLIOGRAPHY . . . . .	32
FIGURES . . . . .	38

## NATIONAL ADVISORY COMMITTEE FOR AERONAUTICS

RESEARCH MEMORANDUM

## JET EFFECTS ON BASE PRESSURES OF CONICAL AFTERBODIES

AT MACH 1.91 AND 3.12

By L. Eugene Baughman and Fred D. Kochendorfer

## SUMMARY

Data are presented which show the effect of a jet on base pressure for a series of conical afterbody-jet-nozzle combinations having boat-tail angles that varied from  $0^\circ$  to  $11^\circ$  and base-to-jet diameter ratios that varied from 1.11 to 2.67. The jet nozzles had exit angles from  $0^\circ$  to  $20^\circ$  and were designed for exit Mach numbers from 1.0 to 3.2. Pressure ratios up to 30 were tested for both a cold (air) and a hot (rocket) jet. The investigation was conducted at free-stream Mach numbers of 1.91 and 3.12.

In general, base pressure increased for increasing values of boat-tail angle, nozzle angle, jet temperature, and jet total pressure and for decreasing values of base-to-jet diameter ratio, jet Mach number, and free-stream Mach number. The addition of tail surfaces produced only small changes in base pressure.

For all variables, base pressure is governed by the maximum pressure rise that can be supported by the wake fluid in the region of the trailing shock. The wake pressure ratio is in turn governed by the jet and free-stream Mach numbers adjacent to the wake region and by the state of the boundary layer on the boattail and on the nozzle.

Values of wake pressure ratio computed using the theory of Korst, Page, and Childs were in good agreement with experimental values for convergent nozzles.

## INTRODUCTION

Predicting the pressure on a blunt annular base surrounding a propulsive jet has proven to be a stubborn problem. In the 6 years it has received attention, a completely general and consistently successful approach has not been forthcoming.

Part of the difficulty arises from the large number of variables in the problem and the relatively tedious calculations required in analyzing the flow field in the base region. Geometric parameters include boattail and nozzle shapes and base size; flow variables include temperature, pressure, Reynolds number, Mach number, and gas properties of both the external stream and the jet. Actual base-pressure calculations require a detailed analysis of the flow conditions of both the jet and the external stream in the base region as well as the mixing process in the wake.

As a result, most of the investigations into this problem area have been experimental in nature and limited in scope. Until recently, the most successful approaches to predicting the pressure on a base surrounding a jet have been empirical in nature, having used experimentally determined values of the governing pressure rise across the region of the trailing-shock formation (e.g., refs. 1 to 4). These studies, in general, parallel similar approaches to the base-pressure problem without a jet (refs. 5 and 6). The extensive studies of the pressure rise associated with shock-induced boundary-layer separation and reattachment have contributed greatly to the progress of this field.

More recently, theoretical approaches have been evolved for the two-dimensional laminar (ref. 7) and turbulent (ref. 8) base-pressure problem. The latter theory was applied to a base separating two different streams and has been modified herein to apply to the annular base.

The present report provides base-pressure data for a systematic set of afterbody and nozzle geometries. The data are then used to calculate the important wake parameters in an attempt to gain further insight into the factors that govern base pressure.

The ranges of the important parameters are as follows: free-stream Mach numbers, 1.91 and 3.12; jet Mach number, 1.0 to 3.2; boattail angle, 0° to 11°; nozzle angle, 0° to 20°; base-to-jet diameter ratio, 1.11 to 2.67; jet temperatures, 540° R (air) and 4200° R (rocket); and jet total-to-free-stream static-pressure ratio, jet off to 30.

Part of the present data has been discussed previously in reference 1. A bibliography of investigations concerning jet-stream interaction effects is included.

#### SYMBOLS

$C_p$  pressure coefficient,  $\frac{2}{\gamma M^2} \left( \frac{p}{p_0} - 1 \right)$

$c$  chord

$d$  diameter

L length  
M Mach number  
P total or stagnation pressure  
p static pressure  
R gas constant  
r radius  
T total temperature  
t thickness  
V velocity  
x axial distance from base  
y radial distance from boattail  
 $\alpha$  deflection angle at trailing shock of fluid just outside mixing region, deg  
 $\beta$  angle of boattail, deg  
 $\gamma$  ratio of specific heats  
 $\delta$  boundary-layer thickness  
 $\epsilon$  angle of nozzle at exit station, deg  
 $\nu$  Prandtl-Meyer angle (angle through which a supersonic stream is turned to expand from  $M = 1$  to  $M > 1$ ), deg  
 $\phi$  angle of internal flow with axis, deg  
 $\psi$  angle of external stream with axis, deg

## Subscripts:

a boattail station just upstream of base for jet-off conditions  
B body maximum

- b base
- c just ahead of trailing shock
- e external stream between a and c
- i internal stream between j and c
- j jet conditions at nozzle exit
- l limiting streamline
- t throat
- w wake conditions downstream of interaction point of jet and external streams
- o free stream

## MODELS

### Basic Models

The model (fig. 1) was composed of a strut-mounted  $8^\circ$  cone-cylinder forebody and interchangeable conical boattails. The over-all length was 20.44 inches, and the fineness ratio  $L/d_B$  of the body was 10.2. The boattail and base instrumentation was located behind and  $90^\circ$  from the struts. The average jet total pressure was measured by a single-calibrated pitot tube located ahead of the convergent portion of the nozzle.

Boattails with half-angles  $\beta$  from  $3^\circ$  to  $11^\circ$  and body-to-base diameter ratios  $d_B/d_j$  from 1.11 to 2.67 were used (fig. 2(a)). The location of the boattail pressure taps is shown.

The convergent and convergent-divergent jet nozzles had a body-to-jet diameter ratio  $d_B/d_j$  of 2.67 except for one convergent-divergent nozzle which had a  $d_B/d_j$  of 1.89. Other nozzle parameters and pressure tap locations are shown in figure 2(b).

### Rocket Model

A propane-oxygen rocket (fig. 3(a)) with the same size and shape nozzle and external configuration as the basic model was used in order to obtain a heated jet. The propellants were gaseous and were metered

to permit control of the fuel-air ratio over the range of combustor pressures used. A schematic diagram of the fuel system is shown in figure 3(b). The propane tank was immersed in a heated water tank to increase its pressure. The fuel and oxidant were injected into the combustion chamber through 1/4-inch diametrically opposed tubes. The mixture was ignited from the end of the model by means of a retractable spark source. Water was circulated through the model in order to keep the nozzle and combustion-chamber-wall temperatures low enough for continuous rocket operation.

The afterbody configuration of the rocket model was modified with shells to give base-to-jet diameter ratios  $d_b/d_j$  of 1.40, 1.67, and 2.00 and boattail angles  $\beta$  of  $5.63^\circ$ ,  $7.03^\circ$ , and  $11.00^\circ$ . Two nozzles, a convergent and a convergent-divergent with a design pressure ratio of 10.5, were run.

The base pressure was measured with four static taps located  $90^\circ$  apart. Boattail instrumentation (for the  $5.63^\circ$  boattail angle only) consisted of five static taps just ahead of the base duplicating that of the basic "cold" model. In order to determine the jet pressure ratio, a wall static tap was placed inside the nozzle as close to the exit as possible.

The static temperature of the jet was determined using the sodium D line reversal method. The temperature was approximately  $4200^\circ$  R in the center of the jet just downstream of the base. The specific heat ratio of the jet was estimated to be between 1.15 and 1.25.

#### Tail Interference Model

Rectangular planform tails were attached to the basic model afterbody (fig. 4). The tails had a thickness ratio  $t/c$  of 5 percent with a  $\frac{1}{2}$ -inch chord and a 4.5-inch span. The tails could be moved fore and aft by repositioning in longitudinal slots. The supporting boattails had angles of  $0^\circ$ ,  $5.63^\circ$ , and  $9.33^\circ$ . The cylindrical or  $0^\circ$  boattail had a base-to-jet diameter ratio of 2.67 while the  $5.63^\circ$  and  $9.33^\circ$  boattails had a base-to-jet diameter ratio of 1.40. Base pressure was measured with four static taps  $90^\circ$  apart in line with the tail surfaces.

#### Air Supply

Air for the jet was supplied by a 125-pound-per-square-inch service air line. The range of pressure ratios available varied from the no-jet-flow condition to a jet pressure ratio  $P_j/P_0$  of 18 for the convergent nozzle to a  $P_j/P_0$  of 38 for the convergent-divergent nozzles. To

obtain the effect of specific heat ratio, carbon dioxide was also used as the jet fluid. Liquid carbon dioxide was heated in a heat exchanger and converted to a gas at the desired pressure and temperature.

### Tunnel Installation

The models were run in two facilities, the Lewis 18- by 18-inch Mach 1.91 supersonic tunnel and the 12- by 12-inch Mach 3.12 supersonic tunnel. The basic model installed in the tunnels is shown in figure 5. The Reynolds number per foot for the Mach 1.91 tunnel was  $3.2 \times 10^6$  and for the Mach 3.12 tunnel was variable from 2.33 to  $8.16 \times 10^6$ .

Support struts. - The model was supported in the tunnel with 9.3-percent-thick double struts located 3.75 body diameters ahead of the base (fig. 1). Air or carbon dioxide for the jet and the fuel-oxidant for the rocket were ducted through the struts to the model along with the instrumentation lines.

Effect of struts on flow. - In order to determine the effect of the struts on afterbody pressures, the model was run both with single and with double struts. The boattail pressures near the base for both the single and double struts were in good agreement with Van Dyke's second-order theory (ref. 9) and the splitter-plate model of reference 10 (fig. 6(a)).

The base pressures showed some effect of the number of struts. With a double strut, base-pressure coefficients were lower than those of the single strut by 0.03 and were in better agreement with those of reference 10. If the base pressures are adjusted for the differences in boattail pressures between the present data and those of reference 10 ( $\Delta C_{p,b} = 0.03$  from fig. 6(a)), the agreement is excellent. Double struts were used for all subsequent experiments.

The curves for the boattail pressure  $90^\circ$  from the strut (fig. 7(a)) show a rise near the base, and those for pressures behind the strut show a bump just ahead of the base. These increases result from the shock from the interaction of strut leading edge and the wall boundary layer (fig. 7(b)). Similar effects were observed for all boattails.

### Boundary Layer

The boundary layer on the boattail was measured with a pitot rake. In order to keep the transition point the same for all runs, transition was forced with a 0.005-inch wire ring  $1/2$  inch in diameter on the nose cone of the model. Typical velocity profiles of the boundary layer just ahead of the base are shown in figure 8 for Mach 1.91 and 3.12. The

difference between the side and bottom profiles is due to the strut shocks as well as to the strut wake. For the afterbody configurations with boattails, the boundary layer thickened slightly with a  $\delta_a/d_B$  of approximately 0.06.

#### DATA REDUCTION

The jet total pressure was found directly from the calibrated pitot tube just upstream of the nozzle. Jet static pressures were calculated only for  $P_j/P_b > (P_j/P_j)_{\text{design}}$  (fig. 2(b)). The jet Mach number was assumed equal to the design value, and  $p_j$  was computed from  $p_j = (P_j)_{\text{measured}} / (P_j/P_j)_{\text{design}}$ .

With respect to this calculation it should be mentioned that the pressures measured on the nozzle wall near the jet exit (fig. 2(b)) were compared with the theoretical design values. For the two divergent nozzles designed for a pressure ratio of 20, the measured values were high by 8 percent. For all other values the discrepancy did not exceed 3 percent.

For the rocket model no internal pitot was used, and the jet static-pressure ratio was computed directly from the exit wall tap.

The base-pressure coefficient was calculated from an average of the two measured base pressures.

#### INTRODUCTORY CONCEPTS

##### Flow Geometry

Typical schlieren photographs of the flow in the base region are presented in figures 9(a) and (b), and a simplified sketch showing the important features of the flow in the interaction region is shown in figure 9(c). It is convenient to consider three distinct regions. In the first, upstream of the base, the static pressures  $p_j$  and  $p_a$ , the Mach numbers  $M_j$  and  $M_a$ , and the flow directions  $\epsilon$  and  $\beta$  of the jet and the stream are, in general, all unequal.

The second region is that downstream of the base and upstream of the trailing shock. In this region the flow directions of the jet and the stream can still be unequal; however, since the two flows are separated by a core of semidead air, their boundary pressures  $p_e$  and  $p_i$  can be assumed equal to the base pressure. (It should be noted that this is a somewhat simplified picture since  $p_b$  may vary somewhat, particularly

in the region just upstream of the trailing shock.) The jet deflection at the base  $\varphi_b - \epsilon$  depends on  $p_j/p_b$ ,  $M_j$ , and  $\gamma_j$ ; the stream deflection  $\psi_b - \beta$  depends on  $p_a/p_b$  and  $M_a$ . For the three-dimensional case the constant-pressure boundaries of both the jet and the stream are curved so that both  $\varphi$  and  $\psi$  will vary with the distance downstream of the base  $x$ . Since  $\varphi = f\left(\frac{x}{d_j}\right)$  and  $\psi = g\left(\frac{x}{d_b}\right)$ , the variable  $d_b/d_j$  will play an important role in determining  $\varphi_c$  and  $\psi_c$ , the flow directions just upstream of the trailing shock.

In the third region, downstream of the trailing shock, the flow directions as well as the static pressures must be equal. Therefore, the pressure of both streams must equal the wake pressure  $p_w$ , and from geometry the deflections  $\alpha_i$  and  $\alpha_e$  must be such that  $\alpha_i + \alpha_e = \varphi_c + \psi_c$ .

Brief consideration shows that the value of the base pressure is not determined uniquely by these requirements. The previous equation can be satisfied for all values of  $p_b$  less than that for which the two flows are parallel ( $\varphi_c = \psi_c$ ;  $\frac{p_w}{p_b} = 1.0$ ) and greater than that for which the pressure ratio  $p_w/p_b$  equals the normal shock value corresponding to  $M_i$  or  $M_e$ , whichever is lower. Thus, the appropriate unique value of the wake pressure ratio  $p_w/p_b$  must be known before the base pressure is determined.

#### Wake Pressure Rise Ratio

It has been suggested (refs. 1, 4, and 6) that the amount by which the wake pressure exceeds the base pressure is simply the maximum pressure rise which can be sustained by the wake in the region of the trailing shock and must, therefore, be directly dependent on some physical characteristic of the wake.

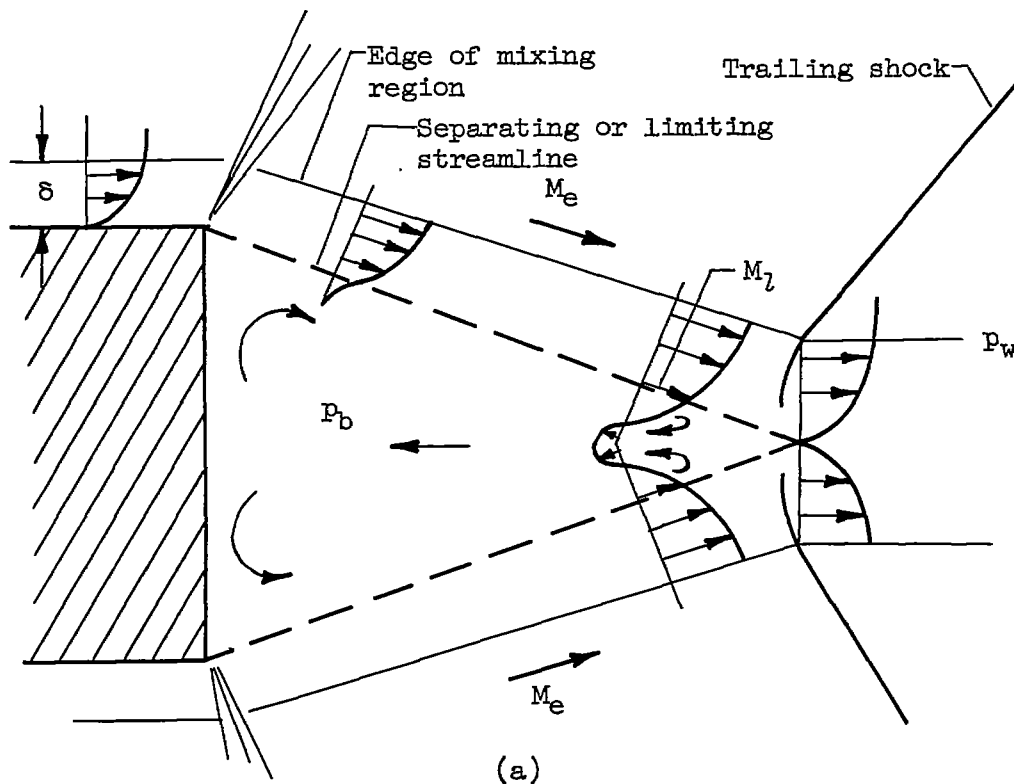
Data from forward- and rearward-facing steps (refs. 11 and 5) and from blunt-based bodies and airfoils (refs. 6 and 12) show that the pressure rise ratio depends on the Mach number, the form of the boundary layer, and the ratio of boundary-layer thickness to step or base height. When the boundary layer is turbulent and thin relative to the base or step, the pressure rise apparently depends only on the value of the Mach number ahead of the shock. The variation of shock pressure rise ratio with approach Mach number is shown in figure 10 for steps and airfoils having thin turbulent boundary layers. The results for the airfoils follow the same trend as those for the rearward-facing steps over the Mach

3808

number range but begin to depart from those for the forward-facing steps at Mach numbers above 2.0.

### Theoretical Flow Model

Some insight into the similarities between the wake flows for the rearward-facing step and the blunt-based airfoil as well as into the nature of the factors governing the wake pressure rise itself can be obtained from a flow model proposed in references 7 and 8.



The previous sketch shows that as the stream passes into the wake region the velocity profile is altered first by the expansion around the base and then by the turbulent mixing in the wake region. Of particular importance in the theory are the "separating" streamlines (dashed lines). A separating streamline is defined as that streamline outside of which the mass flow is equal to that flowing over the body just ahead of the base. (It should be noted, however, that, because of mixing, both stream and wake fluid can cross the separating streamline. It is not intended that the term "separating" denote a division in the absolute sense.) From continuity all fluid outside the separating streamlines must continue downstream through the trailing shock. The inside fluid must reverse

direction and move toward the base. Since of all fluid that must pass downstream the fluid on the separating streamline possesses the lowest dynamic head (or total head or Mach number), the separating streamline must also be the streamline which limits the wake pressure rise ratio  $P_w/P_b$ .

For simplicity, the separating streamlines are shown in sketch (a) to change direction abruptly at the trailing shock. Actually, the higher pressure will be transmitted upstream, and the inner streamlines will change direction smoothly beginning some distance upstream of the shock. The compression process along the separating or limiting streamlines may therefore be almost isentropic so that  $P_z/P_b = P_w/P_b$  where  $P_z$  is the stagnation pressure on the limiting streamline. The Mach number  $M_z$  must then be

$$M_z = \sqrt{\frac{2}{\gamma - 1} \left[ \left( \frac{P_w}{P_b} \right)^{\frac{\gamma-1}{\gamma}} - 1 \right]}$$

Application of this method obviously requires detailed information on the velocity profiles in the wake region. The analysis of two-dimensional jet mixing (refs. 7 and 13) was used in reference 8 to estimate base pressures. However, since the only available information was for fully developed turbulent profiles, the results should apply strictly only to the case for which the distance to the trailing shock is large relative to the boundary-layer thickness; the condition  $x_c/\delta > 20$  is stated as a requirement in reference 13. If it is assumed that the velocity profiles are relatively unaffected by the presence of a surface, the results should apply to the rearward-facing step as well as to the blunt-based airfoil. The solid curve of figure 10 shows the excellent agreement obtained between the theory and the data for blunt-based airfoils or rearward-facing steps.

A similar model can be applied to the problem of jet effects on base pressure. In this case the total pressures of the jet and the stream are, in general, unequal. Figure 11 shows the case for  $P_j > P_0$ , and, since  $P_j/P_b$  is then greater than  $P_0/P_b$ ,  $M_j$  must be greater than  $M_e$ . In general, then, the stagnation pressure on the separating streamline in the jet will be greater than that along the separating streamline in the external flow. Since the two limiting streamlines, which are just able to negotiate the wake pressure rise, by definition must have equal stagnation pressure, the separating streamlines cannot be the limiting streamlines for  $P_j \neq P_0$ . There will exist, however, two new streamlines, one in the internal flow and one in the external flow, which satisfy the following conditions:

(1) The stagnation pressures (or Mach numbers) are equal.

(2) The mass flow between the new streamline and the separating streamline in the internal flow must equal that between the new and separating streamlines in the external flow.

The second condition satisfies the requirement that the total flow that passes downstream through the trailing shock must equal that upstream of the base. The new streamlines are therefore the limiting streamlines so that the Mach number will equal the value of  $M_7$  defined previously.

For the case illustrated in figure 11 ( $P_j > P_0$ ), the two limiting streamlines lie outside their corresponding separating streamlines. A portion of the stream fluid is continually being "trapped" in the wake, and an equal amount of wake fluid is carried downstream by the higher energy jet. It is interesting to note that for a high-temperature jet the jet-stream pressure ratio should play an important role in determining the wake temperature; high wake temperatures should accompany low jet pressures ( $P_j/P_0 < 1$ ) and vice versa.

Calculations for the theoretical values of wake pressure rise ratio were made for  $P_j \neq P_0$  by using the tabulated turbulent mixing quantities of reference 14. Details of the procedure are given in appendix A, and the results are presented in figure 12. Wake pressure rise ratio is plotted as a function of external Mach number  $M_e$  for several values of jet total-pressure ratio, which is defined as the ratio of the jet total pressure to the free-stream total pressure  $P_j/P_0$ . Also shown are lines of constant internal Mach number  $M_i$ , where  $M_i$  is related to  $P_j/P_0$  and  $M_e$  through

$$\frac{\gamma - 1}{2} M_i^2 = \left( \frac{P_j}{P_0} \right)^\gamma \left( 1 + \frac{\gamma - 1}{2} M_e^2 \right) - 1$$

It can be seen that increasing the pressure ratio (at constant  $M_e$ ) results in a significant increase in wake pressure rise ratio. The curve for  $P_j/P_0 = 1.0$  along which  $M_e = M_i$  is identical to the solid curve of figure 10.

#### Role of Variables

As a result of the wake pressure rise concept, base pressure can be expressed as a product of two more fundamental quantities, the wake pressure and the wake pressure rise ratio, as follows:

$$p_b = p_w \frac{1}{\frac{p_w}{p_b}}$$

Any of the parameters which tend to increase  $p_w$  or decrease  $p_w/p_b$  or both will increase base pressure. It has been shown that  $p_w/p_b$  depends on mixing conditions in the wake and on the Mach numbers  $M_i$  and  $M_e$ . The wake pressure, on the other hand, is essentially fixed by jet and stream conditions (i.e., by afterbody and nozzle geometry, free-stream Mach number, and jet pressure ratio) and is relatively independent of conditions in the wake. This is illustrated in figure 13. The curve was obtained by calculating the wake pressure for the experimentally observed value of base pressure as well as for several higher and lower base pressures. (This method is presented in appendix B.) The afterbody and nozzle geometry,  $M_0$ , and  $P_j/p_0$  were held constant. If the wake mixing process could be altered in some manner, thereby changing the wake pressure rise ratio (e.g., by bleeding air through the base), the wake pressure itself would remain essentially constant. Actually, for large changes in wake pressure rise ratio, wake pressure will change; the important point is that the change in wake pressure is small compared with the change in wake pressure rise ratio.

The effects of the different variables can now be summarized as follows:

(1) The value of the wake pressure is determined primarily by the geometry of the nozzle and the afterbody, the free-stream and jet Mach numbers, and the jet pressure ratio.

(2) The base pressure is lower than the wake pressure by a factor which depends on the local Mach numbers in the base region, on the trailing-shock distance, and on the form and size of the boundary layers ahead of the base.

#### BOATTAIL AND WAKE PRESSURES

At this point it is clear that in order to obtain the quantities necessary for an analysis of jet effects on base pressures (i.e.,  $M_e$ ,  $M_i$ ,  $p_w$ , and  $p_w/p_b$ ), values must be known for the pressures  $p_a$ ,  $p_j$ , and  $p_b$  and for the Mach numbers  $M_i$  and  $M_j$ . The methods for obtaining  $p_j$  and  $M_j$  have been discussed previously. Boattail and wake quantities were obtained as follows.

## Boattail

Theoretical and experimental boattail pressure coefficients are compared for a boattail angle of  $5.63^\circ$  in figures 14(a) and (b) for  $M_0 = 1.91$  and in figure 14(c) for  $M_0 = 3.12$ . These data are for jet-off operation and are shown for all the  $5.63^\circ$  boattails tested. The theoretical values are Van Dyke's second-order theory from reference 9. The strut-body interference near the boattail break and the effect of the strut-tunnel wall shock discussed with figure 7(a) are again apparent in figure 14. Except for these local disturbances, however, good agreement was obtained. Results were similar for other boattail angles. Consequently, in order to avoid effects of the local disturbances, the theoretical values of pressure at the end of the boattail will be used where needed to analyze base-pressure data. These values are shown in figure 15 as a function of the base-to-jet diameter ratio for several values of boattail angle.

The boattail Mach number  $M_a$  was computed from  $p_a/P_a$  where the pressure ratio was obtained as follows:

$$\frac{P_a}{P_a} = \frac{P_a}{P_0} \frac{P_0^*}{P_0} \frac{P_0}{P_a}$$

where  $p_a/P_0$  was obtained from figure 14,  $p_0/P_0$  from tunnel calibrations, and  $P_0/P_a = 1$ .

## Wake

The wake pressure was calculated using the observed value of the base pressure. (Details are given in appendix B.) Briefly, the process was as follows: (1) From the observed base pressure, values were computed for the Mach numbers  $M_1$  and  $M_e$  and for the flow directions  $\varphi_c$  and  $\psi_c$ . (2) A value was assumed for the wake pressure ratio, the deflection angles  $\alpha_1$  and  $\alpha_e$  were computed, and the sum of the deflection angles was compared to the sum of the flow angles. (3) The process of step (2) was repeated until the relation  $\alpha_1 + \alpha_e = \varphi_c + \psi_c$  was satisfied.

## RESULTS AND DISCUSSION

## Effect of Jet Pressure Ratio

The effect of jet pressure ratio  $P_j/p_0$  on afterbody pressures is shown in figure 16 for  $d_b/d_j = 1.11$ ,  $\beta = 5.63^\circ$ , and  $M_0 = 1.91$ . The

conventional ratio of jet total pressure to free-stream static pressure is shown in this and in many of the figures concerning jet pressure ratio. Jet pressure ratio should not be confused with jet total-pressure ratio  $P_j/P_0$  (fig. 12) or with jet static-pressure ratio  $p_j/p_0$ , which will be considered subsequently.

Base-pressure coefficient is presented in figure 16(a). Also shown are schlieren photographs corresponding to operation at several pressure ratios. As the jet pressure ratio is increased above the no-flow value, base pressure first increases, then decreases, then again increases almost linearly. The jet at first adds low-energy air to the wake, thus reducing the allowable value of  $p_w/p_b$  and, as a result, increasing the base pressure. This is the region of "base-bleed" operation. The jet flow is so small that the wake configuration is more nearly that of the no-jet-flow case (sketch (a)). The maximum base pressure with base bleed marks the transition between the two types of wake flow. It can be seen that the base-bleed pressure can be considerably higher than the jet-off value.

In the second region, the jet and the stream combine to aspirate the base and base-pressure decreases, the minimum value being considerably lower than the jet-off value. Finally, as jet pressure ratio becomes sufficiently high, base pressures again increase.

For the case shown, the rate at which base-pressure coefficient increases begins to fall for pressure ratios greater than 12 ( $C_{p,b} > 0.15$ ). This occurs because the base pressure becomes sufficiently high to separate the boattail boundary layer. The effect on the location of the trailing shock can be seen in the schlieren photographs (fig. 16(a)); the effect on boattail pressure distribution is shown in figure 16(b). Variation of pressure coefficient with distance along the boattail is plotted for several jet pressure ratios. Also shown are the corresponding base-pressure coefficients. At low pressure ratios ( $P_j/P_0 < 5$ ) the base pressure is lower than the jet-off pressure near the end of the boattail  $p_a$ , and all boattail pressures equal the jet-off values. At higher pressure ratios, however, the base pressure exceeds  $p_a$ , the higher pressures feed upstream, and pressures near the aft end of the boattail increase. At a pressure ratio of 16 large pressure changes can be observed. The flow deflections resulting from these pressure gradients tend to increase the effective value of  $d_b/d_j$  and, as will be shown, this should decrease the rate at which base pressure increases with jet pressure ratio.

Reasons for certain of the base-pressure variations of figure 16 are more apparent if base pressure is factored into component pressure ratios as follows:  $p_b/p_0 = \frac{p_w/p_0}{p_w/p_b}$ . Values of these components calculated

from the experimental data and the corresponding values of internal and external Mach number are plotted in figure 17. Also shown are the appropriate theoretical wake pressure rise ratios from figure 12. It should be noted that the base-to-jet diameter ratio is 2.0 rather than 1.11 as in figure 16. The change was made because more data were available near the minimum base-pressure point for the larger diameter ratio.

Jet pressure ratios greater than that corresponding to minimum base pressure (i.e.,  $P_j/p_0 > 4$ ) should be considered first. As pressure ratio increases (1) wake pressure increases rapidly because the angle of approach  $\phi_c + \psi_c$  increases, and (2) wake pressure rise is almost constant because the Mach numbers  $M_e$  and  $M_1$  vary only slightly and, in addition, in opposite directions (see fig. 12). In general, agreement between theory and experiment is excellent. Base pressure therefore increases because of the increase in wake pressure.

As jet pressure ratio decreases below the value corresponding to minimum base pressure, the jet total pressure (or  $M_1$ ) becomes so low that wake pressure rise ratio must decrease rapidly. Base pressure consequently increases even though wake pressure continues to decrease.

Values of wake pressure could not be calculated for conditions in the base-bleed region. The jet becomes subsonic and, as stated previously, the flow more closely resembles that of the jet-off condition.

#### Effect of Base-to-Jet Diameter Ratio

The effect of varying the base-to-jet diameter ratio is shown in figures 18 and 19 for several values of jet Mach number and for free-stream Mach numbers of 1.91 and 3.12. The boattail angle is constant at  $5.63^\circ$  for these curves.

Increasing the base-to-jet diameter ratio, in general, decreases the base pressure. The form of all the curves, however, is similar; that is, base pressure first increases, then decreases, and finally increases with jet pressure ratio. Also, in general, the maximum base pressure in the base-bleed region is greater than the jet-off value, which in turn is greater than the minimum value. For base-to-jet diameter ratios greater than about 1.67, base pressures increase quite slowly with pressure ratio, and high pressure ratios are required before base pressure exceeds the jet-off value.

The reasons for base pressure decreasing as diameter ratio increases are again clearer if base pressure is factored into components as follows:

$$\frac{P_b}{P_0} = \frac{P_a}{P_0} \frac{P_w}{P_a} \frac{1}{\frac{P_w}{P_b}}$$

These ratios are plotted in figure 20 as a function of base-to-jet diameter ratio for fixed values of boattail angle, Mach number, and jet pressure ratio. As the base-to-jet diameter ratio increases (1) the boattail pressure  $p_a/p_0$  decreases (fig. 14); (2) the wake pressure  $p_w/p_a$  decreases because for the larger bases the trailing-shock distance  $x_c/d_j$  increases, jet curvature effects become more important, and, therefore,  $\phi_c$  decreases; and (3) the wake pressure rise ratio increases because both  $M_e$  and  $M_1$  increase. Since all components vary in a manner that tends to reduce base pressure, the combined effect is large. It is interesting to note that, since the factor that shows the greatest change is the wake pressure itself, jet curvature plays an important role. The theoretical and experimental values of wake pressure rise are again in excellent agreement.

#### Effect of Body-to-Jet Diameter Ratio

The ratio of body-to-jet diameter was held fixed at 2.67 for all but one of the afterbody configurations. For this one configuration the jet diameter was increased such that the ratio  $d_B/d_j = 1.89$ . The effect of this change is shown in figure 21. To minimize effects due to changes in boattail pressure, values of  $p_b/p_a$  are shown. It is apparent that decreasing  $d_B/d_j$  decreases base pressure slightly. Since the ratio of base-to-jet diameter is the same for both configurations, jet or stream curvatures should not be contributing factors. This is confirmed by figure 22 which plots the component pressure ratios for a jet pressure ratio of 15; wake pressure expressed in terms of the boattail pressure ratio  $p_w/p_a$  is independent of diameter ratio.

Base-to-boattail pressure ratio increases with body-to-jet diameter ratio because the boattail and external Mach numbers decrease (i.e.,  $p_a$  increases), and, therefore, wake pressure rise ratio decreases.

Experimental values of wake pressure rise ratio fall below the theoretical values. This trend was observed for all configurations having convergent-divergent nozzles ( $M_j > 1$ ) and will be discussed further in the section Effect of Jet Mach Number.

### Effect of Boattail Angle

The effect of changes in boattail angle  $\beta$  on base-pressure coefficient is shown in figures 23 and 24 for free-stream Mach numbers of 1.91 and 3.12, respectively. In general, for a fixed value of  $d_b/d_j$  increasing boattail angle increases base pressure. However, for the largest angle,  $\beta = 11^\circ$ , the curve levels out at the higher pressure ratios (again due to pressure feedback through the boattail boundary layer), and the trend of base pressure with boattail angle is reversed.

The variation of the component pressures with boattail angle is presented in figure 25 for a jet pressure ratio of 8. It can be seen that wake pressure  $p_w/p_0$  increases only slightly with boattail angle. Even though the wake pressure shows a definite increase when expressed in terms of  $p_a$ , the effect is canceled out by the variation in  $p_a$  itself.

The most important effect on base pressure clearly results from the change in wake pressure rise ratio. It is interesting to note that had the experimental values of  $p_w/p_b$  followed the theory, the effect of boattail angle would have been about half that actually observed.

It has been proposed in reference 1 that the effects of boattail angle can be correlated by use of the stream angle at the base  $\psi_b$  after deflection. This parameter is shown in figure 26 as a function of jet pressure ratio for the data of figures 23(a) and 24(a). At any pressure ratio the values  $\psi_b$  agree within  $1^\circ$  at  $M_0 = 1.91$  and  $1.3^\circ$  at  $M_0 = 3.12$ . Since these angles correspond to pressure coefficient differences of only 0.020 and 0.016, respectively, this simple correlation has been fairly successful.

### Effect of Nozzle Angle

As nozzle-exit angle  $\epsilon$  increases, the internal flow angle  $\phi_c$  increases, so  $\psi_c$  must decrease. Therefore, base pressures must increase. This effect can be seen in figure 27 for jet Mach numbers of 2.19 and 2.60. Increases in pressure coefficient of as much as 0.13 result from increasing nozzle angle from  $0^\circ$  to  $20^\circ$ .

In this case as, in general, for all variables which involve changes in the form of the jet, curvature effects are significant. Jet curvature increases with nozzle angle (ref. 15) and therefore tends to compensate for nozzle angle effects. Since in addition to curvature (or  $d\phi/dx$ ) the change in jet direction  $\phi_c - \phi_b$  depends on  $x_c/d_j$ , the compensating effects of curvature should be greater for a larger value of  $d_b/d_j$ . For

example, at a pressure ratio of 20 increasing nozzle angle from  $0^\circ$  to  $20^\circ$  increases base-pressure coefficient by 0.11 for  $d_b/d_j = 1.40$ , but the same change in nozzle angle for  $d_b/d_j = 1.67$  increases base-pressure coefficient by only 0.05 (fig. 27(b)).

The effect of nozzle angle on the component pressure ratios is shown in figure 28 for a jet Mach number of 2.19 and a jet pressure ratio of 15. In contrast to the trend with boattail angle (fig. 25), increasing nozzle angle significantly increases wake pressure. This increase and the reduction in wake pressure rise ratio combine to produce a large increase in base pressure.

Although experimental and theoretical wake pressure ratios show similar trends, the experimental values are lower. The magnitude of the difference is similar to that observed previously for a supersonic jet Mach number (see fig. 22).

In the preceding section it was found that boattail angle effects could be correlated by the use of the stream angle  $\psi_b$ . A similar correlation for nozzle angle using internal flow angle  $\phi_b$  has been attempted in figure 29. For the smaller diameter ratio ( $d_b/d_j = 1.40$ , fig. 29(a)) base pressure is relatively independent of nozzle angle when plotted against internal flow angle  $\phi_b$ . For the larger diameter ratio, however, jet curvature effects become of sufficient importance to render the correlation useless (fig. 29(b)).

#### Effect of Jet Mach Number

The effect of jet Mach number on base-pressure coefficient is shown in figure 30. At a fixed value of jet pressure ratio  $P_j/p_0$ , increasing jet Mach number produces a large reduction in base pressure. This occurs because for equal values of  $P_j/p_0$  increasing jet Mach number decreases the jet angle  $\phi_b$  and hence the wake pressure. This effect can be seen clearly in the component pressure plots of figure 31(a). The curves represent the effect of jet Mach number at constant jet pressure ratio. As jet Mach number increases, wake pressure decreases rapidly. Therefore, since wake pressure rise ratio remains essentially constant, base pressure decreases rapidly.

The agreement between theoretical and experimental wake pressure rise ratios follows the trend noted previously; at  $M_j = 1$  agreement is good, but as  $M_j$  increases, theory and experiment diverge.

It has been reasoned (ref. 1) that, since the jet angle  $\phi_b$  depends mainly on the jet-to-base static-pressure ratio  $p_j/p_b$ , the large effect

of jet Mach number on wake pressure (and hence on base pressure) could be reduced if the jet static-pressure ratio rather than the jet pressure ratio itself were held constant. The component pressures are presented in figure 31(b) for a jet static-pressure ratio  $p_j/p_0$  of 2.0. The resulting variation in jet total-pressure ratio  $P_j/P_0$  is also shown. The effect of jet Mach number on both wake pressure and base pressure has been reduced considerably by holding jet static-pressure ratio constant.

A good correlation is also obtained for other geometries and jet pressure ratios as shown in figures 32 and 33. Again base pressure is relatively independent of jet Mach number when plotted as a function of jet static-pressure ratio. The largest discrepancies amount to 0.030 at  $M_0 = 1.91$  and 0.016 at  $M_0 = 3.12$ .

The utility of jet angle as a parameter may again be questioned at this point. For each jet Mach number, the two-dimensional expansion angle  $\phi_b - \epsilon$  can be obtained for any value of jet-to-base static-pressure ratio  $p_j/p_b$  (fig. 34), and the data can then be replotted as shown in figure 35. Obviously, the correlation using  $\phi_b$  is not as good as that obtained with the jet static-pressure ratio  $p_j/p_0$ . Since base pressure is largely determined by the jet angle just ahead of the trailing shock  $\phi_c$ ,  $p_j/p_0$  must be a better measure of  $\phi_c$  than is  $\phi_b$ . The reason is that as the jet Mach number is increased the jet curvature decreases (ref. 15). This means that for a given value of  $\phi_c$  increasing jet Mach number decreases  $\phi_b$ . Fixing the static-pressure ratio does, in fact, correspond to decreasing  $\phi_b$  as jet Mach number increases (fig. 34). As a result, use of the jet static-pressure ratio  $p_j/p_0$  as a parameter corrects fortuitously for the change in curvature.

Actually, the good correlation obtained for jet Mach number effects presents a dilemma. If wake pressure rise ratio had followed the theory (fig. 31(b)), base pressure would have decreased considerably as jet Mach number increased. Therefore, if the theory is correct jet static-pressure ratio should not correlate the effects of jet Mach number. This problem will be discussed in the section WAKE PRESSURE RISE RATIO.

#### Effect of Free-Stream Mach Number

Comparison of figures 18 and 19 or 23 and 24 shows that variations in base-pressure coefficient are similar at free-stream Mach numbers of 1.91 and 3.12. The effect on base pressure itself is shown in figure 36. Base pressure expressed in terms of free-stream static pressure  $p_0$  is plotted as a function of jet pressure ratio for two configurations. If other conditions are held fixed, base-pressure ratio decreases as free-stream Mach number increases. The reasons for this trend can be seen from the effect of free-stream Mach number on the component pressures for a

constant jet pressure ratio of 8.0 (fig. 37). It can be seen that, despite the fact that boattail pressure ratio decreases, wake pressure ratio increases slightly as free-stream Mach number increases. The predominant effect, however, is the large increase in wake pressure rise ratio and the base-pressure decreases.

### Effect of Fluid Properties

The most important fluid property from the standpoint of jet geometry and variation in jet geometry with pressure ratio is the ratio of specific heats  $\gamma$ . The effect on base pressure of changing the jet fluid from air ( $\gamma = 1.4$ ) to carbon dioxide ( $\gamma = 1.3$ ) is shown in figure 38. Base pressures with the carbon dioxide jet are consistently higher than those with the air jet. Two factors can contribute to this result: (1) the effect of  $\gamma$  on the jet geometry (and, therefore, on the wake pressure), and (2) a possible effect of  $\gamma$ , density, and/or viscosity on the wake pressure rise ratio. If the effect on jet geometry can be determined, at least approximately, the effect on wake pressure rise ratio can be evaluated.

For convenience the effect of  $\gamma$  on jet geometry can be broken into two parts: the effect on the jet-to-base static-pressure ratio  $p_j/p_b$  required to produce any given initial jet angle  $\phi_b$ , and the effect on jet curvature and hence on the final angle  $\phi_c$ . Characteristic solutions presented in reference 15 show that, for the case  $M_j = 2.0$ ,  $p_j/p_b = 1.0$ , and  $\epsilon = 10^\circ$ , the effect of  $\gamma$  on curvature is negligible, at least as far downstream as the point for which the internal angle  $\phi = 0$ . For lack of additional information, it will be assumed that this result is general; that is,  $\gamma$  will be assumed to have no effect on jet curvature. It is therefore necessary to consider only the effect on the relation between the pressure ratio and the deflection angle.

The two-dimensional, Prandtl-Meyer relation is essentially

$$p_j/p_b = f[(\phi_b - \epsilon), M_j, \gamma]$$

If for simplicity  $M_j$  is taken equal to 1 and  $\epsilon$  equal to zero, the pressure ratio corresponding to any value of  $\gamma$  divided by the ratio for  $\gamma = 1.4$  can be expressed as

$$\frac{(p_j/p_b)_\gamma}{(p_j/p_b)_{\gamma=1.4}} = \frac{f(\phi_b, \gamma)}{f(\phi_b, \gamma=1.4)} = F(\phi_b, \gamma)$$

This ratio is plotted in figure 39 for several values of  $\gamma$ . These curves can be used directly to estimate base-pressure effects resulting from changes in jet geometry.

In figure 38 the abscissa of each point for the dashed curve is equal to the abscissa of the curve for air multiplied by the corresponding value of  $F(\phi_p, \gamma=1.3)$ . Agreement with the experimental data is good. The small difference indicates that the effect of the properties of carbon dioxide on the pressure rise ratio must be small.

#### Effect of Jet Temperature

The effect of jet temperature on base pressure is shown in figure 40. Effects are included for several values of base-to-jet diameter, several values of boattail angle, and two jet Mach numbers (figs. 40(a), (b), and (c), respectively). The hot jet was obtained from a propane-oxygen rocket with a combustion-chamber temperature of approximately  $4000^\circ$  R. Except for  $\beta = 11^\circ$  where separation occurs (fig. 40(b)), the curves are essentially parallel, those for the hot jet shifting upward from those of the cold jet by a pressure coefficient of about 0.08.

A question which immediately occurs is whether temperature effect can be explained solely by the associated change in specific-heat ratio. Curves for several values of  $\gamma$  predicted from the cold air jet ( $\gamma = 1.4$ ) are shown in figure 41. Although the proper value of  $\gamma$  for the rocket jet is not known exactly, the value is probably not less than 1.15. Therefore, additional factors (heat transfer, etc.) must come into play. In this respect it should be noted that for a cooler ( $2000^\circ$  R) gasoline-air jet good agreement has been obtained using the  $\gamma$  correction alone (see ref. 1).

#### Effect of Tail Interference

The effect on base pressure of the addition of tail surfaces is shown in figure 42. Tail interference expressed as change in base-pressure coefficient is plotted as a function of jet pressure ratio for several values of boattail angle in figure 42(a). The effect is a slight reduction in base pressure ( $\Delta C_{p,b} \approx -0.01$ ). No trend with either pressure ratio or boattail angle is apparent.

Figure 42(b) shows the effect of the number of surfaces. Except for the double-surface configuration, interference seems to be proportional to the number of surfaces. An additional factor, however, may be the location of the tail surfaces with respect to the model support struts.

The effect of the axial position of the tail is shown in figure 42(c). The greatest effect results if the trailing edge is located ahead of the base by 0.5 chord length ( $x/c = -0.5$ ).

## WAKE PRESSURE RISE RATIO

In the preceding discussion it was found that theoretical wake pressure rise ratios were in relatively good agreement with experiment if the jet Mach number  $M_j$  equalled unity. As jet Mach number increased above unity, these pressure rise ratios fell below the theory by an increasing amount (see fig. 31(b)).

A similar trend is apparent in the summary curves of figure 43 in which wake pressure rise ratios calculated from the data are compared with the theoretical values for a wide range of geometries and pressure ratios and for free-stream Mach numbers of 1.91 and 3.12. Wake pressure rise ratio is plotted as a function of the external Mach number  $M_e$  for several values of jet total-pressure ratio  $P_j/P_0$ . (It should be remembered that fixing  $M_e$  and the total-pressure ratio is equivalent to fixing both  $M_e$  and  $M_j$ .) Each dashed curve represents a given geometry; the points represent different pressure ratios as indicated on the figure.

When considering the results for the convergent nozzle ( $M_j = 1$ ) (fig. 43(a)), the agreement is quite good, especially at the higher pressure ratios. At a free-stream Mach number of 3.12 the highest jet pressure ratio  $P_j/P_0$  was 24, so the highest jet total-pressure ratio for which a comparison can be made is 0.50.

In contrast to the good agreement obtained for the convergent nozzle, the experimental data for the convergent-divergent nozzle (fig. 43(b)) fall below the theoretical values. The trends with respect to both pressure ratio and Mach number follow those of the theory, but the values are low.

Certain differences between theory and experiment of figure 43 are to be expected. The theoretical values are associated with a fully developed turbulent mixing profile and should therefore represent the highest wake pressure ratios obtainable. For the convergent nozzle (fig. 43(a)) and for the lowest diameter ratio  $d_b/d_j = 1.11$ , distances to the trailing shock  $x_c/\delta_a$  vary from 0.9 to 1.4, depending on the pressure ratio. Since these distances are small for fully developed profiles, it is not surprising that the experimental values fall below the theoretical. Also, since the trailing-shock distances increase with diameter ratio ( $x_c/\delta_a$  varies from 2 to 3 for  $d_b/d_j = 1.4$  and from 4 to 5 for  $d_b/d_j = 2.00$ ), agreement between theory and experiment should and does improve as diameter ratio increases.

Reasons for the differences for the convergent-divergent nozzle are not so obvious. One possibility is that the internal boundary layer could have been thicker for the convergent-divergent nozzles. The thickness unfortunately was not measured; however, a calculation based on the static wall pressures for the nozzle of figure 43(b) ( $M_j = 2.6$ ) showed that the internal boundary layer was thinner than the external ( $\delta_j/\delta_a \approx 0.5$ ). Consequently, it is difficult to believe that boundary-layer thickness could be a primary factor.

Another possibility is that the internal mixing process may not have been completely turbulent for the convergent-divergent configurations. Laminar or transitional mixing could greatly reduce the theoretical values of figure 43.

In view of the good correlations obtained for the convergent nozzle, it is unlikely that the trouble could be with factors such as departure from two-dimensional mixing (which would affect the theoretical values) and/or inaccuracies in the values of jet or free-stream curvature which were used to calculate wake pressure ratio from the experimental data (see appendix B). An investigation of the effect of nozzle configuration on the internal mixing process appears necessary before these questions can be answered.

#### PREDICTION OF BASE-PRESSURE COEFFICIENT

Values of base-pressure coefficient corresponding to the theoretical values of wake pressure ratio were calculated for the convergent nozzle. The results are compared with the experimental values in figure 44. Except for a diameter ratio of 1.11 at low pressure ratios, the agreement is excellent as was expected. Although a corresponding calculation for the convergent-divergent nozzle was not made, a difference of 0.1 in wake pressure ratio is equivalent to a difference of from 0.01 to 0.02 in base-pressure coefficient at  $M_0 = 1.91$ . Theoretical base-pressure coefficients should then be too low by an average of 0.06.

Reference 4, published prior to the present report, suggests that wake pressure rise ratio can be approximated by using a curve similar to that of figure 10 with  $M_1 = \frac{1}{2} (M_e + M_i)$ . Figure 45 presents an example of the results obtained by this method. Wake pressure rise ratio is plotted as a function of jet pressure ratio for a given configuration ( $d_b/d_j = 2.00$ ,  $\beta = 5.63^\circ$ ) for free-stream Mach numbers of 1.91 and 3.12. The solid curve is the result of using figure 10 with  $M_1 = \frac{1}{2} (M_e + M_i)$ , the data points come from experimental base-pressure measurements, and

the dashed curve was obtained by using figure 12. Good agreement is obtained except at low pressure ratios for the data at  $M_0 = 3.12$ , that is, except for cases where  $M_e$  is greatly different from  $M_i$  as shown in the following table:

Case	External Mach number, $M_e$	Internal Mach number, $M_i$	Wake pressure rise ratio from fig. 12, $P_w/P_b$	Wake pressure rise ratio from fig. 10, $P_w/P_b$
A	2.6	2.6	2.76	2.76
B	2.7	2.5	2.75	2.76
C	2.2	3.0	2.70	2.76

In all three cases  $M_1 = \frac{1}{2} (M_e + M_i) = 2.60$ . For  $M_e = M_i$  (case A) the two methods are of course identical. For  $M_e$  close to  $M_i$  (case B) figure 10 is still in good agreement with figure 12. As  $M_e$  and  $M_i$  become greatly different (case C), however, the agreement becomes poorer.

With respect to the over-all value of the correlations obtained in figure 43, it should be pointed out that calculation of the base pressure from the wake pressure rise ratio is a trial-and-error process which involves knowledge of the shape of both the jet and the stream in the base region. This information is not generally available for noncircular afterbodies or for unusual nozzle configurations (ejector-type nozzles, etc.) so experimental methods will still be required for base-pressure information. Nevertheless, the correlation is of considerable value since it shows that the flow model of figure 11 is essentially correct.

#### SUMMARY OF RESULTS

An investigation was conducted on the effect of a central jet on supersonic base pressures to provide data for a systematic set of afterbody and nozzle geometries and, in addition, to gain further insight into the factors which govern base pressure. The results are as follows:

1. Other quantities remaining constant, the ratio of base pressure to ambient pressure was, in general, increased by (a) decreasing base-to-jet diameter ratio, (b) increasing boattail angle, (c) increasing nozzle angle, (d) decreasing jet Mach number (at constant jet pressure ratio), (e) decreasing free-stream Mach number, (f) increasing jet temperature or decreasing jet specific heat ratio or both, and (g) increasing jet pressure ratio (for pressure ratios greater than design nozzle pressure ratio).

2. Addition of tail surfaces produced only small changes in base pressure. The largest effect at a free-stream Mach number of 1.91 was a change in base-pressure coefficient nearly equal to -0.02.

3. For certain variables (boattail angle, specific heat ratio, and jet Mach number) base-pressure data could be correlated by means of relatively simple parameters. For jet Mach number, however, the results may be somewhat fortuitous because of associated changes in nozzle boundary layer.

4. For all variables, base pressure is governed by the maximum pressure rise which can be supported by the wake fluid in the region of the trailing shock. The wake pressure rise ratio therefore determines the strength of the trailing shock.

5. The wake pressure rise ratio in turn was found to increase with free-stream Mach number and jet-to-stream total-pressure ratio (or with free-stream and jet Mach numbers).

6. Wake pressure rise ratio decreases as the boundary-layer thickness on the boattail increases above some critical value.

7. Values of wake pressure rise ratio computed using previously published results of an analysis of two-dimensional constant-pressure jet mixing by Korst, Page, and Childs were in good agreement with experimental values for the convergent nozzle. For the convergent-divergent nozzle, however, the experimental values were consistently lower than the computed values. The effects of nozzle boundary layer on wake pressure ratio require additional investigation.

Lewis Flight Propulsion Laboratory  
National Advisory Committee for Aeronautics  
Cleveland, Ohio, May 15, 1957

CW-4

## APPENDIX A

## CALCULATION OF THEORETICAL WAKE PRESSURE RISE RATIO

The calculation is based on an analysis presented in reference 13 of two-dimensional turbulent mixing of a compressible jet expanding into a constant-pressure region. From an asymptotic solution corresponding to a fully developed velocity profile in the mixing region, several quantities of importance in the base-pressure problem have been calculated and are tabulated in reference 14.

The following symbols are essentially those of reference 14 but are listed here only if different from those of the present report:

$$C \quad \frac{u}{u_{\max}} = M \sqrt{\frac{\gamma - 1}{2 \left( 1 + \frac{\gamma - 1}{2} M^2 \right)}}$$

g acceleration of gravity

$G_s$  weight flow per unit width between streamlines s and j

$$I_1(C_2 \eta) \quad \int_{-\infty}^{\eta} \frac{\varphi d\eta}{1 - C_2^2 \varphi^2} \quad (\text{tabulated in ref. 14})$$

u velocity in X-direction

X distance from base along boundary (x used in ref. 14)

Y distance normal to X (y used in ref. 14)

$$\eta \quad \sigma \frac{Y}{X}$$

$\sigma$  proportionality factor (approximately 12 for  $M \ll 1$ )

$\varphi(\eta)$  velocity ratio,  $\frac{u}{u_2}$  (tabulated in ref. 14)

Subscripts:

j conditions on separating streamline

max maximum

- s conditions on limiting streamline (used to denote conditions along an arbitrary streamline in ref. 14)
- 2 conditions just outside of mixing region

With the assumption that the total temperature is constant through the mixing region, the weight flow per unit width between streamline s and the separating streamline j is

$$G_s = \frac{X}{\sigma} \sqrt{\frac{g}{R}} \sqrt{\frac{2\gamma}{\gamma-1}} \frac{P}{\sqrt{T}} C_2 \left[ I_1(C_2 \eta_s) - I_1(C_2 \eta_j) \right] \quad (A1)$$

and the velocity ratio is

$$\phi(\eta_s) = \frac{u_s}{u_2} = \frac{C_s}{C_2} \quad (A2)$$

Since streamline s is taken as the limiting streamline, conditions which must be satisfied are as follows:

- (1) The jet flow between s and j must equal the free-stream flow between j and s; that is,  $G_{s_i} = -G_{s_e}$  or from equation (A1), assuming  $\sigma_i = \sigma_e$ ,  $\gamma_i = \gamma_e$ ,  $R_i = R_e$ , and  $T_i = T_e$ :

$$\frac{X_i C_{2_i}}{X_e C_{2_e}} = - \frac{I_1(C_{2_e} \eta_{s_e}) - I_1(C_{2_e} \eta_{j_e})}{I_1(C_{2_i} \eta_{s_i}) - I_1(C_{2_i} \eta_{j_i})} \quad (A3)$$

- (2) Since the Mach number along both  $s_e$  and  $s_i$  must be such that the fluid can just negotiate the wake pressure rise,  $M_{s_e}$  must equal  $M_{s_i}$ . This means that  $C_{s_e} = C_{s_i}$ , or with equation (A2):

$$\frac{\phi_e(\eta_{s_e})}{\phi_i(\eta_{s_i})} = \frac{C_{2_i}}{C_{2_e}} \quad (A4)$$

Equations (A3) and (A4) are sufficient to determine wake pressure rise if the boattail geometry and the Mach numbers  $M_e$  and  $M_i$  are specified. For the present calculation, however, a further simplifying assumption was made. It was assumed that the jet and free-stream angles were either small or equal so that  $X_i = X_e$ . The ratio  $X_i/X_e$  can then be dropped from equation (A3), and the solution is independent of after-body geometry.

For given values of  $C_{2e}$  and  $C_{2i}$  the calculation procedure is as follows:

- (1) Calculate  $M_e$ ,  $M_i$ , and  $P_j/P_0$   $\left( M = C \sqrt{\frac{2}{(\gamma - 1)(1 - C^2)}} \right)$
- (2) Calculate  $C_{2i}/C_{2e}$
- (3) From tables (ref. 14) find  $I_1(C_{2e} \eta_{j_e})$  and  $I_1(C_{2i} \eta_{j_i})$
- (4) Assume  $\varphi_e(\eta_{s_e})$
- (5) Find  $\varphi_i(\eta_{s_i})$  from equation (A4).
- (6) From tables (ref. 14) find  $I_1(C_{2e} \eta_{s_e})$  and  $I_1(C_{2i} \eta_{s_i})$
- (7) Calculate right side of equation (A3) and compare with value of  $C_{2i}/C_{2e}$  (step (2)). Repeat starting with step (4) until agreement is obtained.
- (8) Calculate  $C_s$  from value of  $\varphi_e(\eta_{s_e})$  for which equation (A3) is satisfied:

$$C_s = C_{s_i} = C_{s_e} = \varphi_e(\eta_{s_e}) C_{2e}$$

- (9) Calculate  $M_s$  and  $p_w/p_b = \left( 1 + \frac{\gamma - 1}{2} M_s^2 \right)^{\frac{\gamma}{\gamma - 1}}$

Calculations were made for a range of values for  $M_e$  and  $M_i$  from 1.4 to 3.6, and the resulting values of wake pressure ratio are plotted in figures 12 and 43 as a function of  $M_e$  for several values of  $P_j/P_0$ .

## APPENDIX B

CALCULATION OF EXPERIMENTAL PRESSURE RISE RATIO  $p_w/p_b$ 

In order to calculate the wake pressure ratio  $p_w/p_b$ , it is necessary to know the flow geometry (fig. 9(c)) just ahead of the trailing shocks, namely  $\psi_c$  and  $\phi_c$ , and the internal and external Mach numbers  $M_i$  and  $M_e$ . Then, by an iteration procedure a wake pressure ratio can be found that will satisfy the flow conditions.

An important point in making the wake pressure calculations for an axisymmetric body and jet is the sizeable changes in internal- and external-flow direction that can occur between the base and the point of intersection. The streamlines can be calculated by the method of characteristics or determined from experimental data. In this report the shape of the jet as a function of jet pressure ratio, Mach number, and nozzle angle was determined from quiescent air schlieren photographs. Recently, however, a report (ref. 15) has been published with a convenient method of determining the jet boundaries. These boundaries are approximated by circular arcs defined by the initial flow direction and the maximum jet diameter. The values of reference 15 agree well in general and vary at most by  $2^\circ$  from the values of the present report and probably would be more convenient to use. Calculated jet boundaries can also be obtained from reference 17.

Since the curvature of the external stream was small compared with that of the internal stream, an approximate correction was used. This was obtained from reference 16 by interpolation and extrapolation of the theoretical boundaries. These boundaries compared favorably with those determined from schlieren photographs.

A typical calculation of pressure rise ratio is as follows:

Given these conditions:

- (1) Base pressure  $p_b/p_0$
- (2) Boattail flow direction  $\beta$ , boattail Mach number  $M_a$ , and boattail static-pressure ratio  $p_a/p_0$  (from fig. 15)
- (3) Nozzle flow direction  $\epsilon$ , jet Mach number  $M_j$ , and jet static-pressure ratio  $p_j/p_0$
- (4) Base-to-jet diameter ratio  $d_b/d_j$ ,

the direction of the external streamline just downstream of the base and the external Mach number can be obtained from the following isentropic flow relations:

~~CONFIDENTIAL~~

$$v_a = f(M_a)$$

$$M_e = g(p_b/P_0)$$

$$v_e = f(M_e)$$

$$\psi_b = (v_e - v_a) + \beta$$

Similarly, the initial direction of the internal streamline and the internal Mach number can be obtained from

$$v_j = f(M_j)$$

$$M_i = g(p_b/P_j)$$

$$v_i = f(M_i)$$

$$\phi_b = (v_i - v_j) + \epsilon$$

By knowing the conditions just downstream of the base, the jet and free-stream streamline curvatures can be determined from references 15, 16, and 17. The flow field at the point of intersection  $x_c$  can be constructed, and  $\psi_c$  and  $\phi_c$  can be measured by combining the internal and external streamlines. By using the curves of the static-pressure ratio across an oblique shock  $p_w/p_b$  as a function of free-stream Mach number  $M_e$  or  $M_i$  (fig. 46), a value of wake pressure ratio  $p_w/p_b$  is chosen and the corresponding deflection angle  $\alpha$  is determined. This process is repeated until  $\psi_c + \phi_c = \alpha_e + \alpha_i$  for the value of  $p_w/p_b$  chosen.

#### REFERENCES

1. Cortright, Edgar M., Jr., and Kochendorfer, Fred D.: Jet Effects on Flow over Afterbodies in Supersonic Stream. NACA RM E53H25, 1953.
2. Coletti, Donald E.: Measurements and Predictions of Flow Conditions on a Two-Dimensional Base Separating a Mach Number 3.36 Jet and a Mach Number 1.55 Outer Stream. NACA RM L54C08, 1954.
3. Raymond, J. L., and Rodden, W. P.: Base Pressures for Bodies of Revolution. RM-1544, Rand Corp., Aug. 24, 1955.
4. Cortright, Edgar M., Jr.: Some Aerodynamic Considerations of Nozzle-Afterbody Combinations. Aero. Eng. Rev., vol. 15, no. 9, Sept. 1956, pp. 59-65.

~~CONFIDENTIAL~~

5. Beastall, D., and Eggink, H.: Some Experiments on Breakaway in Supersonic Flow, pt. II. Tech. Note AERO. 2061, British RAE, June 1950.
6. Love, Eugene S.: The Base Pressure at Supersonic Speeds of Two-Dimensional Airfoils and Bodies of Revolution (With and Without Fins) Having Turbulent Boundary Layers. NACA RM L53C02, 1953.
7. Chapman, Dean R., Kuehn, Donald M., and Larson, Howard K.: Investigation of Separated Flows in Supersonic and Subsonic Streams with Emphasis on the Effect of Transition. NACA TN 3869, 1957.
8. Korst, H. H., Page, R. H., and Childs, M. E.: A Theory for Base Pressures in Transonic and Supersonic Flow. Tech. Note 392-2, Eng. Exp. Station, Univ. Ill., Mar. 1955. (Office Sci. Res. Contract AF-18(600)-392.)
9. Jack, John R.: Theoretical Pressure Distributions and Wave Drags for Conical Boattails. NACA TN 2972, 1953.
10. Cortright, Edgar M., Jr., and Schroeder, Albert H.: Investigation at Mach Number 1.91 of Side and Base Pressure Distributions over Conical Boattails Without and With Jet Flow Issuing from Base. NACA RM E51F26, 1951.
11. Love, Eugene S.: Pressure Rise Associated with Shock-Induced Boundary-Layer Separation. NACA TN 3601, 1955.
12. Chapman, Dean R., Wimbrow, William R., and Kester, Robert H.: Experimental Investigation of Base Pressure on Blunt-Trailing-Edge Wings at Supersonic Velocities. NACA Rep. 1109, 1952. (Supersedes NACA TN 2611.)
13. Korst, H. H., Page, R. H., and Childs, M. E.: Compressible Two-Dimensional Jet Mixing at Constant Pressure. Tech. Note 392-1, Eng. Exp. Station, Univ. Ill., Apr. 1954. (Office Sci. Res. Contract AF-18(600)-392.)
14. Korst, H. H., Page, R. H., and Childs, M. E.: Compressible Two-Dimensional Jet Mixing at Constant Pressure. Tables of Auxiliary Functions for Fully Developed Mixing Profiles. Tech. Note 392-3, Eng. Exp. Station, Univ. Ill., Apr. 1955. (Office Sci. Res. Contract AF-18(600)-392.)
15. Love, Eugene S., and Grigsby, Carl E.: Some Studies of Axisymmetric Free Jets Exhausting from Sonic and Supersonic Nozzles Into Still Air and Into Supersonic Streams. NACA RM L54L31, 1955.

16. Chapman, Dean R.: An Analysis of Base Pressure at Supersonic Velocities and Comparison with Experiment. NACA Rep. 1051, 1951. (Supersedes NACA TN 2137.)
17. Love, Eugene S.; Woodling, Mildred J., and Lee, Louise P.: Boundaries of Supersonic Axisymmetric Free Jets. NACA RM L56G18, 1956.

## BIBLIOGRAPHY

## JET-STREAM INTERACTION EFFECTS

- Baker, W. T., Davis, T., and Matthews, S. E.: Reduction of Drag of a Projectile in a Supersonic Stream by the Combustion of Hydrogen in the Turbulent Wake. CM 673, Appl. Phys. Lab., The John Hopkins Univ., June 4, 1951. (Contract NOrd 7386, with Bur. Ord., U. S. Navy.)
- Baughman, L. Eugene: Wind-Tunnel Investigation at Mach 1.91 of Multijet-Missile Base Pressures. NACA RM E54L14, 1955.
- Bressette, Walter E.: Investigation of the Jet Effects on a Flat Surface Downstream of the Exit of a Simulated Turbojet Nacelle at a Free-Stream Mach Number of 2.02. NACA RM L54E05a, 1954.
- Bressette, Walter E.: Some Experiments Relating to the Problem of Simulation of Hot Jet Engines in Studies of Jet Effects on Adjacent Surfaces at Free-Stream Mach Number of 1.80. NACA RM L56E07, 1956.
- Bressette, Walter E., and Faget, Maxime A.: An Investigation of Jet Effects on Adjacent Surfaces. NACA RM L55E06, 1955.
- Bromm, August F., Jr., and O'Donnell, Robert M.: Investigation at Supersonic Speeds of the Effect of Jet Mach Number and Divergence Angle of the Nozzle Upon the Pressure of the Base Annulus of a Body of Revolution. NACA RM L54I16, 1954.
- Coletti, Donald E.: Measurements and Predictions of Flow Conditions on a Two-Dimensional Base Separating a Mach Number 3.36 Jet and a Mach Number 1.55 Outer Stream. NACA RM L54C08, 1954.
- Cortright, Edgar M., Jr., and Schroeder, Albert H.: Investigation at Mach Number 1.91 of Side and Base Pressure Distributions over Conical Boattails Without and With Jet Flow Issuing from Base. NACA RM E51F26, 1951.

Cortright, Edgar M., Jr., and Schroeder, Albert H.: Preliminary Investigation of Effectiveness of Base Bleed in Reducing Drag of Blunt-Base Bodies in Supersonic Stream. NACA RM E51A26, 1951.

Cubbage, James M., Jr.: Jet Effects on Base and Afterbody Pressures of a Cylindrical Afterbody at Transonic Speeds. NACA RM L56C21, 1956.

deMoraes, Carlos A.: Transonic Flight Test of a Rocket-Powered Model to Determine Propulsive Jet Influence on the Configuration Drag. NACA RM L54D27, 1954.

deMoraes, Carlos A., Hagginbothom, William K., Jr., and Falanga, Ralph A.: Design and Evaluation of a Turbojet Simulator, Utilizing a Solid-Propellant Rocket Motor, for Use in Free-Flight Aerodynamic Research Models. NACA RM L54I15, 1954.

deMoraes, Carlos A., and Nowitsky, Albin M.: Experimental Effects of Propulsive Jets and Afterbody Configurations on the Zero-Lift Drag of Bodies of Revolution at a Mach Number of 1.59. NACA RM L54C16, 1954.

Englert, Gerald W., Vargo, Donald J., and Cubbison, Robert W.: Effect of Jet-Nozzle-Expansion Ratio on Drag of Parabolic Afterbodies. NACA RM E54B12, 1954.

Englert, Gerald W., Wasserbauer, Joseph F., and Whalen, Paul: Interaction of a Jet and Flat Plate Located in an Airstream. NACA RM E55G19, 1955.

Falanga, Ralph A.: A Free-Flight Investigation of the Effects of Simulated Sonic Turbojet Exhaust on the Drag of a Boattailed Body with Various Jet Sizes from Mach Number 0.87 to 1.50. NACA RM L55F09a, 1955.

Falanga, Ralph A.: A Free-Flight Investigation of the Effects of a Sonic Jet on the Total-Drag and Base-Pressure Coefficients of a Boattail Body of Revolution from Mach Number 0.83 to 1.70. NACA RM L55L21, 1956.

Falanga, Ralph A., and Judd, Joseph H.: Flight Investigation of the Effect of Underwing Propulsive Jets on the Lift, Drag, and Longitudinal Stability of a Delta-Wing Configuration at Mach Numbers from 1.23 to 1.62. NACA RM L55I13, 1955.

Falk, H.: The Influence of the Jet of a Propulsion Unit on Nearby Wings. NACA TM 1104, 1946.

Fradenburgh, Evan A., Gorton, Gerald C., and Beke, Andrew: Thrust Characteristics of a Series of Convergent-Divergent Exhaust Nozzles at Subsonic and Supersonic Flight Speeds. NACA RM E53L23, 1954.

- Fuller, L., and Reid, J.: Experiments on Two Dimensional Base Flame at  $M = 2.4$ . Rep. No. AERO 2569, British RAE, Feb. 1956.
- Gillespie, Warren, Jr.: Jet Effects on Pressures and Drags of Bodies. NACA RM L51J29, 1951.
- Grigsby, Carl E.: An Investigation of the Effects of Jet Exhaust and Reynolds Number Upon the Flow over the Vertical Stabilizer and Rudder of the Douglas D-558-II Research Airplane at Mach Numbers of 1.62, 1.93, and 2.41. NACA RM L54E03, 1954.
- Hatch, John E., Jr., and Savelle, William M.: Some Effects of a Sonic Jet Exhaust on the Loading over a Yawed Fin at a Mach Number of 3.03. NACA RM L52L02a, 1953.
- Hearth, Donald P., and Gorton, Gerald C.: Investigation of Thrust and Drag Characteristics of a Plug-Type Exhaust Nozzle. NACA RM E53L16, 1954.
- Hearth, Donald P., and Valerino, Alfred S.: Thrust and Pumping Characteristics of a Series of Ejector-Type Exhaust Nozzles at Subsonic and Supersonic Flight Speeds. NACA RM E54HL9, 1954.
- Hearth, Donald P., and Wilcox, Fred A.: Thrust and Drag Characteristics of a Convergent-Divergent Nozzle with Various Exhaust Jet Temperatures. NACA RM E53L23b, 1954.
- Hebrank, W. H., Scanland, T. S., Platou, A. S., and Hicks, B. L.: The Effects on Base Pressure of Air Ejection from the Base of a Model Projectile at  $M = 1.7$  - Partial Evaluation of the External Ram Jet Principles. Memo. Rep. No. 539, Ballistic Res. Labs., Aberdeen Proving Ground (Md.), Aug. 1951. (Proj. No. TB3-0110V, Res. and Dev. Div., Ord. Corps.)
- Henry, Beverly Z., Jr., and Cahn, Maurice S.: Preliminary Results of an Investigation at Transonic Speeds to Determine the Effects of a Heated Propulsive Jet on the Drag Characteristics of a Related Series of Afterbodies. NACA RM L55A24a, 1955.
- Henry, Beverly Z., Jr., and Cahn, Maurice S.: Pressure Distributions over a Series of Related Afterbody Shapes as Affected by a Propulsive Jet at Transonic Speeds. NACA RM L56K05, 1957.
- Hoffman, Sherwood: Free-Flight Tests to Determine the Power-on and Power-off Pressure Distribution and Drag of the NACA RM-10 Research Vehicle at Large Reynolds Numbers Between Mach Numbers 0.8 and 3.0. NACA RM L55H02, 1955.

- Jonas, Julius: On the Interaction Between Multiple Jets and an Adjacent Surface. Aero. Eng. Rev., vol. 11, no. 1, Jan. 1952, pp. 21-25.
- Leiss, Abraham: Free-Flight Investigation of Effects of Simulated Sonic Turbojet Exhaust on the Drag of Twin-Jet Boattail Bodies at Transonic Speeds. NACA RM L56D30, 1956.
- Love, Eugene S.: Aerodynamic Investigation of a Parabolic Body of Revolution at Mach Number of 1.92 and Some Effects of an Annular Supersonic Jet Exhausting from the Base. NACA TN 3709, 1956. (Supersedes NACA RM L9K09.)
- Love, Eugene S.: Initial Inclination of the Mixing Boundary Separating an Exhausting Supersonic Jet from a Supersonic Ambient Stream. NACA RM L55J14, 1956.
- O'Donnell, Robert M., and McDearmon, Russell W.: Experimental Investigation of Effects of Primary Jet Flow and Secondary Flow Through a Zero-Length Ejector on Base and Boattail Pressures of a Body of Revolution at Free-Stream Mach Numbers of 1.62, 1.93, and 2.41. NACA RM L54I22, 1954.
- Olson, Roland E., and Bielat, Ralph P.: An Aerodynamic and Hydrodynamic Investigation of Two Multijet Water-Based Aircraft Having Low Transonic Drag Rise. NACA RM L55A11a, 1955.
- Peck, Robert F.: Jet Effects on Longitudinal Trim of an Airplane Configuration Measured at Mach Numbers Between 1.2 and 1.8. NACA RM L54J29a, 1955.
- Peck, Robert F.: Results of Rocket Model Test of an Airplane Configuration Having an Arrow Wing and Slender Flat-Sided Fuselage. Lift, Drag, Longitudinal Stability, Lateral Force, and Jet Effects at Mach Numbers Between 1.0 and 2.3. NACA RM L55L29, 1956.
- Pel, C., and Rustemeyer, A.: Investigation of Turbojet Exhaust-Interference Drag. Rep. R-0801-12, Res. Dept., United Aircraft Corp., Nov. 1955. (Contract NOa(s)55-134-c.)
- Potter, J. Leith, and Shapiro, Norman M.: Some Effects of a Propulsion Jet on the Flow over the Fins of a Missile. Rep. 2R3F, Ord. Missile Labs, Redstone Arsenal, Jan. 11, 1954. (Proj. TB3-0108.)
- Purser, Paul E., Thibodaux, Joseph G., and Jackson, H. Herbert: Note on Some Observed Effects of Rocket-Motor Operation on the Base Pressures of Bodies in Free Flight. NACA RM L50I18, 1950.

3808

CONFIDENTIAL

- Rainey, Robert W.: The Effects Upon Body Drag of Jets Exhausting from Wing-Mounted Nacelles. NACA RM L56A09, 1956.
- Salmi, Reino J.: Experimental Investigation of Drag of Afterbodies with Exiting Jet at High Subsonic Mach Numbers. NACA RM E54I13, 1954.
- Salmi, Reino J.: Preliminary Investigation of Methods to Increase the Base Pressure of Plug Nozzles at Mach 0.9. NACA RM E56J05, 1956.
- Salmi, R. J., and Cortright, E. M., Jr.: Effects of External Stream Flow and Afterbody Variations on the Performance of a Plug Nozzle at High Subsonic Speeds. NACA RM E56F11a, 1956.
- Salmi, Reino J., and Klann, John L.: Interference Effects at Mach 1.9 on a Horizontal Tail Due to Trailing Shock Waves from an Axisymmetric Body with an Exiting Jet. NACA RM E55J13a, 1956.
- Salmi, Reino J., and Klann, John L.: Investigation of Boattail and Base Pressures of Twin-Jet Afterbodies at Mach Number 1.91. NACA RM E55C01, 1955.
- Scanland, T. S., and Hebrank, W. H.: Drag Reduction Through Heat Addition to the Wake of Supersonic Missiles. Memo. Rep. No. 596, Ballistic Res. Labs., Aberdeen Proving Ground (Md.), June 1952. (Proj. No. TB3-0110, Res. and Dev. Div., Ord. Corps.)
- Squire, H. B.: Jet Flow and Its Effects on Aircraft. Aircraft Eng., vol. XXII, no. 253, Mar. 1950, pp. 62-67.
- Stitt, Leonard E., and Valerino, Alfred S.: Effect of Free-Stream Mach Number on Gross-Force and Pumping Characteristics of Several Ejectors. NACA RM E54K23a, 1955.
- Stoney, William E., Jr., and Katz, Ellis: Pressure Measurements on a Sharply Converging Fuselage Afterbody with Jet on and off at Mach Numbers from 0.8 to 1.6. NACA RM L50F06, 1950.
- Valerino, Alfred S.: Jet Effects on Pressure Loading of All-Movable Horizontal Stabilizer. NACA RM E54C24, 1954.
- Valerino, Alfred S.: Static Investigation of Several Jet Deflectors for Longitudinal Control of an Aircraft. NACA RM E55D04, 1955.
- Valerino, Alfred S., and Stitt, Leonard E.: Effect on Ejector Performance of Varying Diameter Ratio by Simulated Iris Flaps. NACA RM E55B25, 1955.

Valerino, Alfred S., and Yeager, Richard A.: External-Stream Effects on Gross Thrust and Pumping Characteristics of Ejectors Operating at Off-Design Mach Numbers. NACA RM E56C14, 1956.

Vargo, Donald J.: Effects of Secondary-Air Flow on Annular Base Force of a Supersonic Airplane. NACA RM E54G28, 1954.

Vargo, Donald J., and Englert, Gerald W.: Effect of Nozzle Contour on Drag of Parabolic Afterbodies. NACA RM E54D02, 1954.

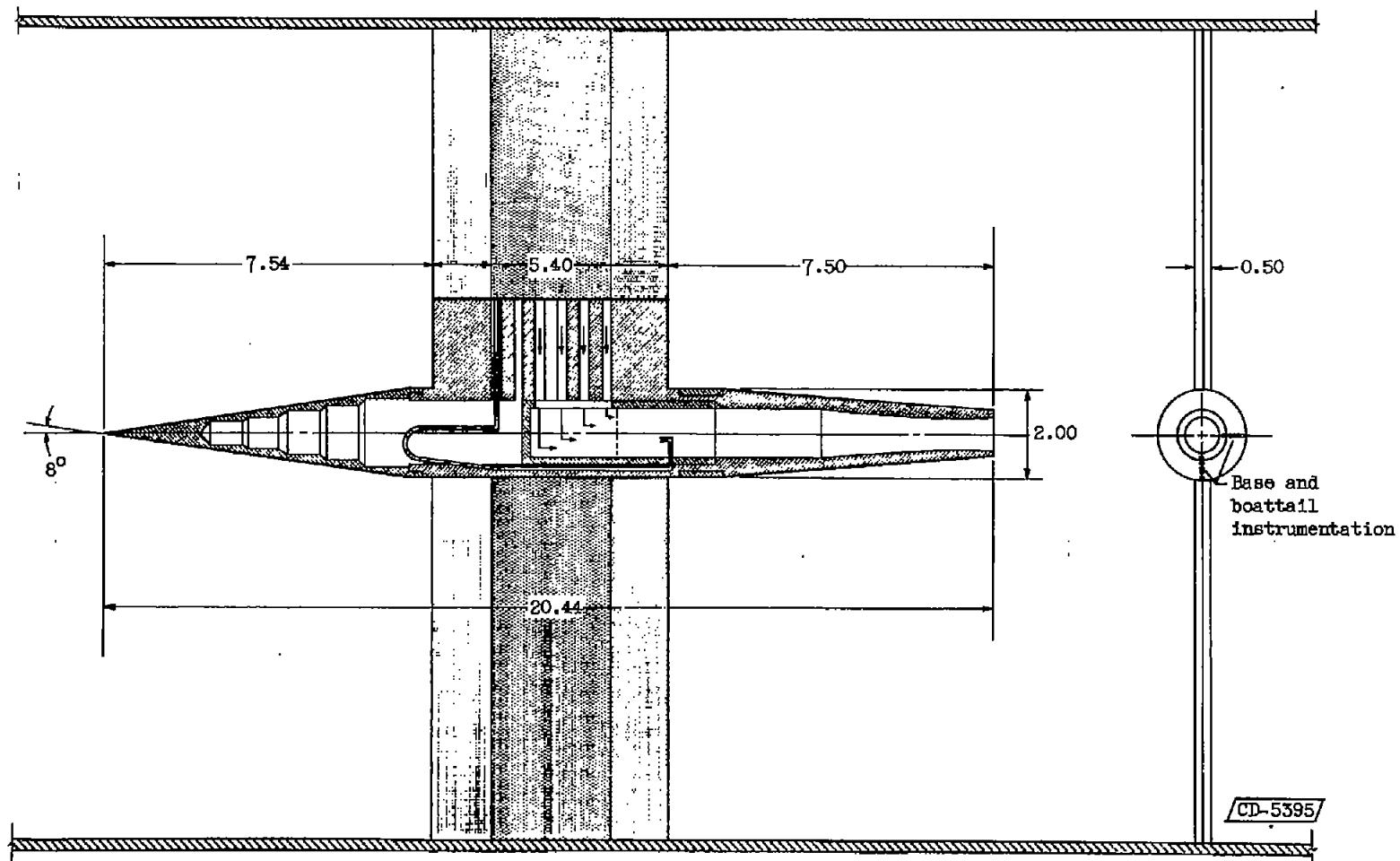
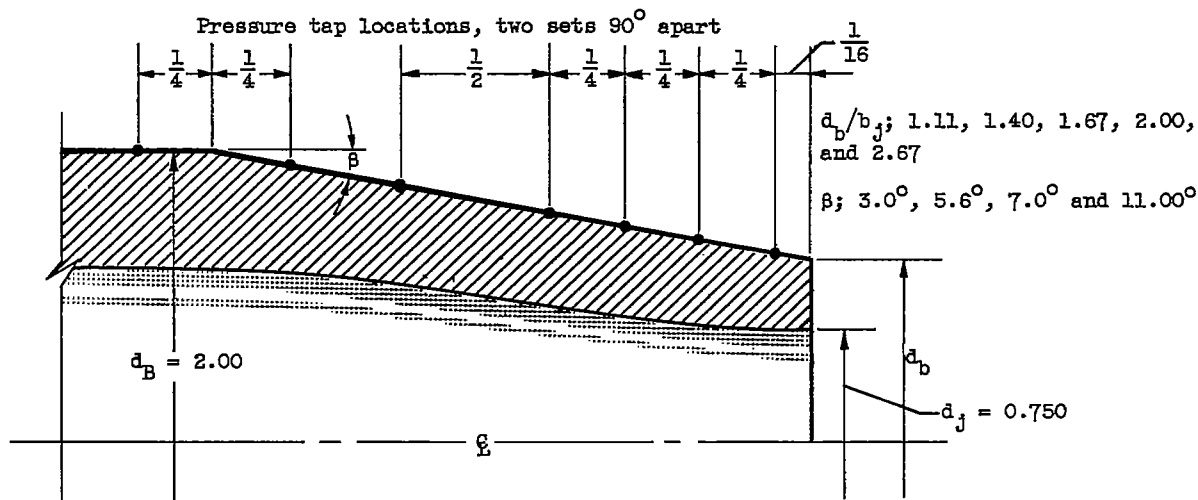
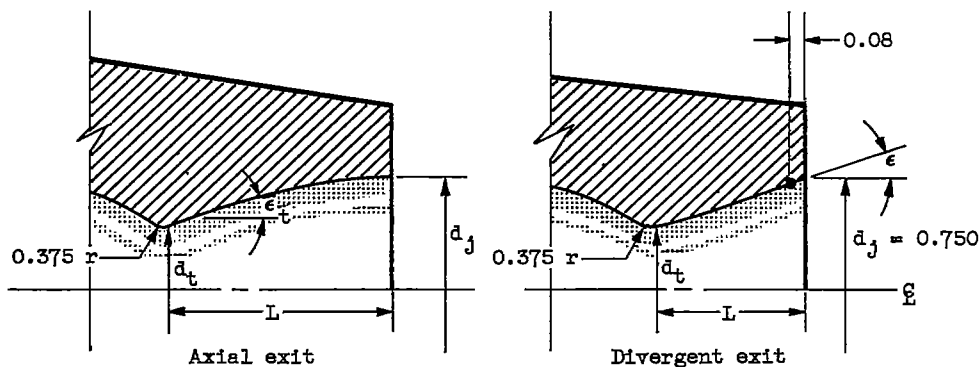


Figure 1. - Schematic of basic model. (All dimensions in inches except where noted.)

3808



(a) Boattail geometries.

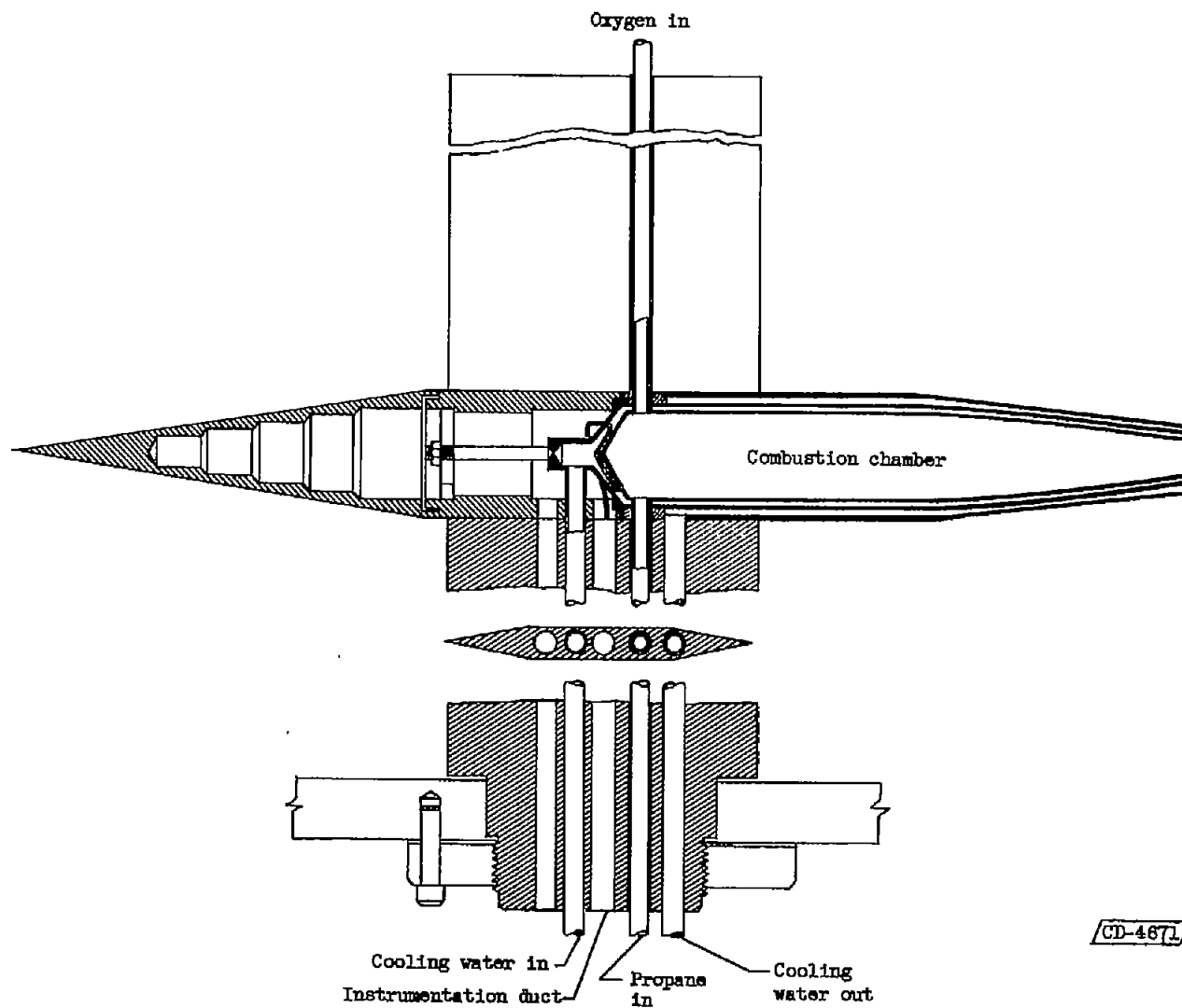


Design jet Mach number, $M_j$	Design jet pressure ratio, $P_j/P_j$	Body-to-jet diameter ratio, $d_B/d_j$	Nozzle angle, $\epsilon$ , deg	Nozzle-throat angle, $\epsilon_t$ , deg	$d_t/d_j$	$L/d_j$
2.2	10.5	2.67	0	11.0	0.710	1.31
2.6	20	2.67	0	20.7	.588	2.41
3.2	50	2.67	0	26.8	.440	2.80
2.2	10.5	2.67	10	10	.712	.79
2.6	20	2.67	10	10	.590	1.17
2.2	10.5	2.67	20	20	.715	.48
2.6	20	2.67	20	20	.596	.64
2.2	10.5	1.89 ( $d_j = 1.056$ )	0	11.0	.710	1.31

(b) Nozzle geometries.

/CD-5396/

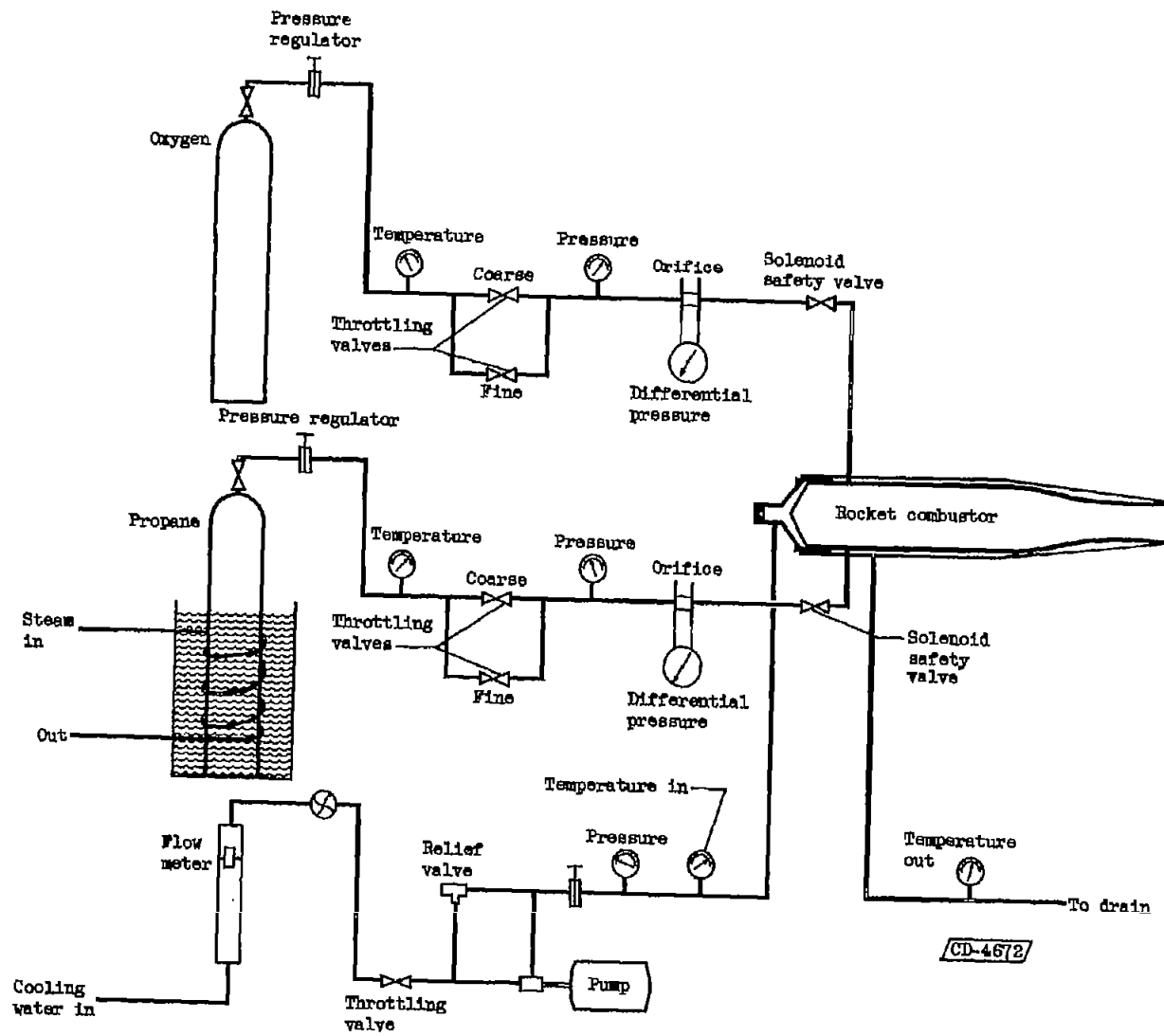
Figure 2. - Boattail and nozzle geometries.



(a) Schematic diagram.

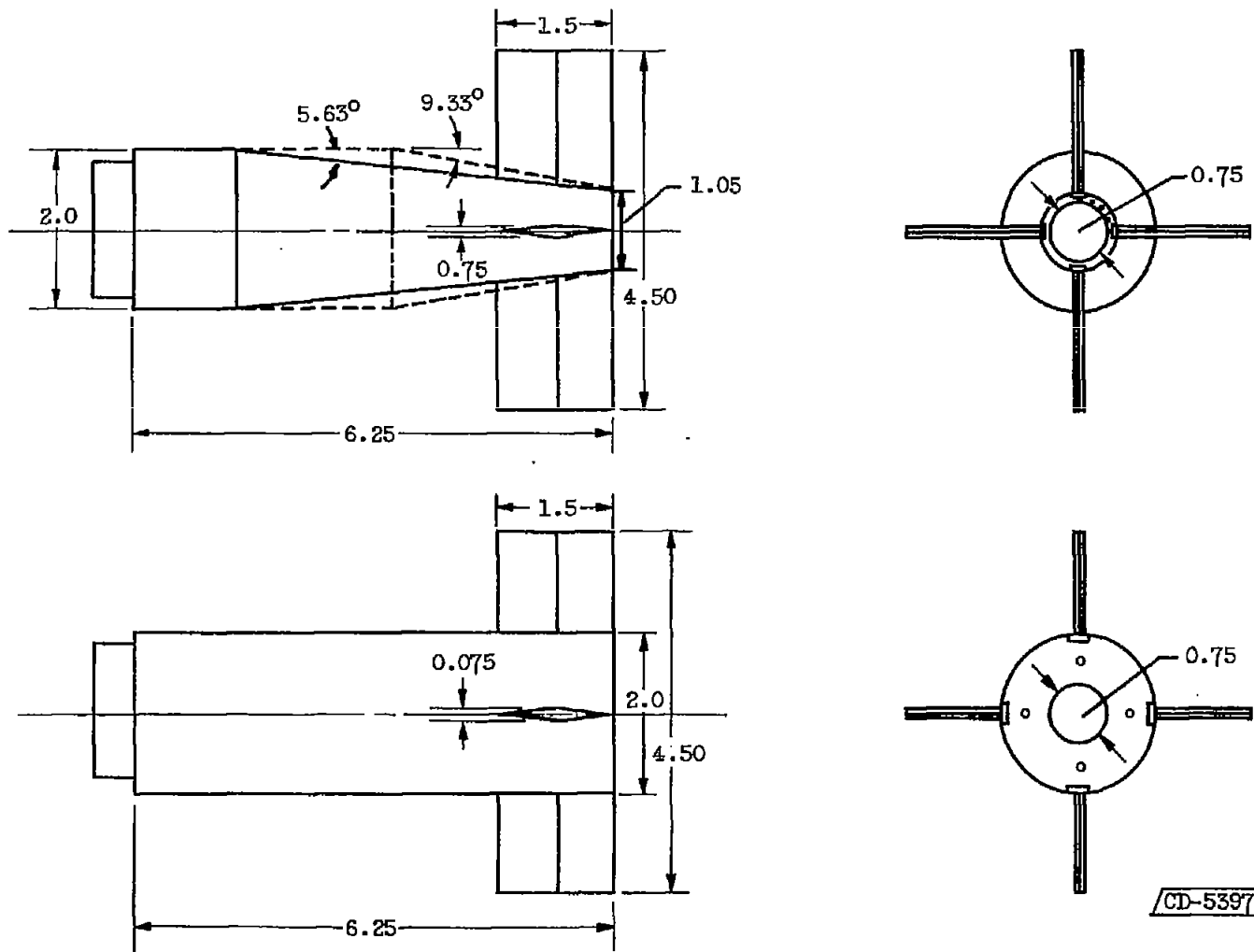
Figure 3. - Rocket model.

CD-487L



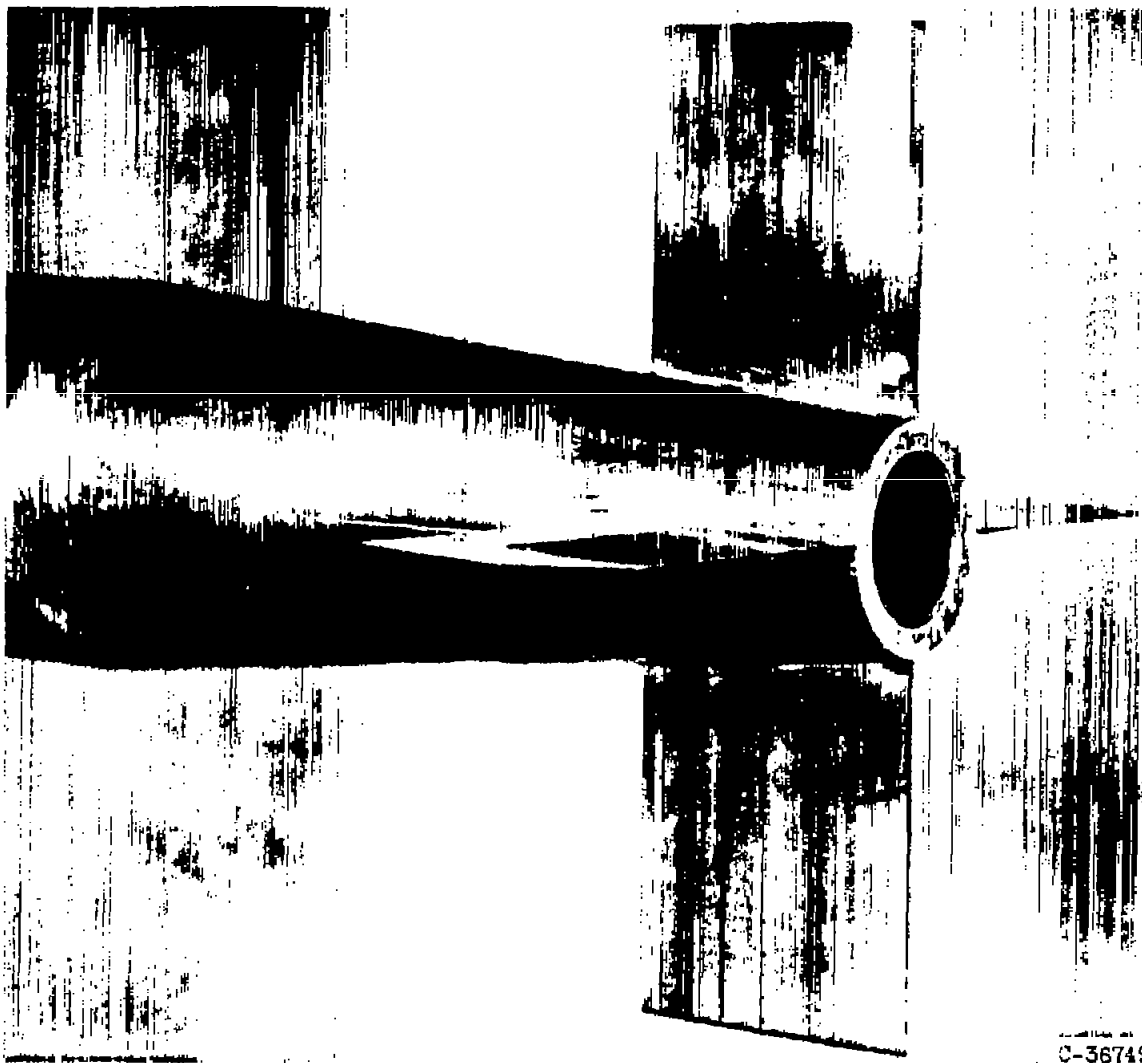
(b) Schematic diagram of fuel and coolant system.

Figure 3. - Concluded. Rocket model.



(a) Schematic diagram of afterbodies with tail surfaces. (All dimensions in inches except where noted.)

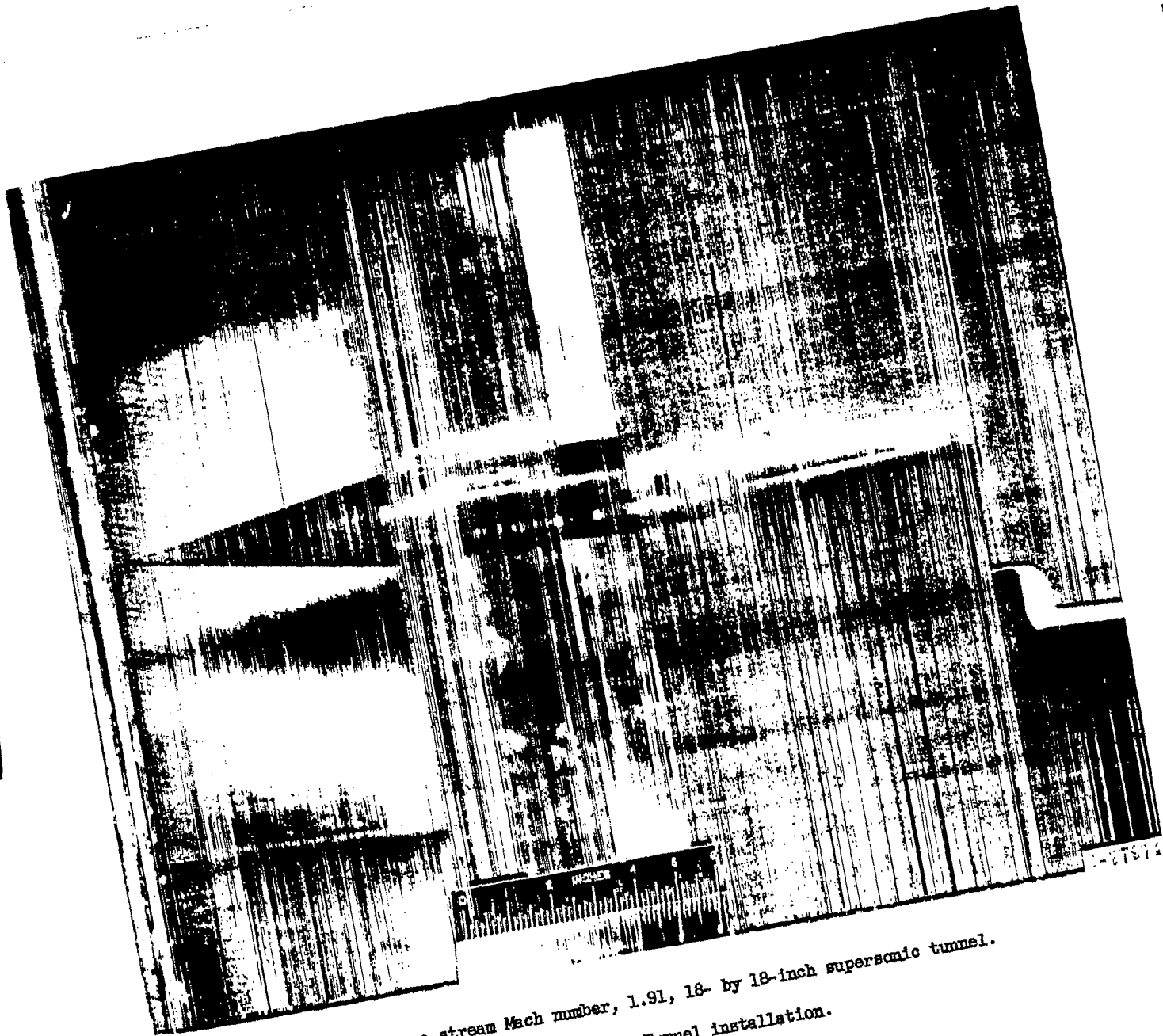
Figure 4. - Tail interference model.



C-36749

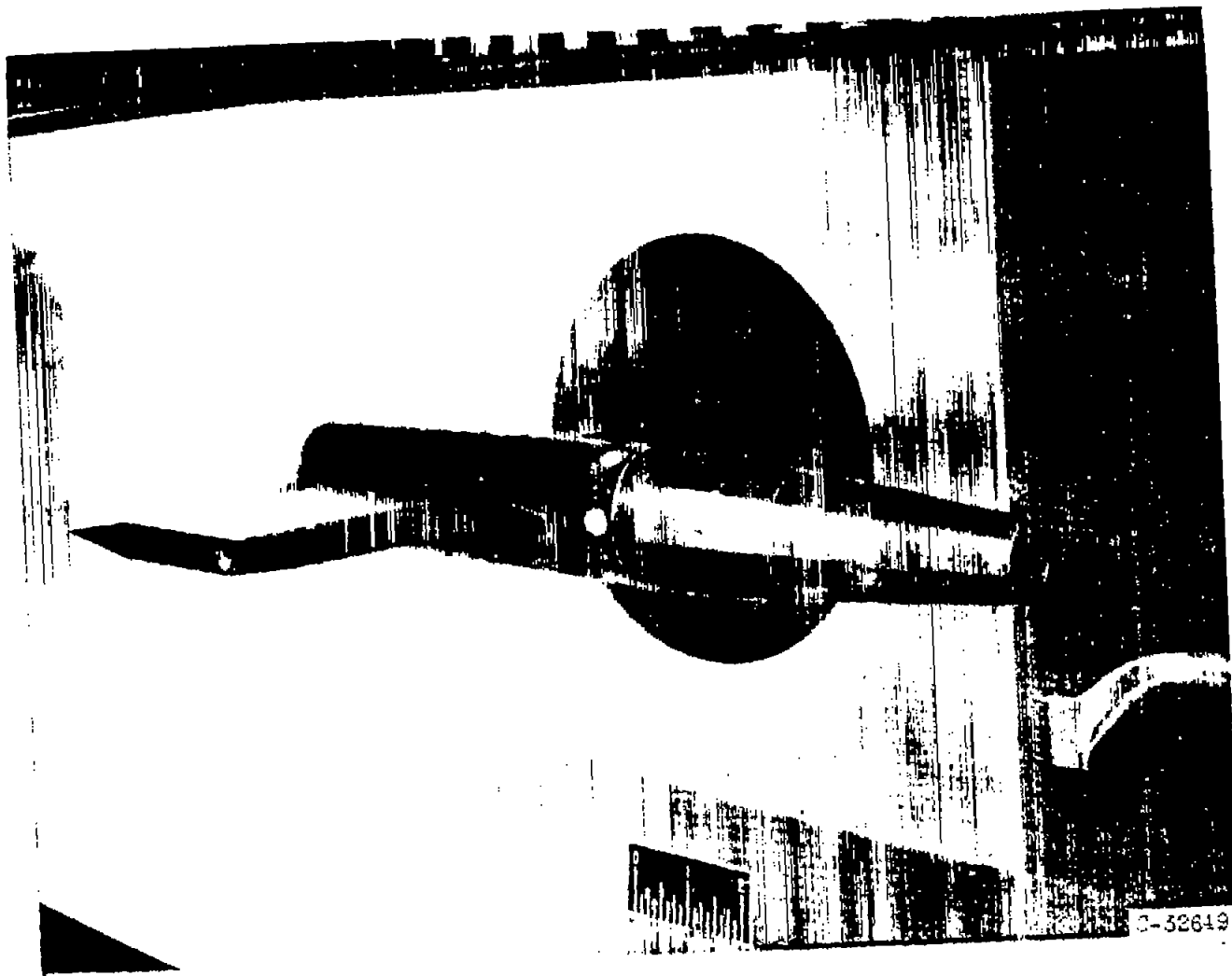
(b) Three-quarter view of cruciform tail on  $5.83^\circ$  boattail.

Figure 4. - Concluded. Tail interference model.



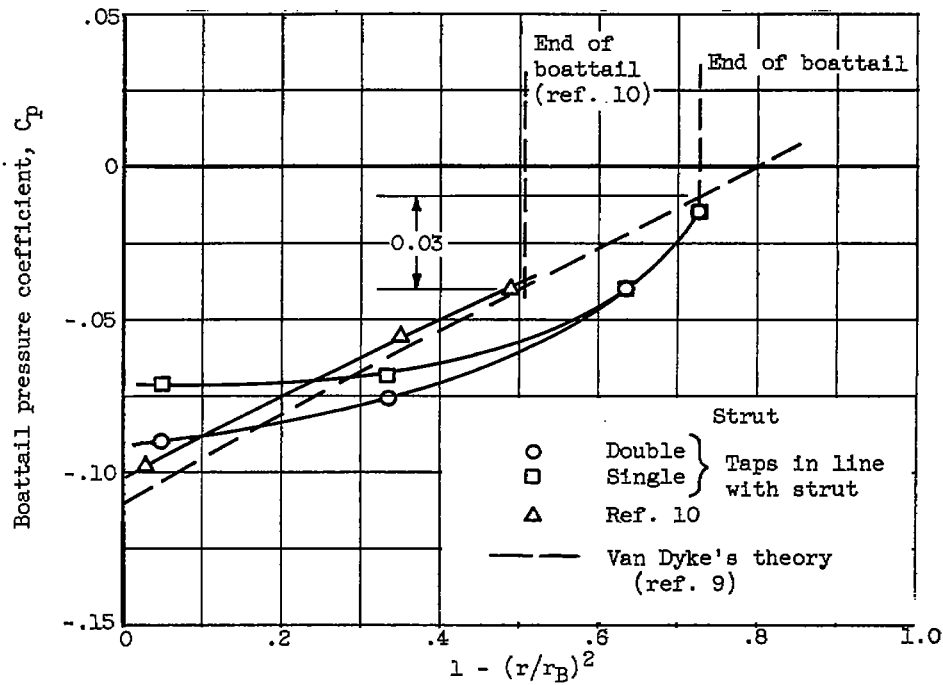
(a) Free-stream Mach number, 1.91, 18- by 18-inch supersonic tunnel.

Figure 5. - Tunnel installation.

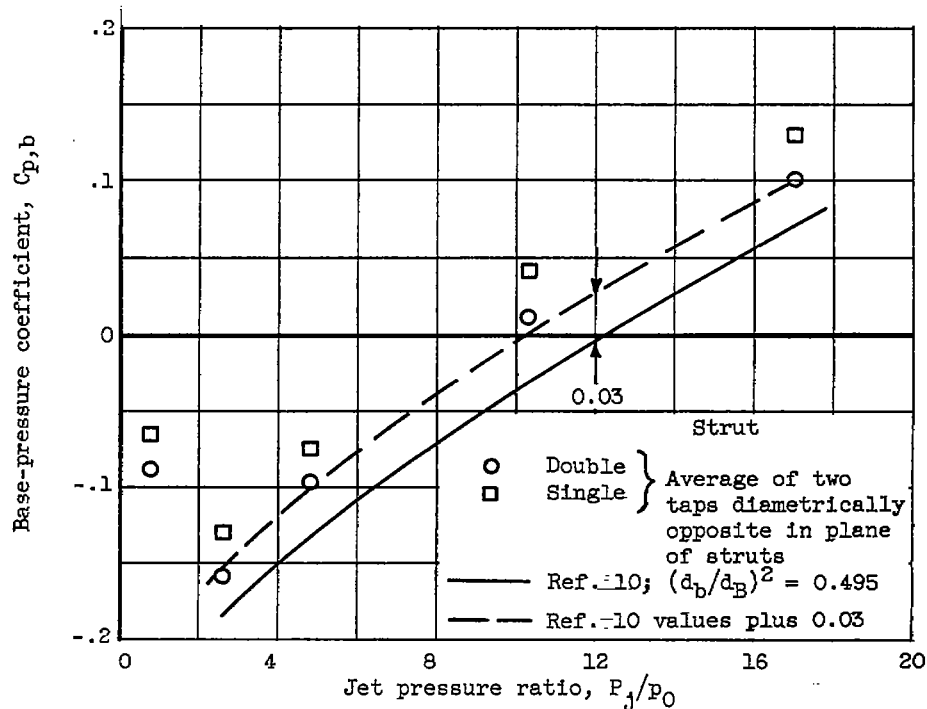


(b) Free-stream Mach number, 3.12, 1- by 1-foot supersonic tunnel.

Figure 5. - Concluded. Tunnel installation.

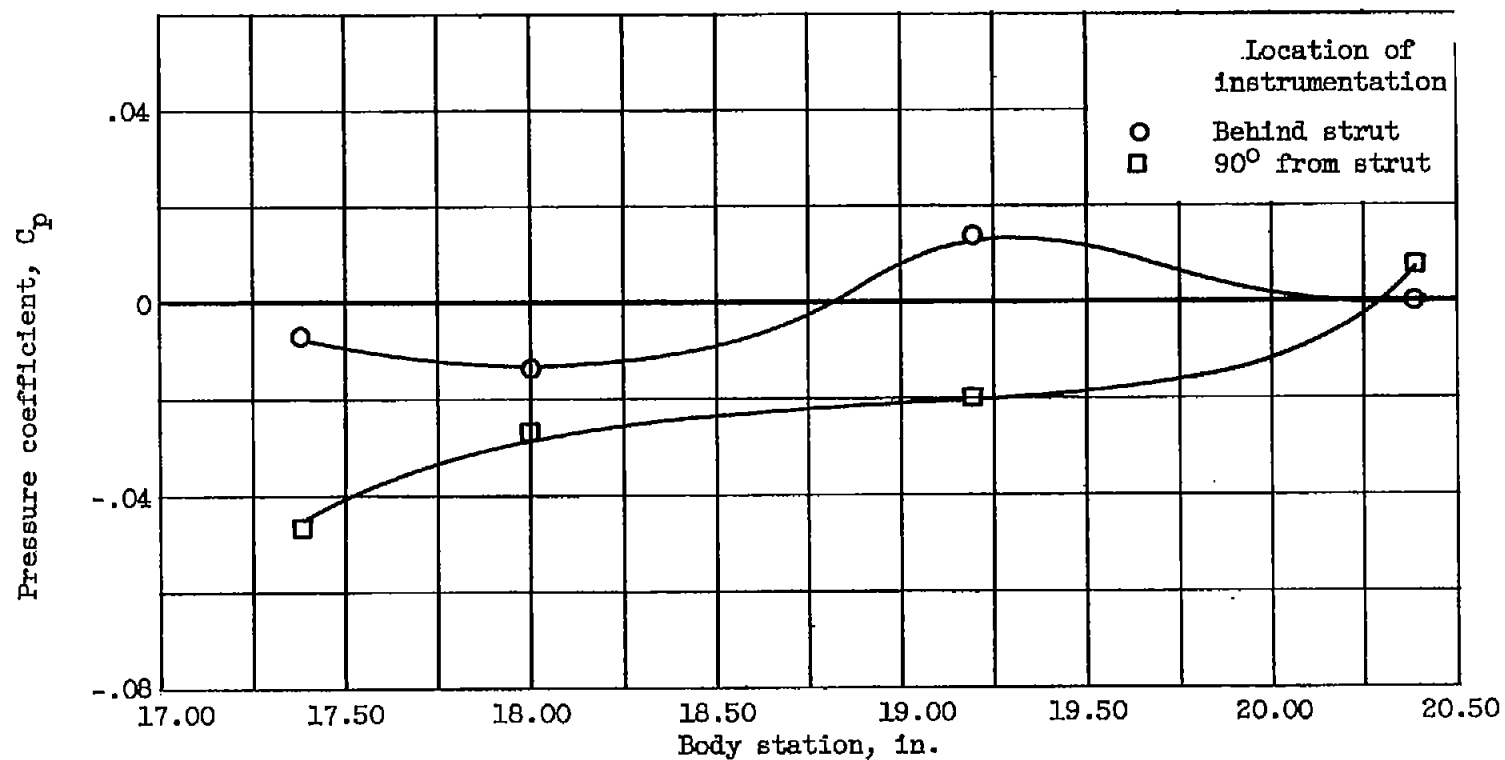


(a) Boattail pressure.



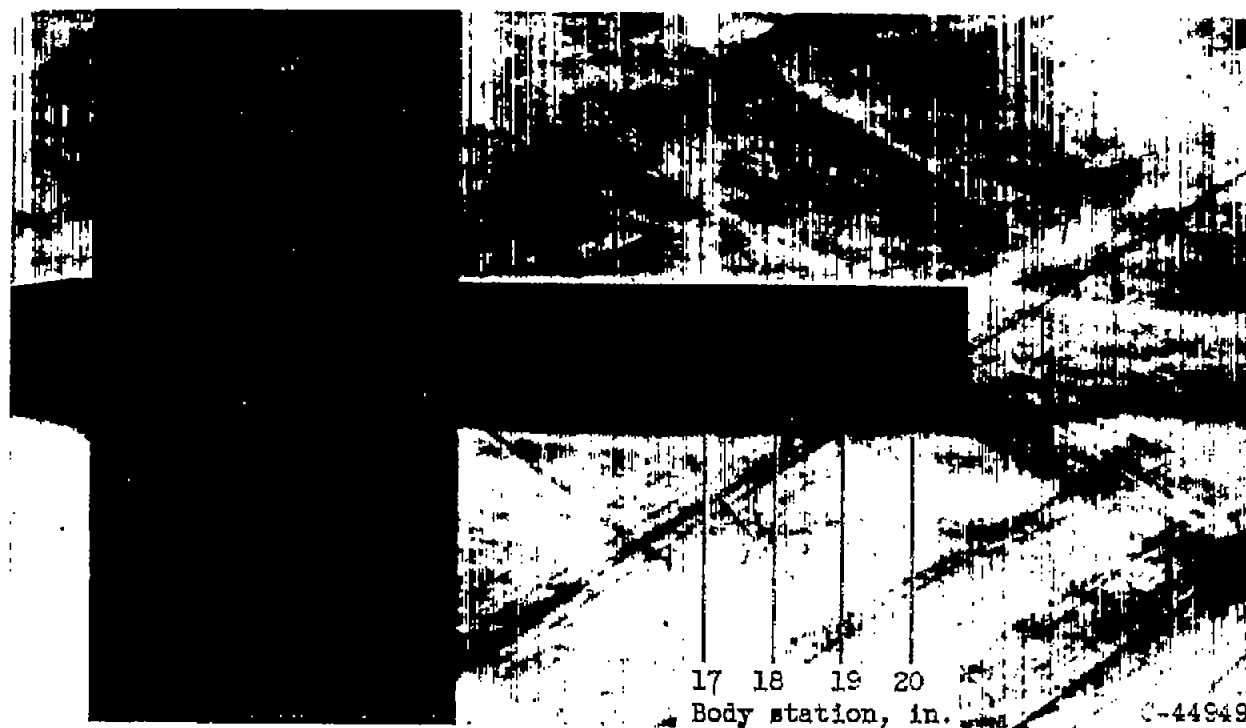
(b) Base pressure; ratio of base area to body area, 0.276.

Figure 6. - Effect of struts on boattail and base pressures. Boattail angle,  $5.63^\circ$ ; free-stream Mach number, 1.91.



(a) Body pressure.

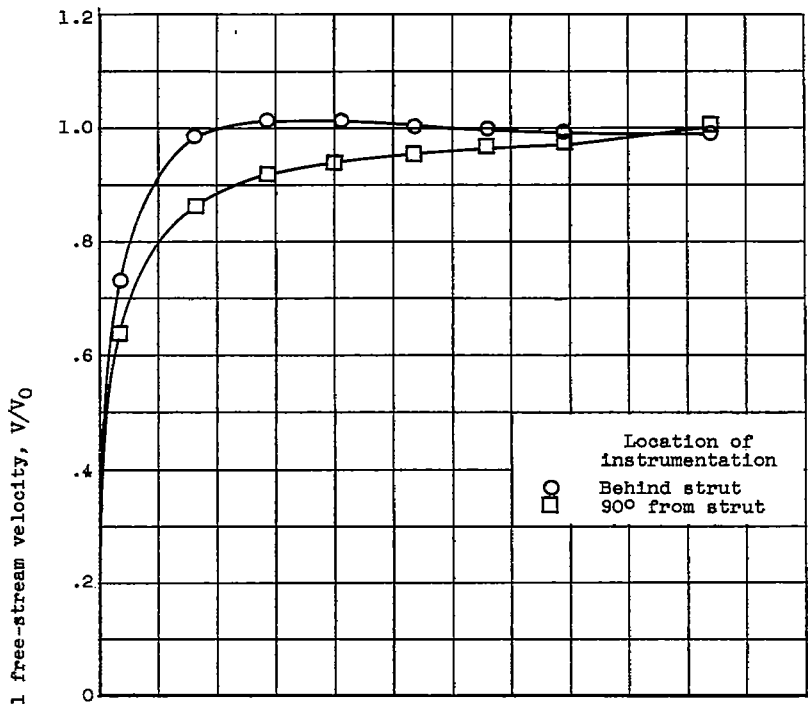
Figure 7. - Effect of struts on body pressure. Cylindrical afterbody; free-stream Mach number, 1.91; no jet flow.



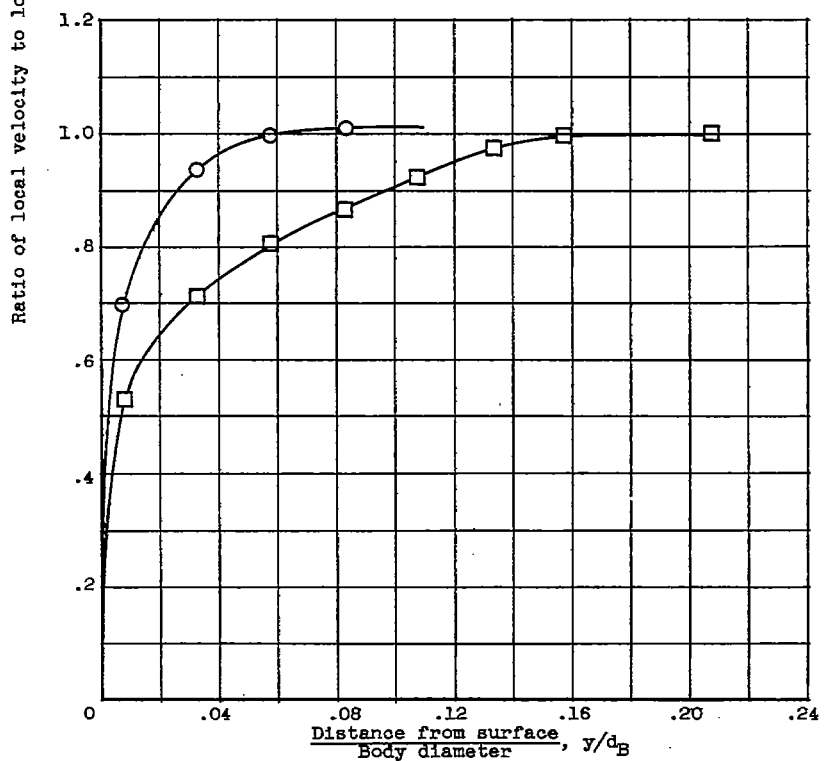
(b) Schlieren photograph.

Figure 7. - Concluded. Effect of struts on body pressure. Cylindrical afterbody; free-stream Mach number, 1.91; no jet flow.

CW-7  
3808



(a) Free-stream Mach number, 1.91.



(b) Free-stream Mach number, 3.12.

Figure 8. - Boundary-layer velocity profiles at end of cylindrical afterbody. No jet flow.



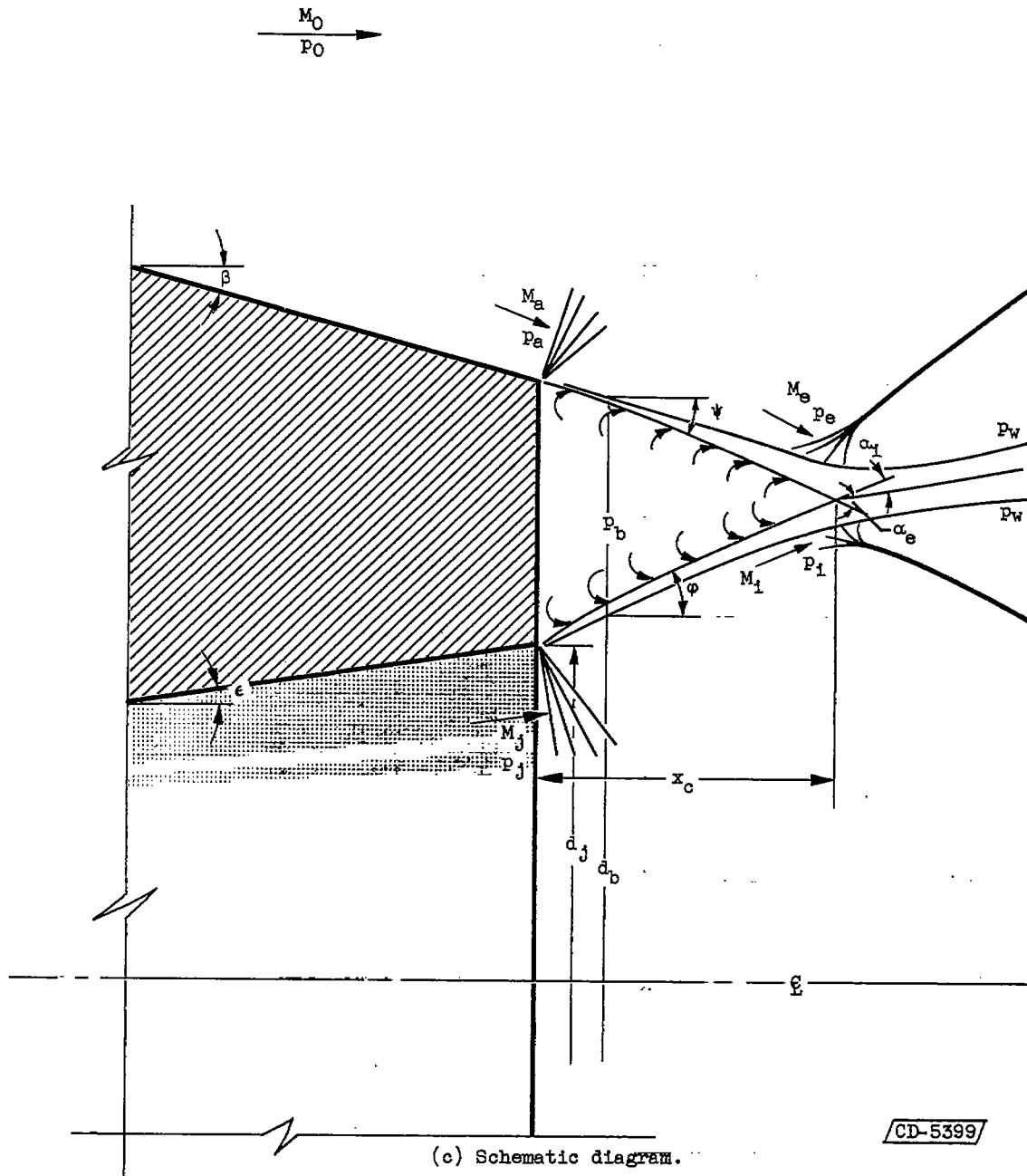
(a) Schlieren photograph. Convergent nozzle; jet pressure ratio, 16.5; boat-tail angle,  $3.0^\circ$ ; free-stream Mach number, 1.91.

Figure 9. - Flow geometry.



(b) Schlieren photograph. Convergent nozzle; jet pressure ratio, 16.0; cylindrical afterbody; free-stream Mach number, 3.12.

Figure 9. - Continued. Flow geometry.



(c) Schematic diagram.

Figure 9. - Concluded. Flow geometry.

3808

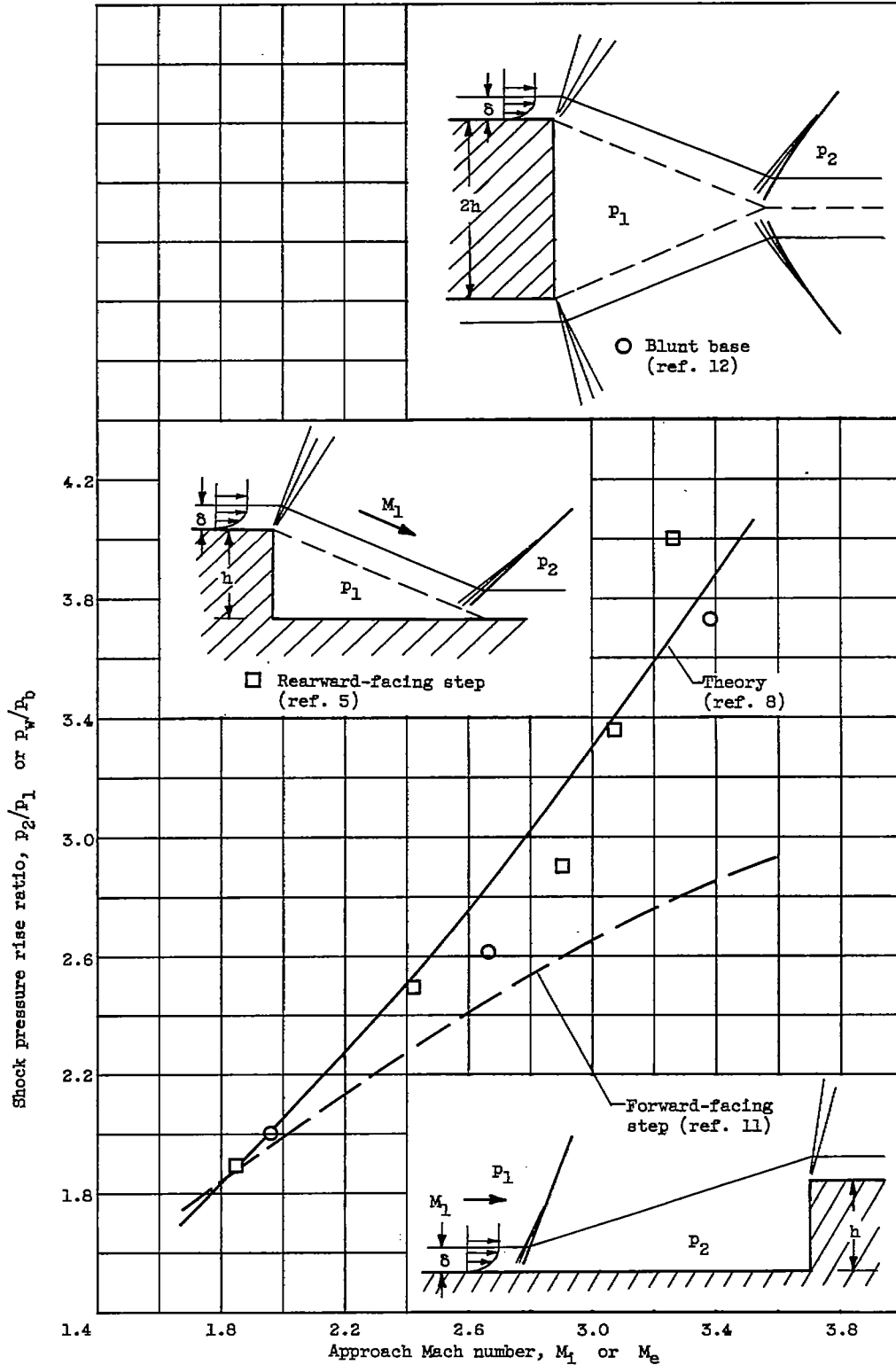


Figure 10. - Summary of pressure rise data. Turbulent mixing;  $h/\delta > \approx 4$ .

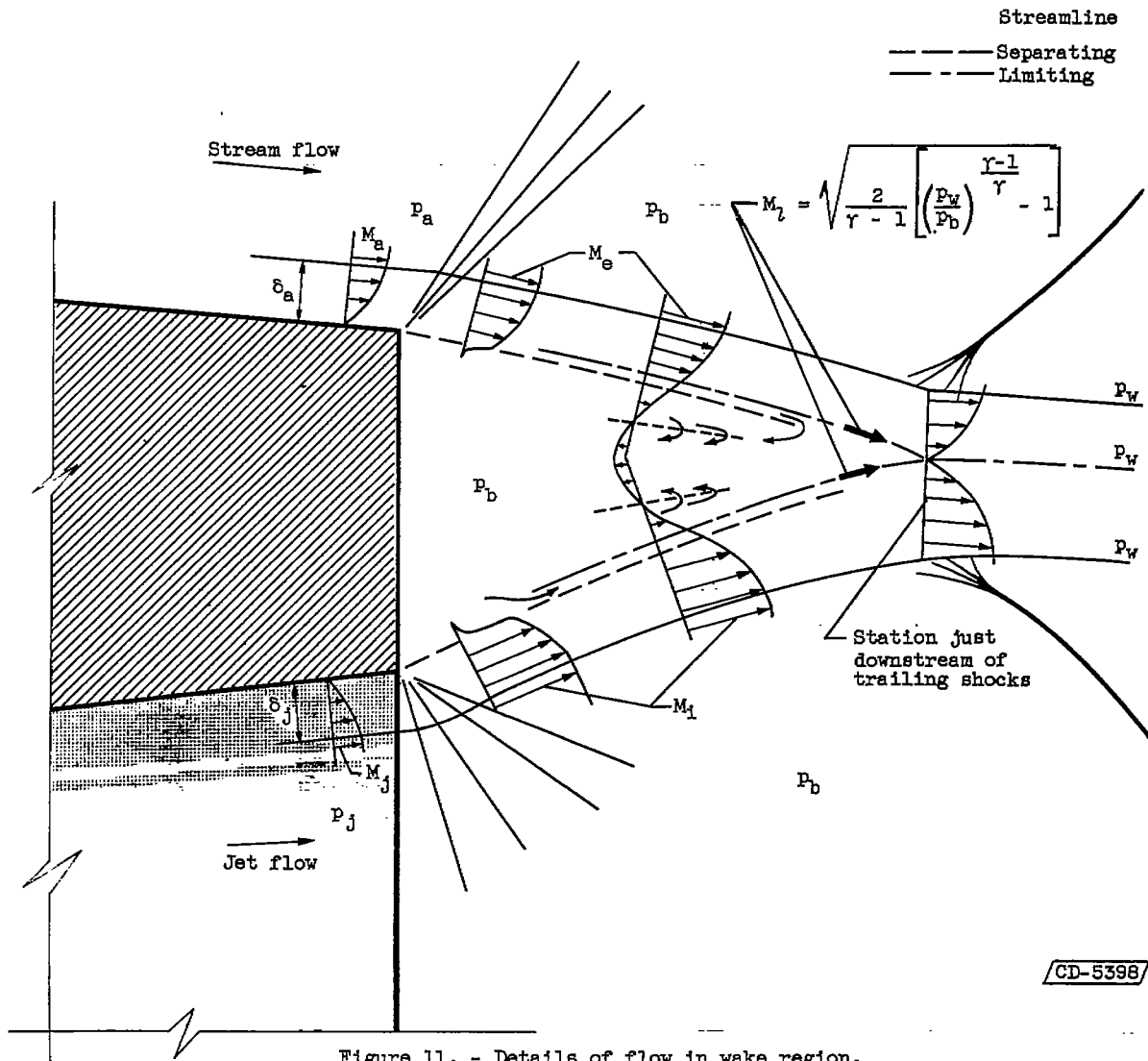


Figure 11. - Details of flow in wake region.

3808

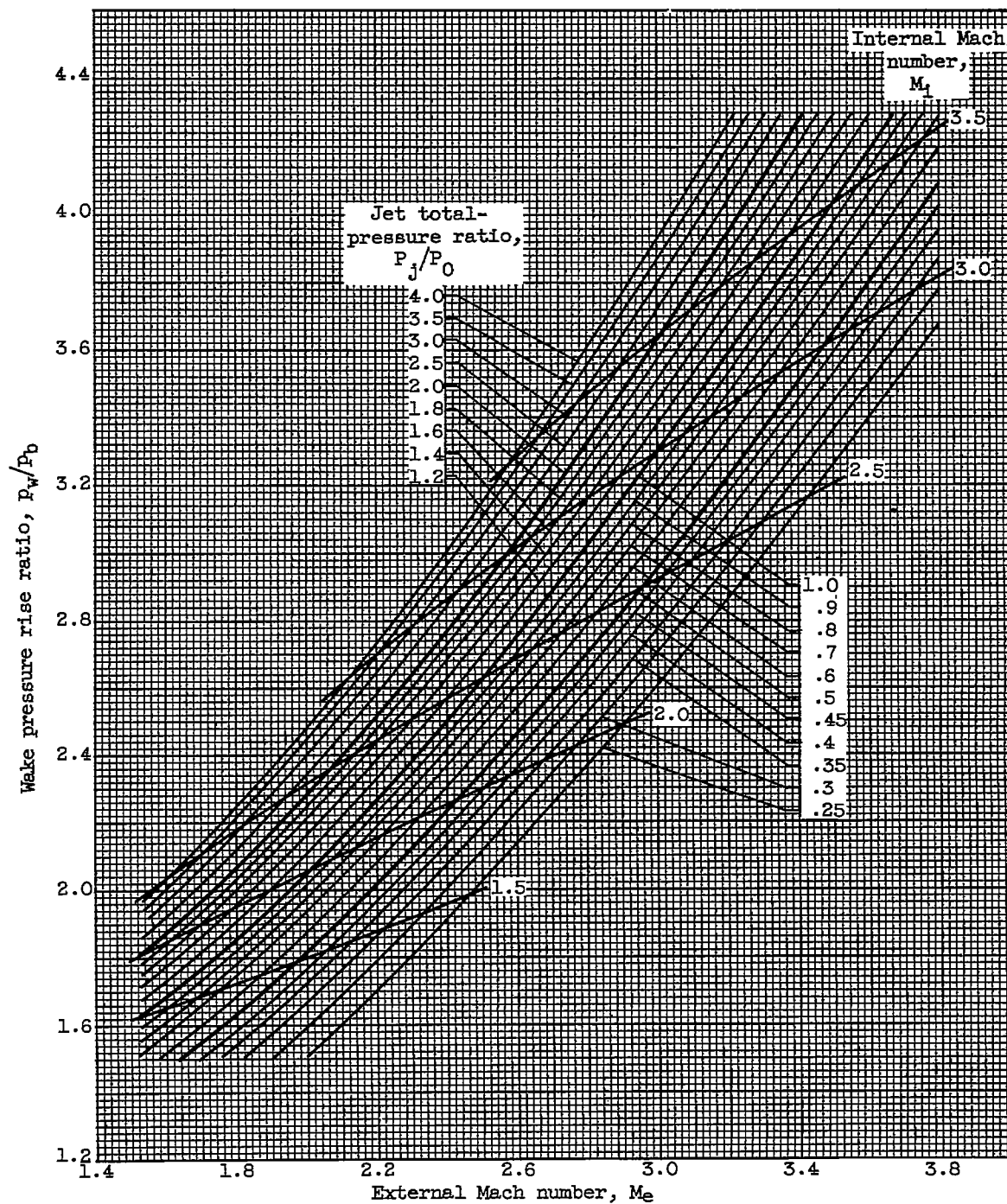


Figure 12. - Theoretical wake pressure rise ratio.  $T_e = T_1$ ;  $X_e = X_1$ ; two-dimensional flow.

CONFIDENTIAL

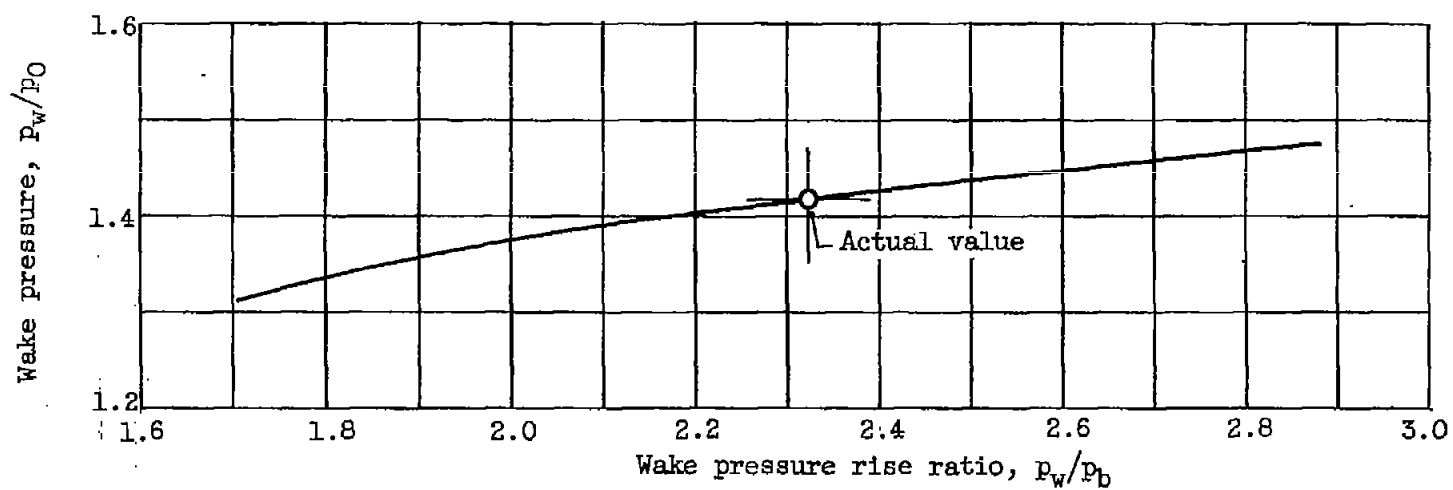


Figure 13. - Change in wake pressure for hypothetical change in wake pressure rise ratio. Base-to-jet diameter ratio, 2.00; boattail angle,  $5.63^\circ$ ; jet Mach number, 1.00; free-stream Mach number, 1.91; jet pressure ratio, 8.0.

3808  
CW-8

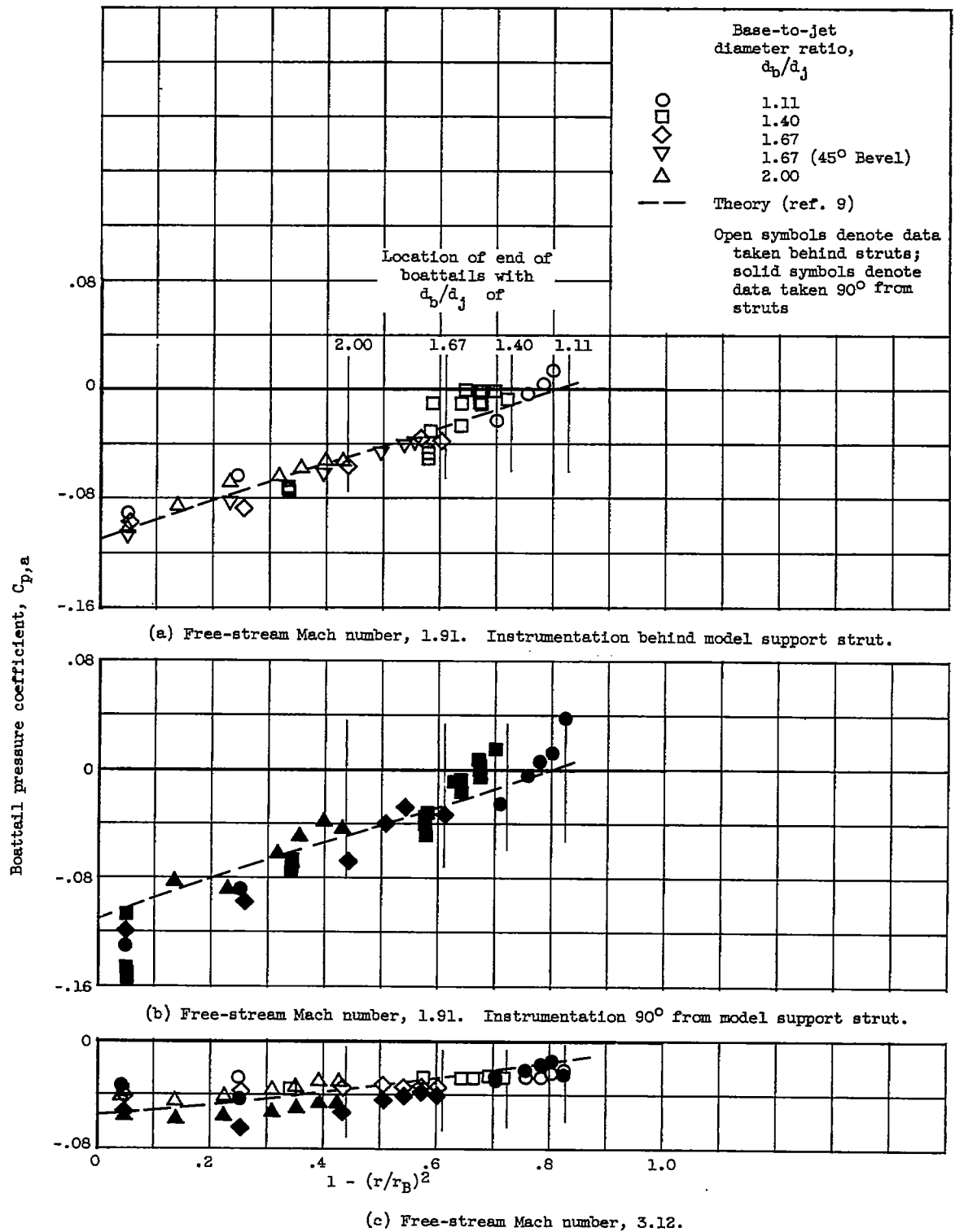
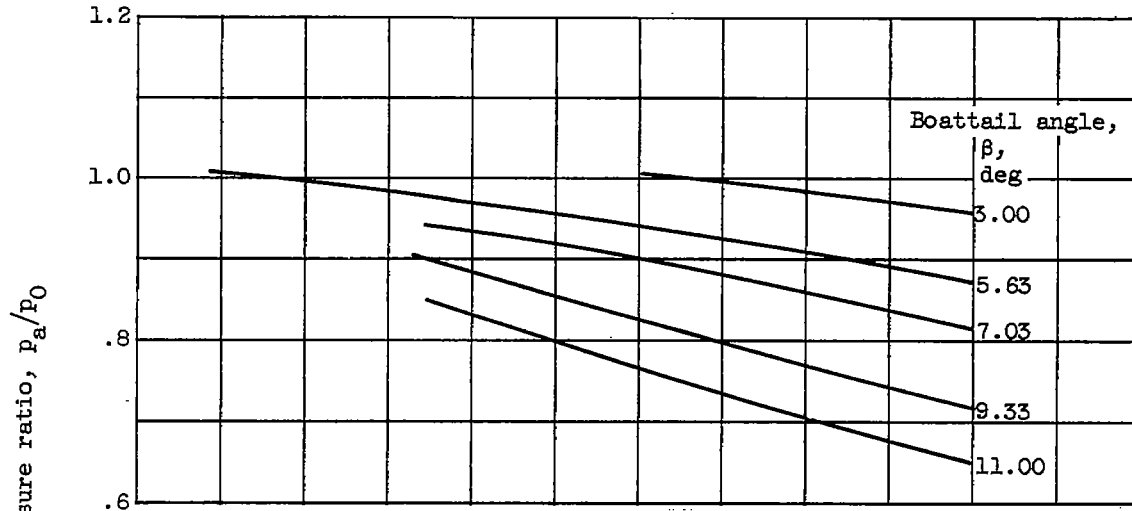
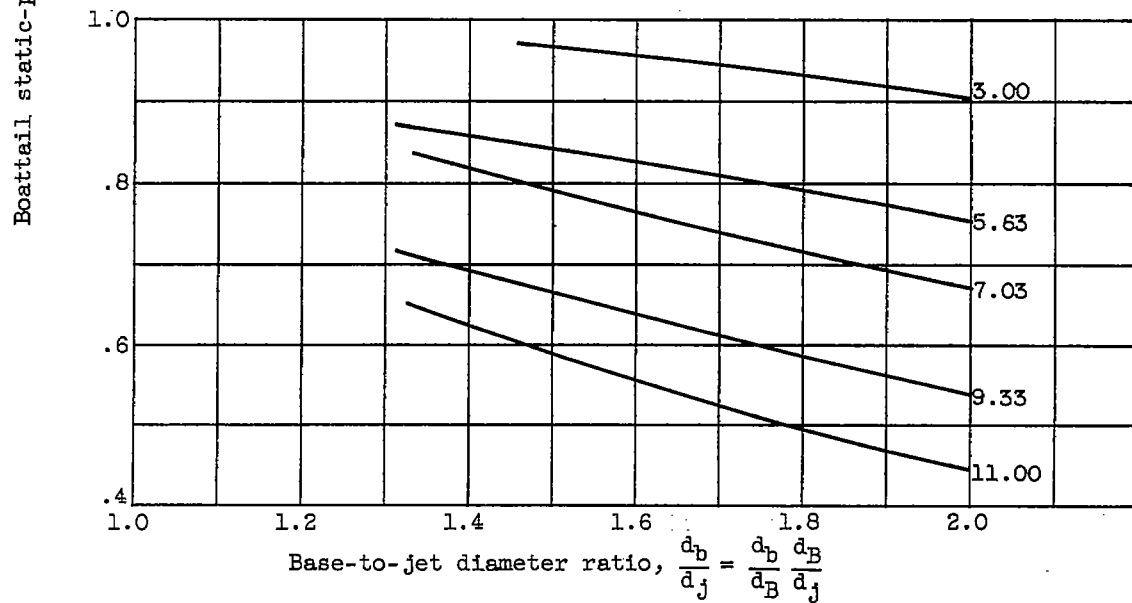


Figure 14. - Pressure distribution on conical boattails. Jet off; boattail angle, 5.63°.

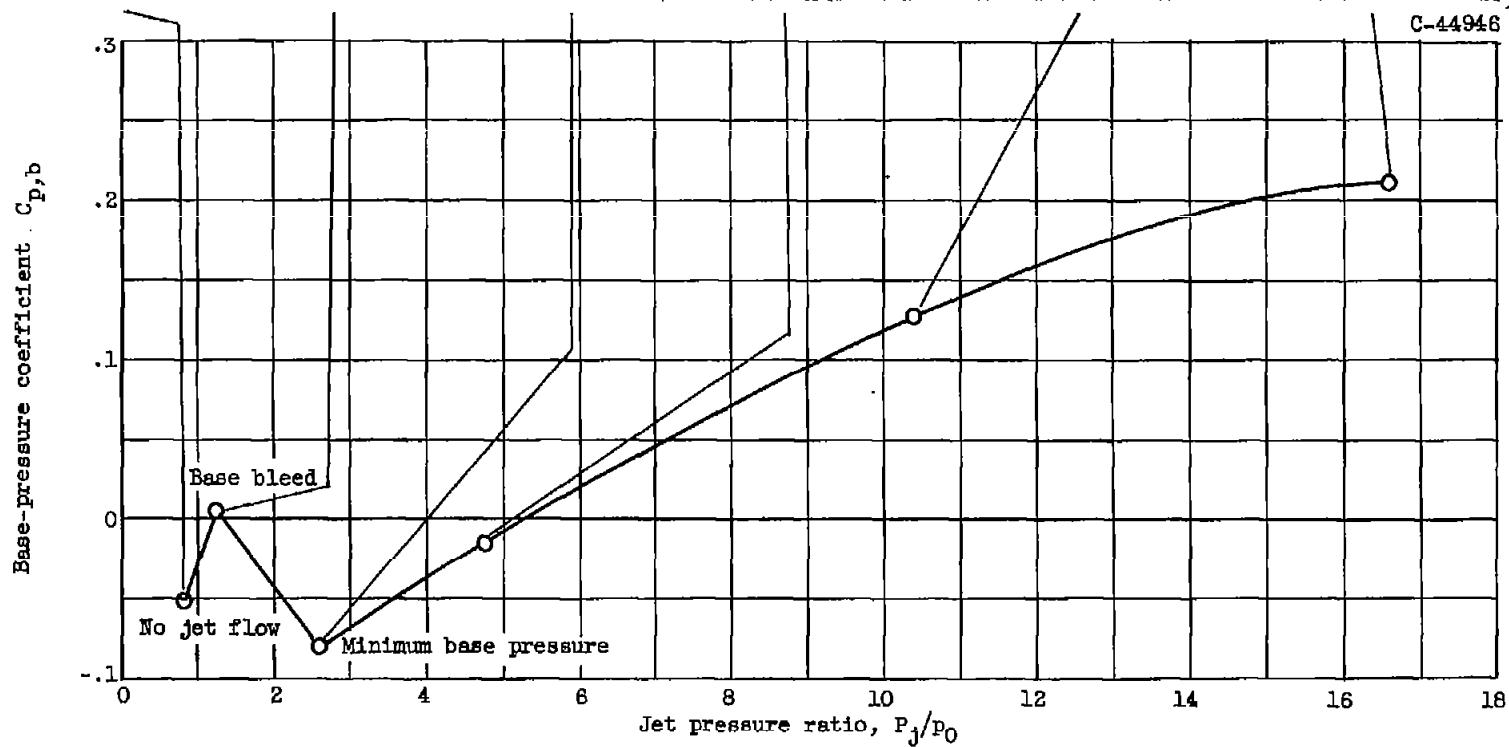


(a) Free-stream Mach number, 1.91.



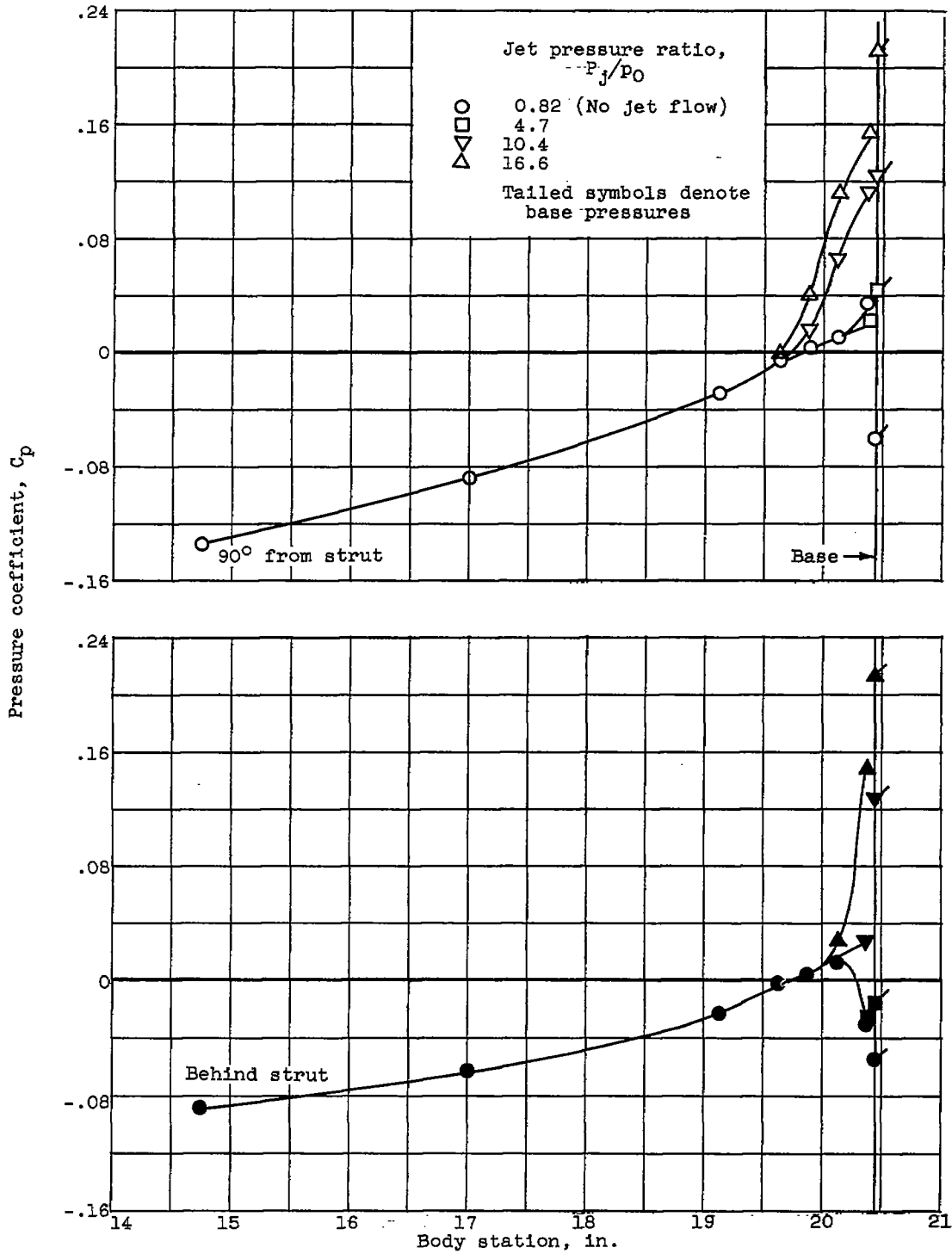
(b) Free-stream Mach number, 3.12.

Figure 15. - Theoretical pressures at end of boattail.



(a) Base pressure.

Figure 16. - Effect of nozzle pressure ratio on afterbody pressures. Base-to-jet diameter ratio, 1.11; boattail angle,  $5.63^\circ$ ; free-stream Mach number, 1.91; convergent nozzle.



(b) Boattail pressure.

Figure 16. - Effect of nozzle pressure ratio on afterbody pressures. Base-to-jet diameter ratio, 1.11; boattail angle, 5.63°; free-stream Mach number, 1.91; convergent nozzle.

3808

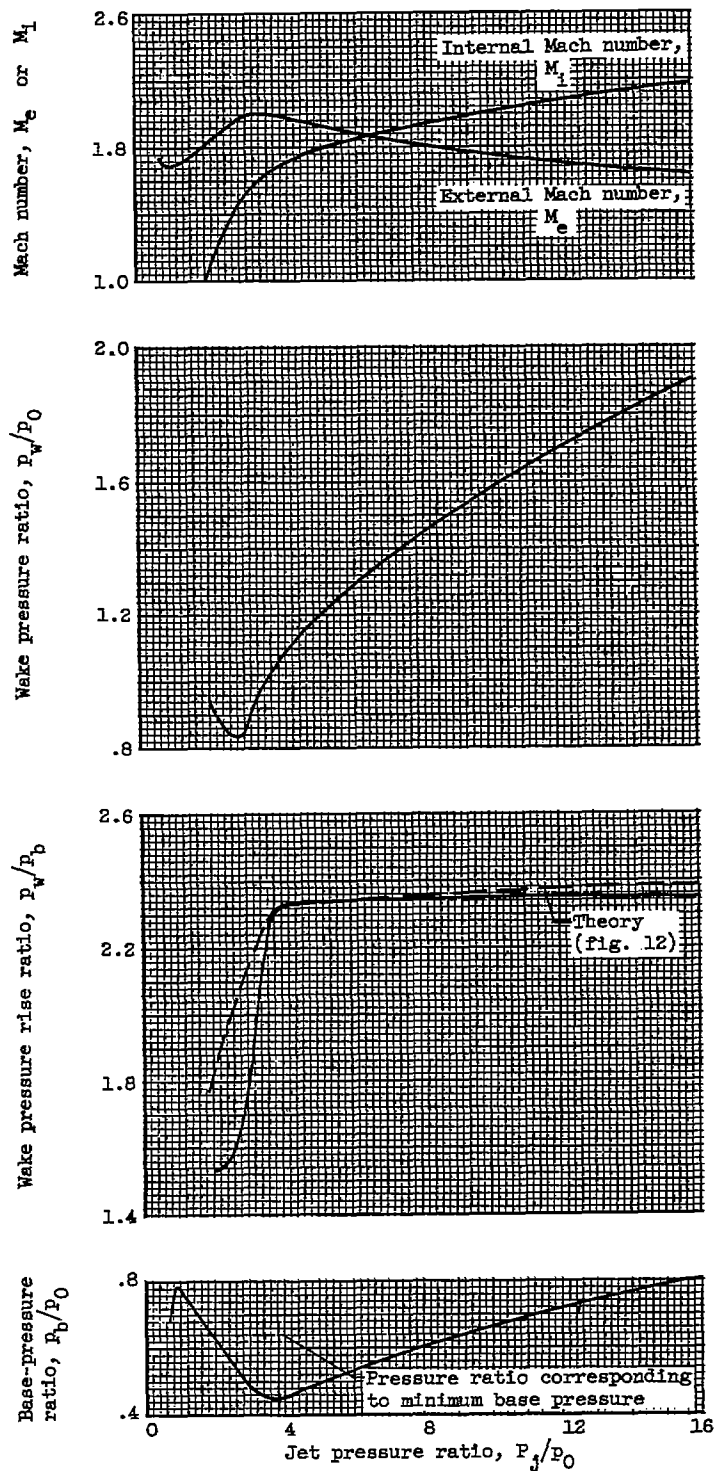
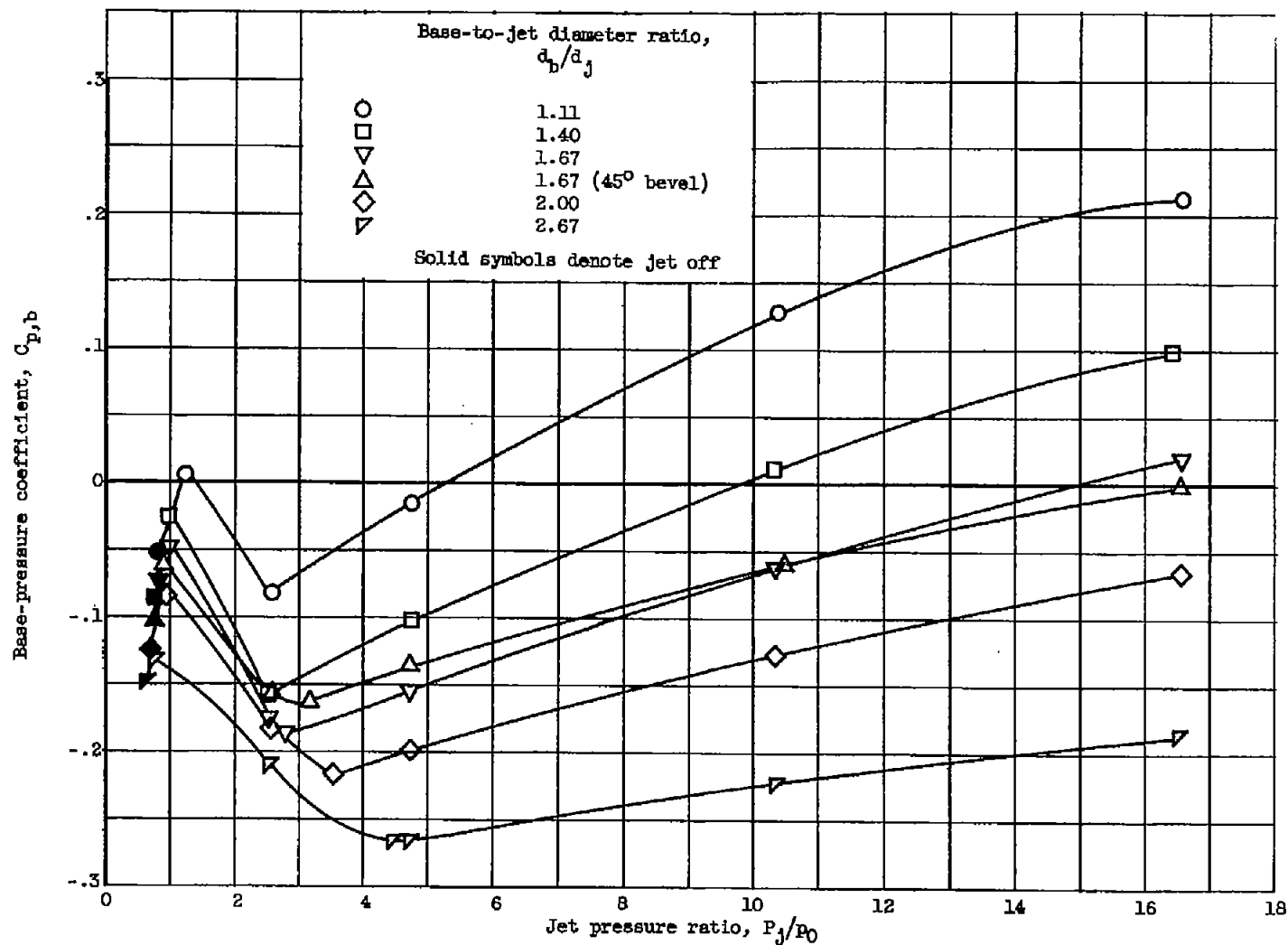
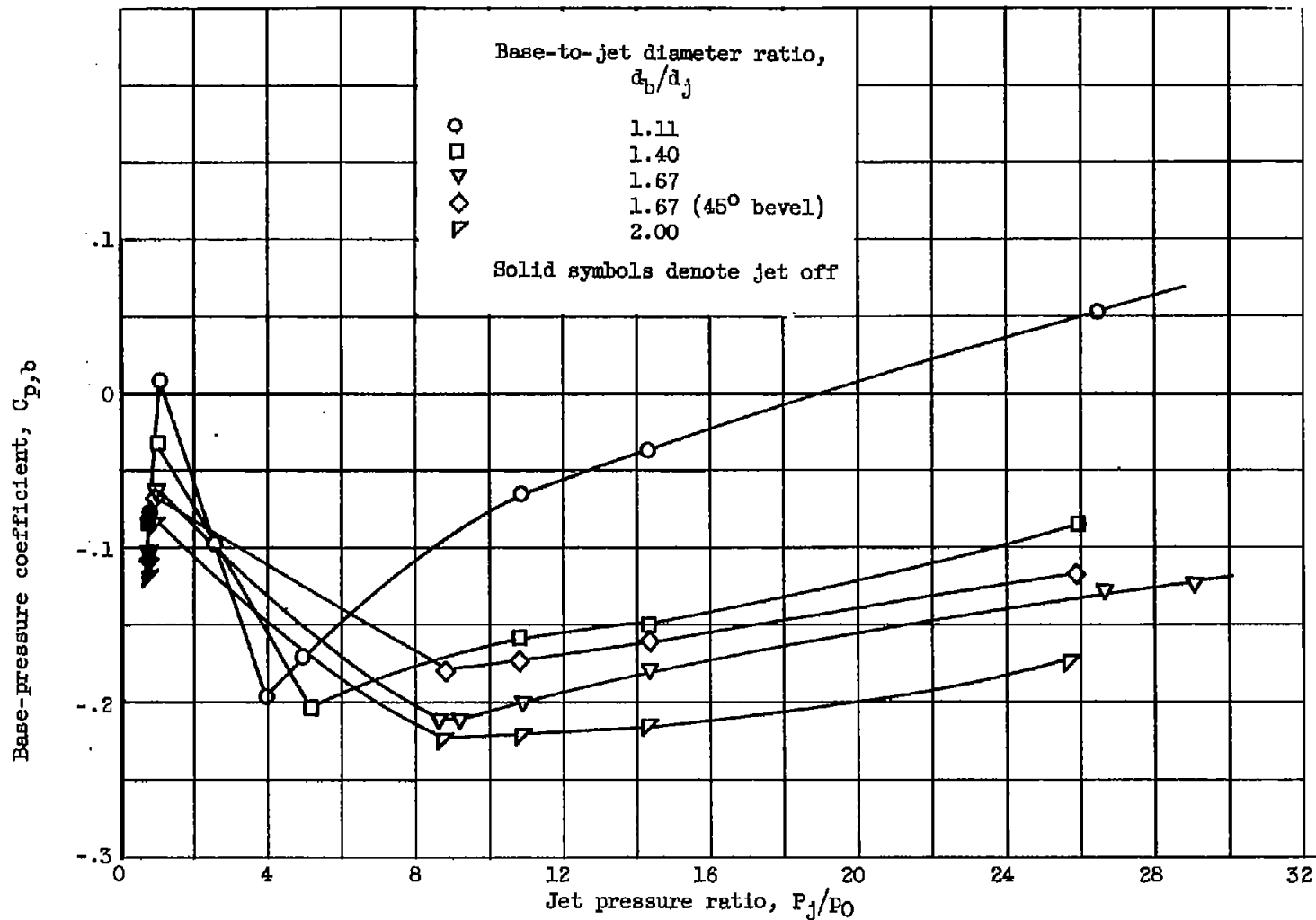


Figure 17. - Variation of base-pressure components with jet pressure ratio. Base-to-jet diameter ratio, 2.00; boattail angle,  $5.63^\circ$ ; jet Mach number, 1.00; free-stream Mach number, 1.91.



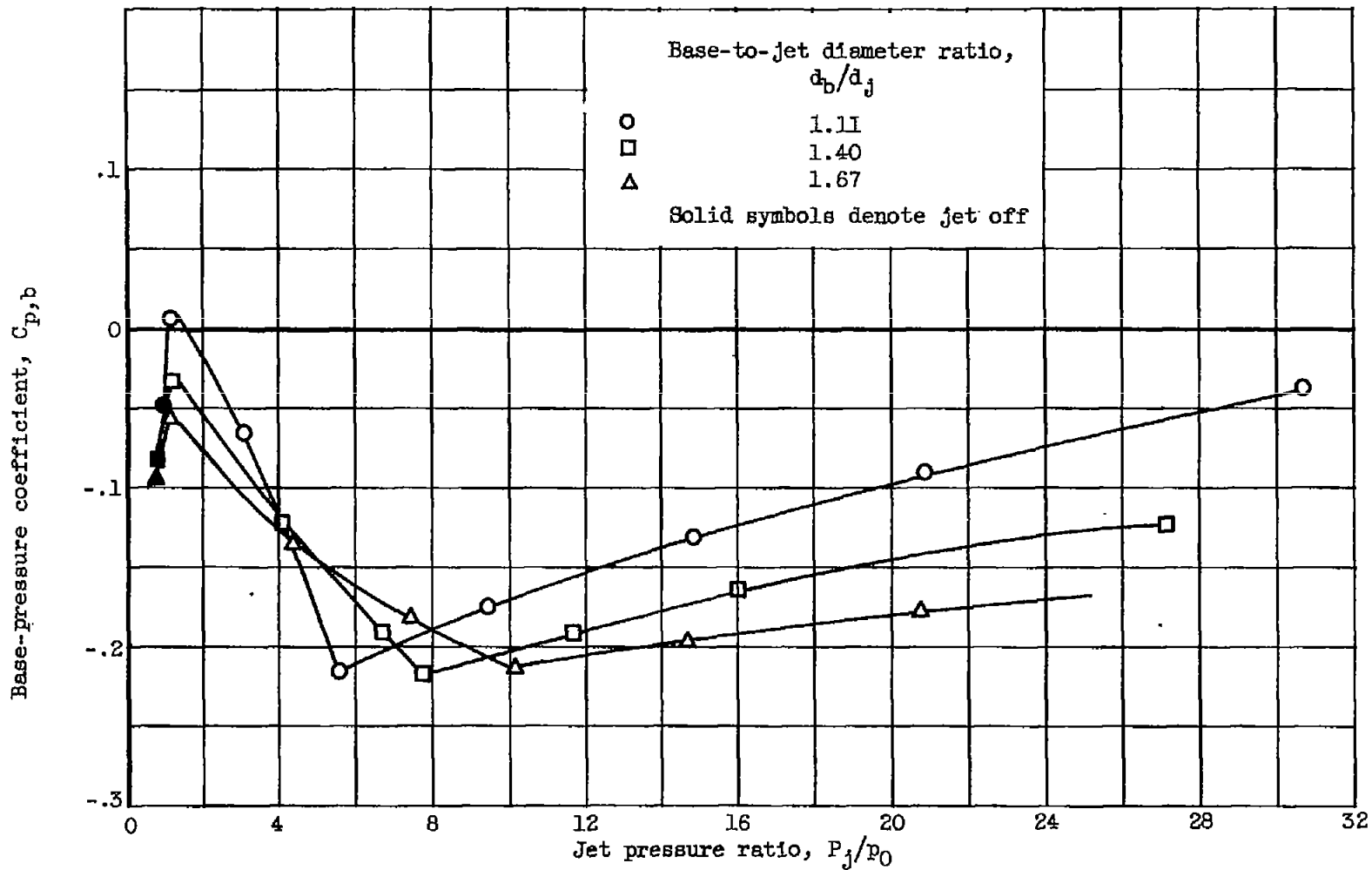
(a) Convergent nozzle; jet Mach number, 1.00.

Figure 18. - Effect of base-to-jet diameter ratio on base pressure at free-stream Mach number of 1.91. Boattail angle,  $5.63^\circ$ ; nozzle angle,  $0^\circ$ .



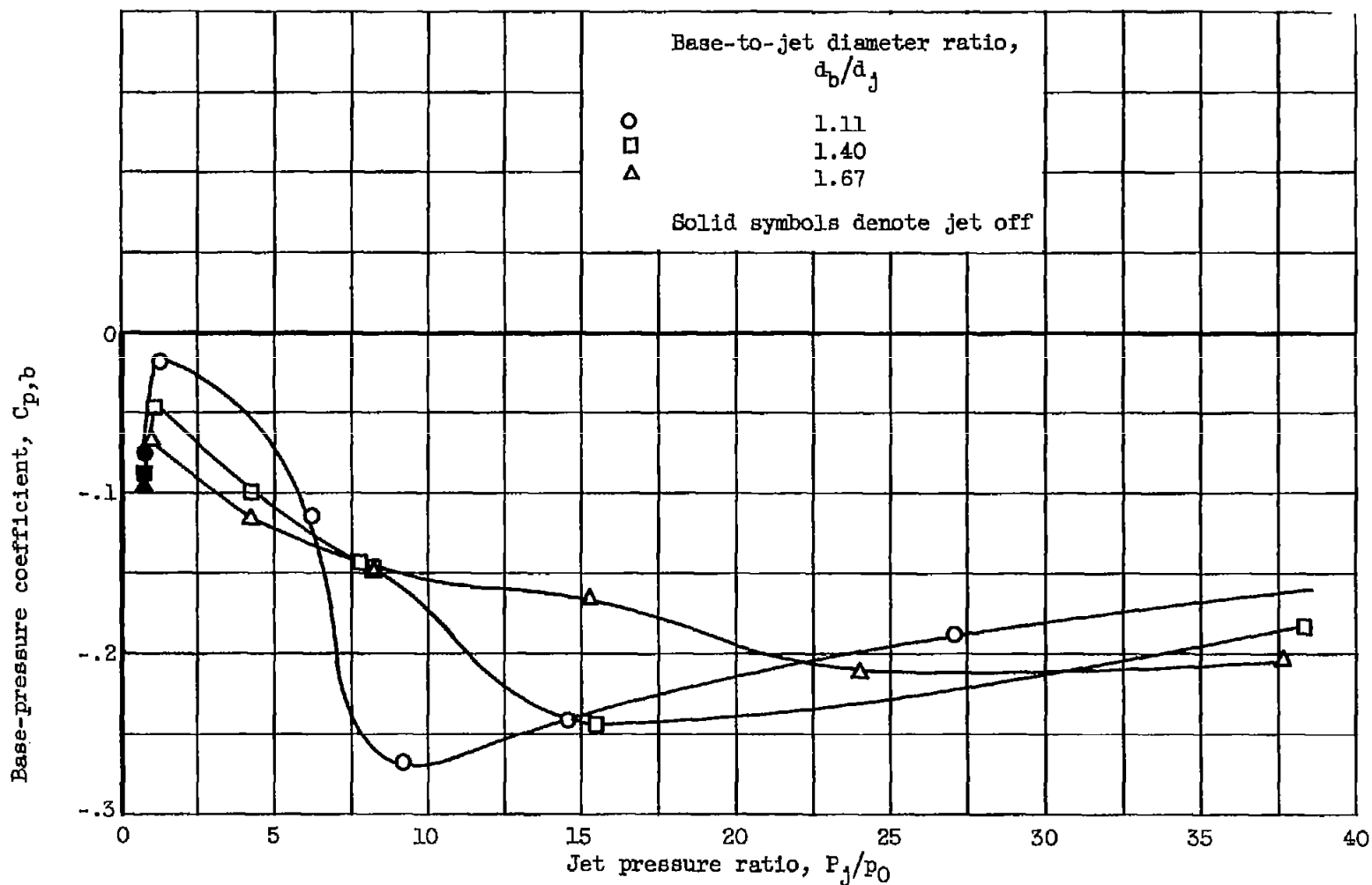
(b) Jet Mach number, 2.19.

Figure 18. - Continued. Effect of base-to-jet diameter ratio on base pressure at free-stream Mach number of 1.91. Boattail angle,  $5.63^\circ$ ; nozzle angle,  $0^\circ$ .



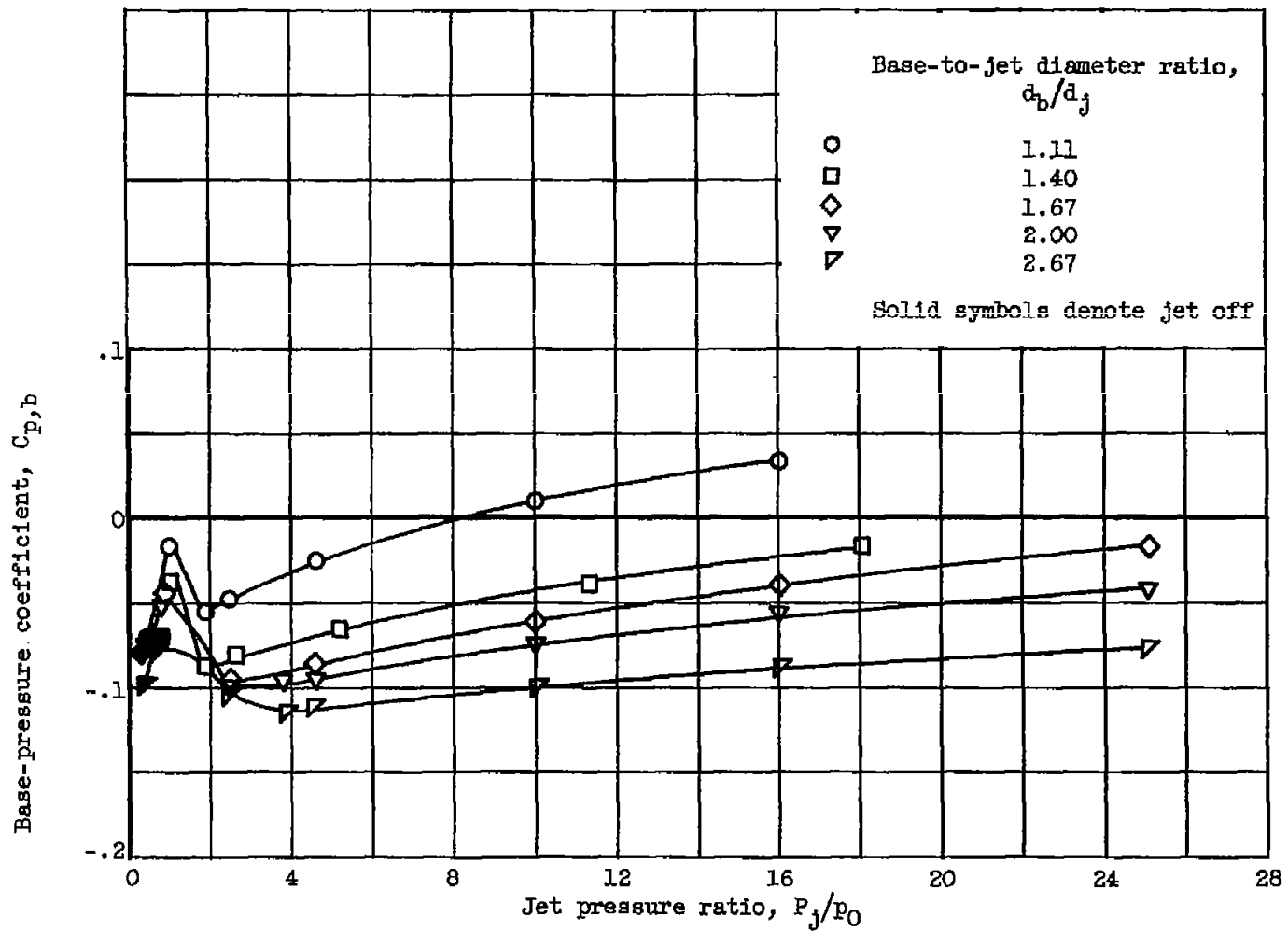
(c) Jet Mach number, 2.60.

Figure 18. - Continued. Effect of base-to-jet diameter ratio on base pressure at free-stream Mach number of 1.91. Boattail angle,  $5.63^\circ$ ; nozzle angle,  $0^\circ$ .



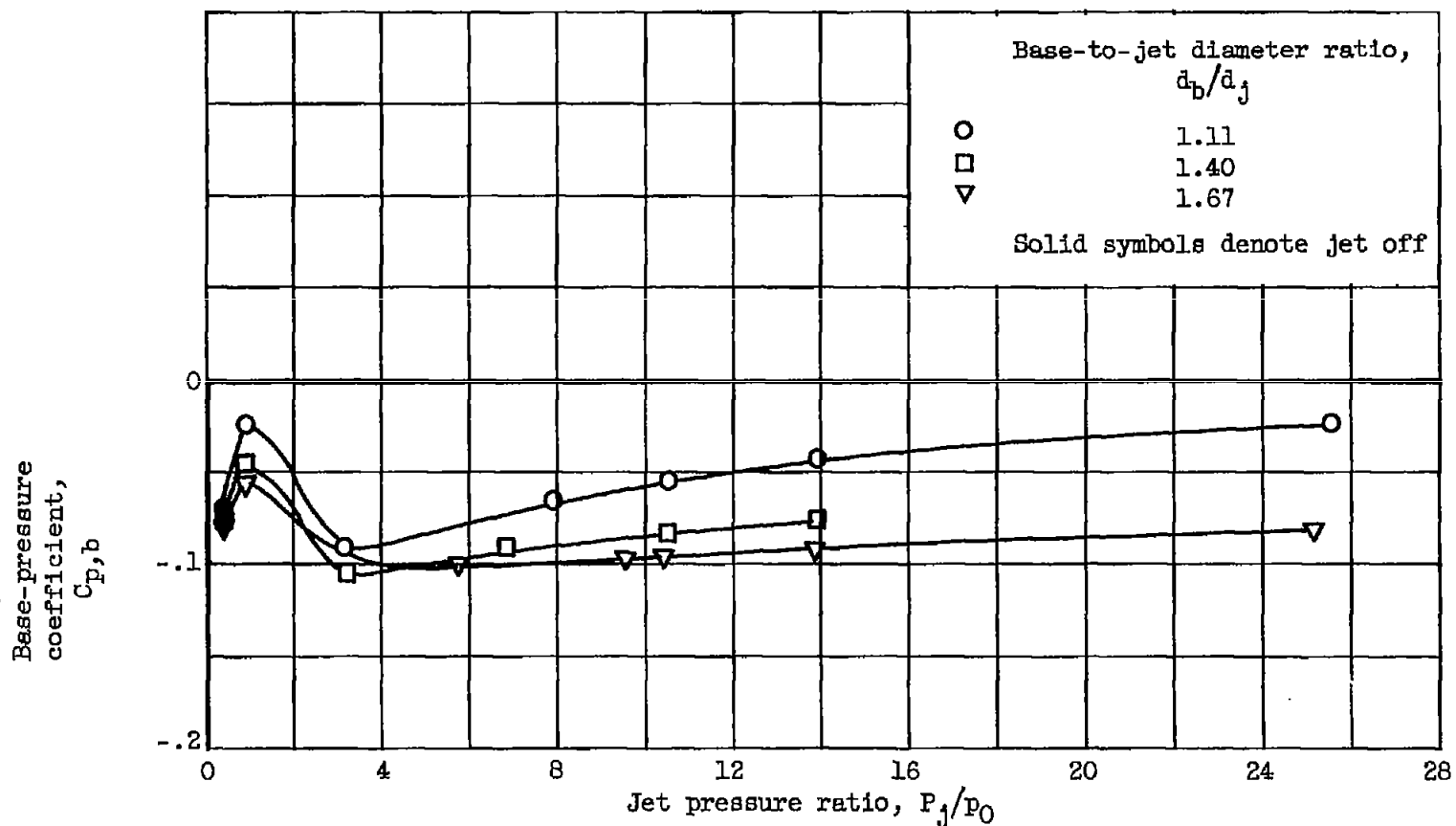
(d) Jet Mach number, 3.21.

Figure 18. - Concluded. Effect of base-to-jet diameter ratio on base pressure at free-stream Mach number of 1.91. Boattail angle,  $5.63^\circ$ ; nozzle angle,  $0^\circ$ .



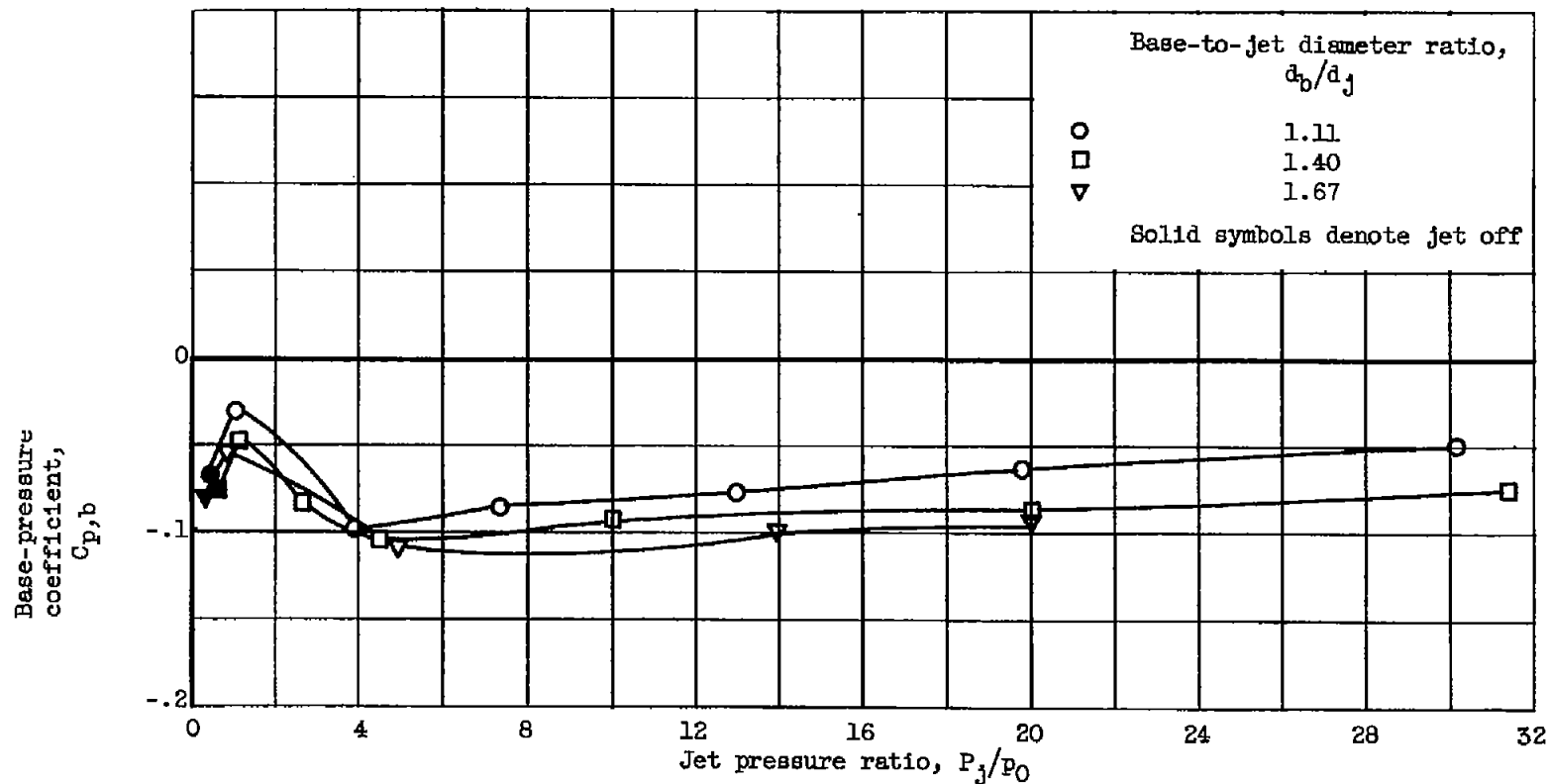
(a) Convergent nozzle; jet Mach number, 1.00.

Figure 19. - Effect of base-to-jet diameter ratio on base-pressure coefficient at free-stream Mach number of 3.12. Boattail angle,  $5.63^\circ$ ; nozzle angle,  $0^\circ$ .



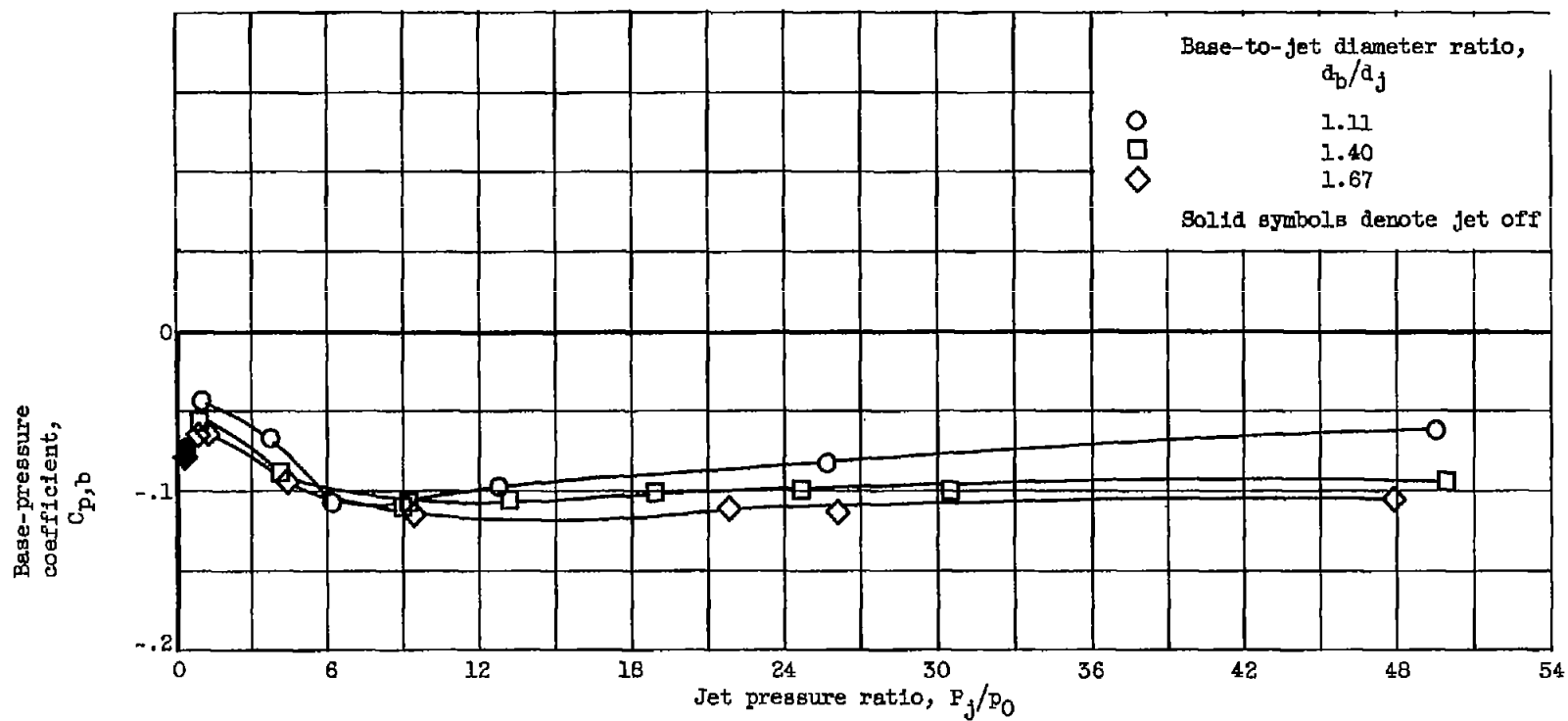
(b) Jet Mach number, 2.19.

Figure 19. - Continued. Effect of base-to-jet diameter ratio on base-pressure coefficient at free-stream Mach number of 3.12. Boattail angle,  $5.63^\circ$ ; nozzle angle,  $0^\circ$ .



(c) Jet Mach number, 2.60.

Figure 19. - Continued. Effect of base-to-jet diameter ratio on base-pressure coefficient at free-stream Mach number of 3.12. Boattail angle,  $5.63^\circ$ ; nozzle angle,  $0^\circ$ .



(d) Jet Mach number, 3.21.

Figure 19. - Concluded. Effect of base-to-jet diameter ratio on base-pressure coefficient at free-stream Mach number of 3.12. Boattail angle,  $5.63^\circ$ ; nozzle angle,  $0^\circ$ .

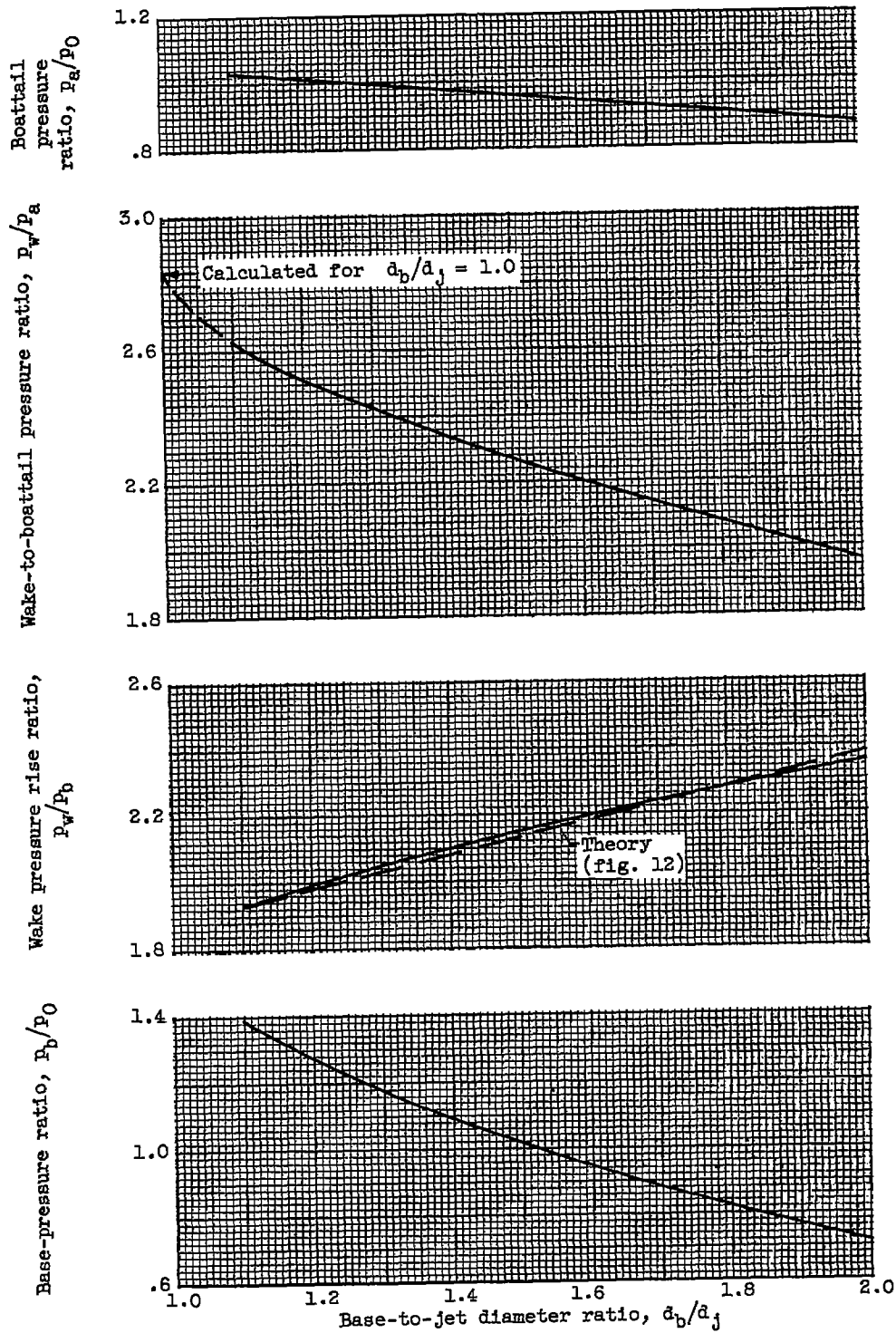


Figure 20. - Variation of base-pressure components with base-to-jet diameter ratio. Boattail angle,  $5.63^\circ$ ; jet Mach number, 1.00; free-stream Mach number, 1.91; jet pressure ratio, 12.

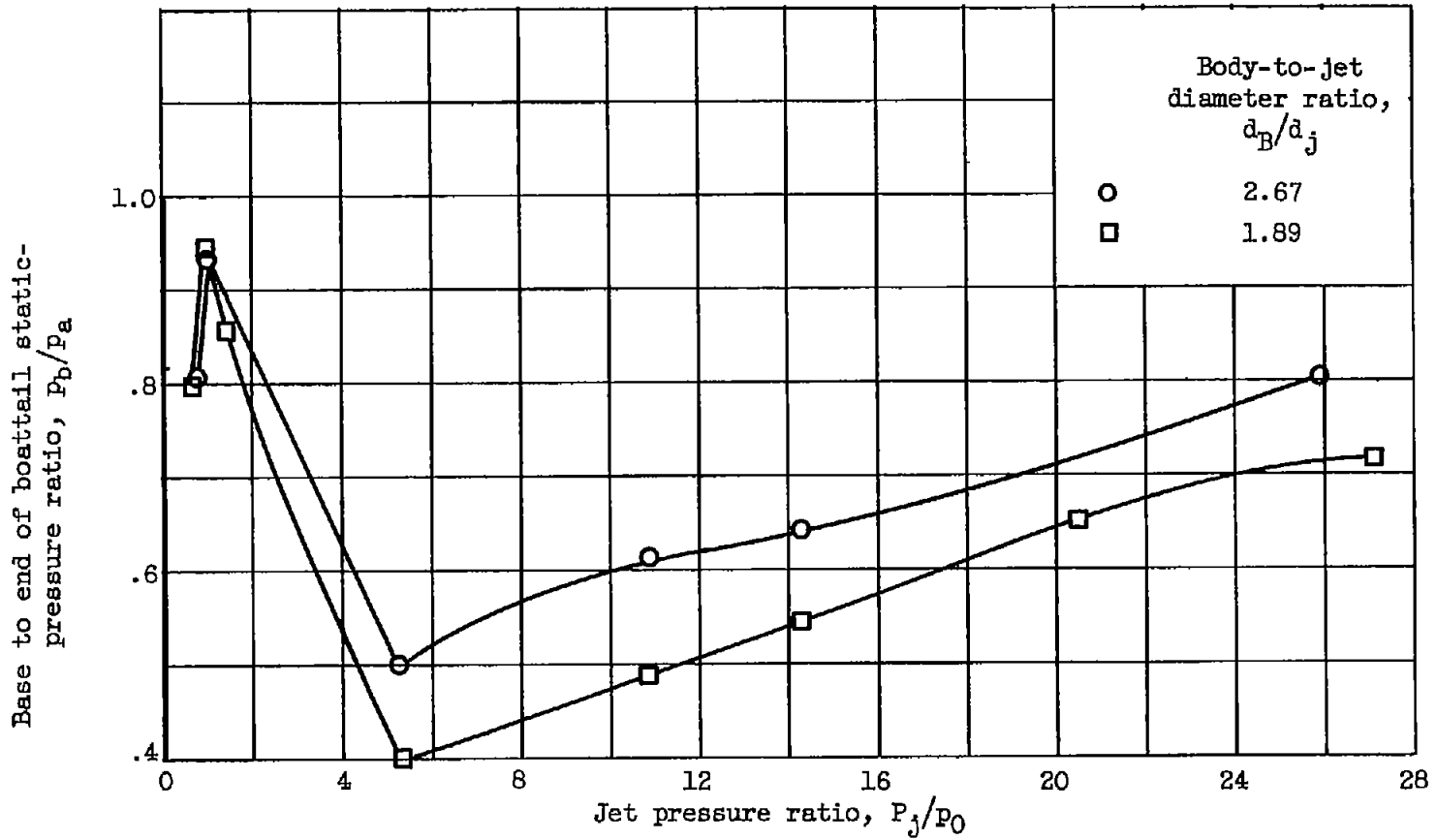


Figure 21. - Effect of body-to-jet diameter ratio on base pressure. Boattail angle,  $5.63^\circ$ ; base-to-jet diameter ratio, 1.40; jet Mach number, 2.19; free-stream Mach number, 1.91.

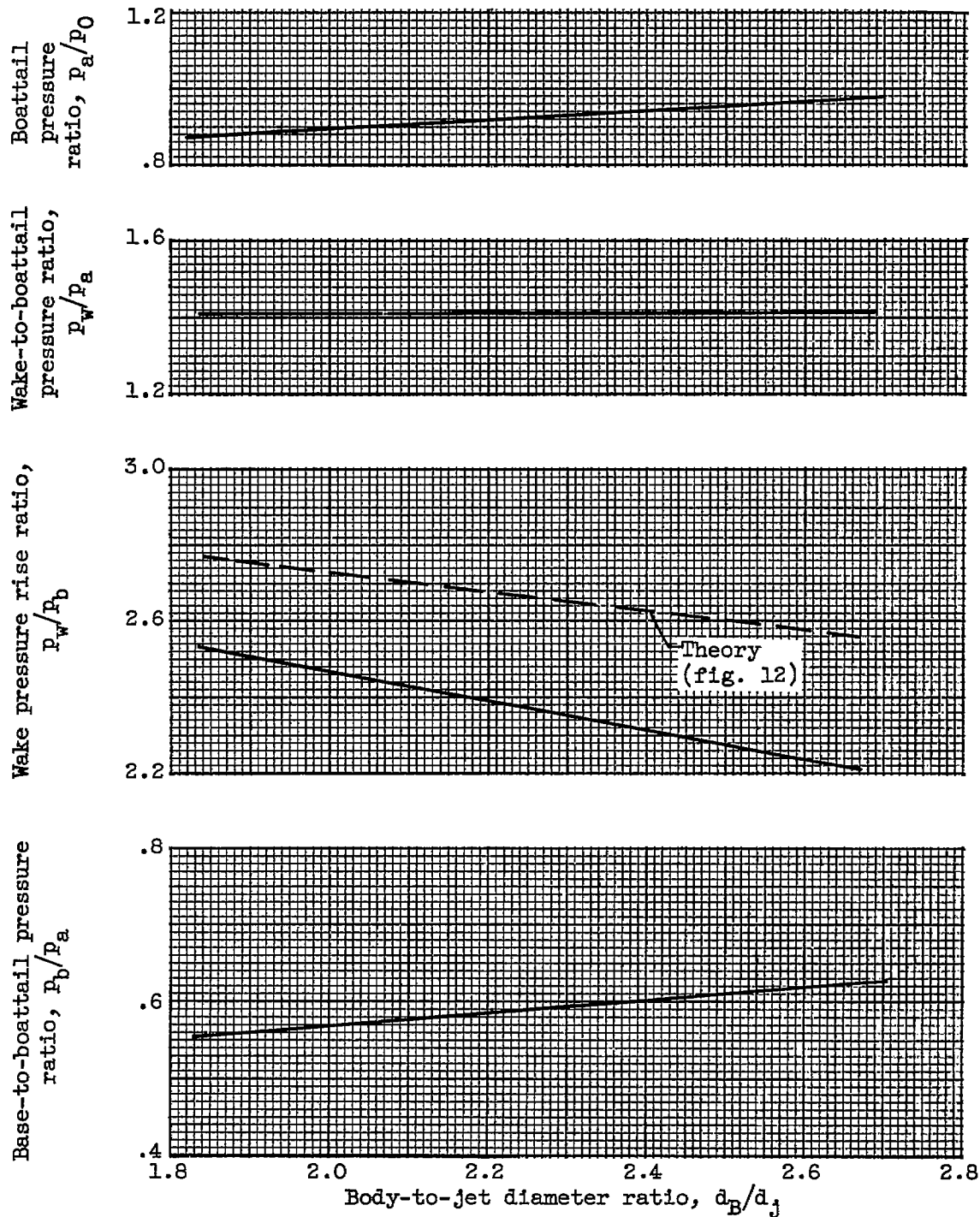
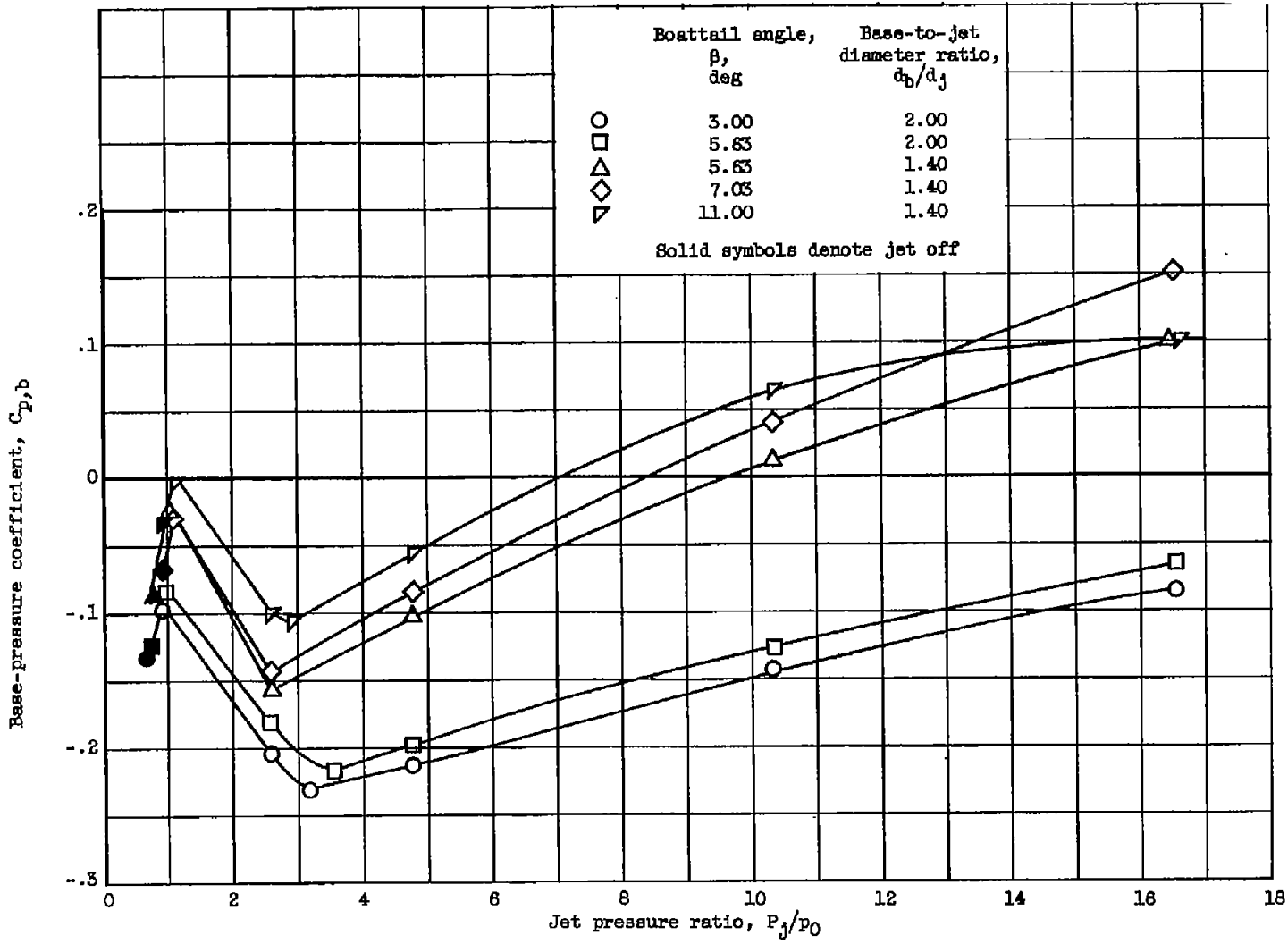
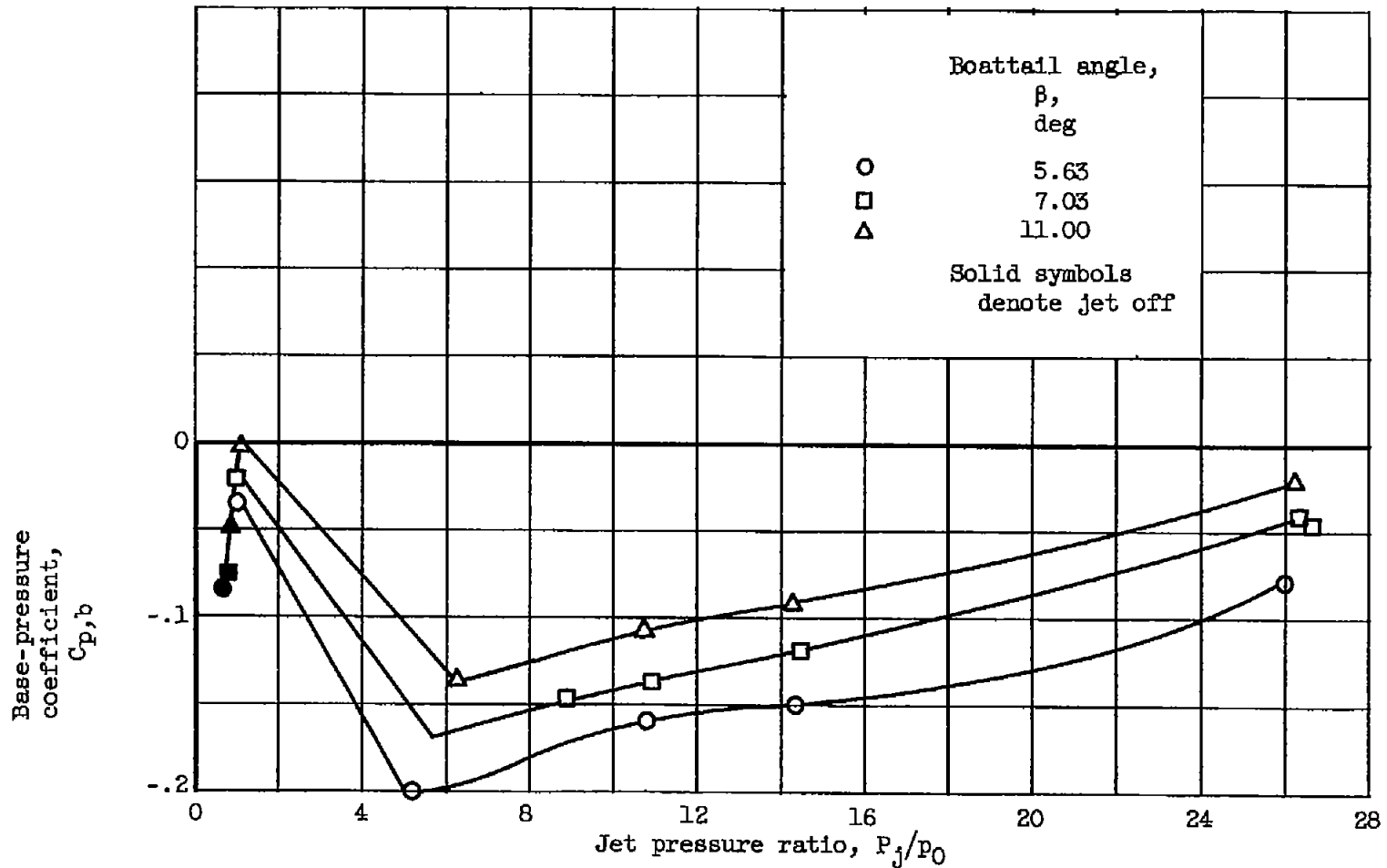


Figure 22. - Variation of base-pressure components with body-to-jet diameter ratio. Base-to-jet diameter ratio, 1.40; boattail angle,  $5.63^\circ$ ; nozzle angle,  $0^\circ$ ; jet Mach number, 2.19; free-stream Mach number, 1.91; jet pressure ratio, 15.



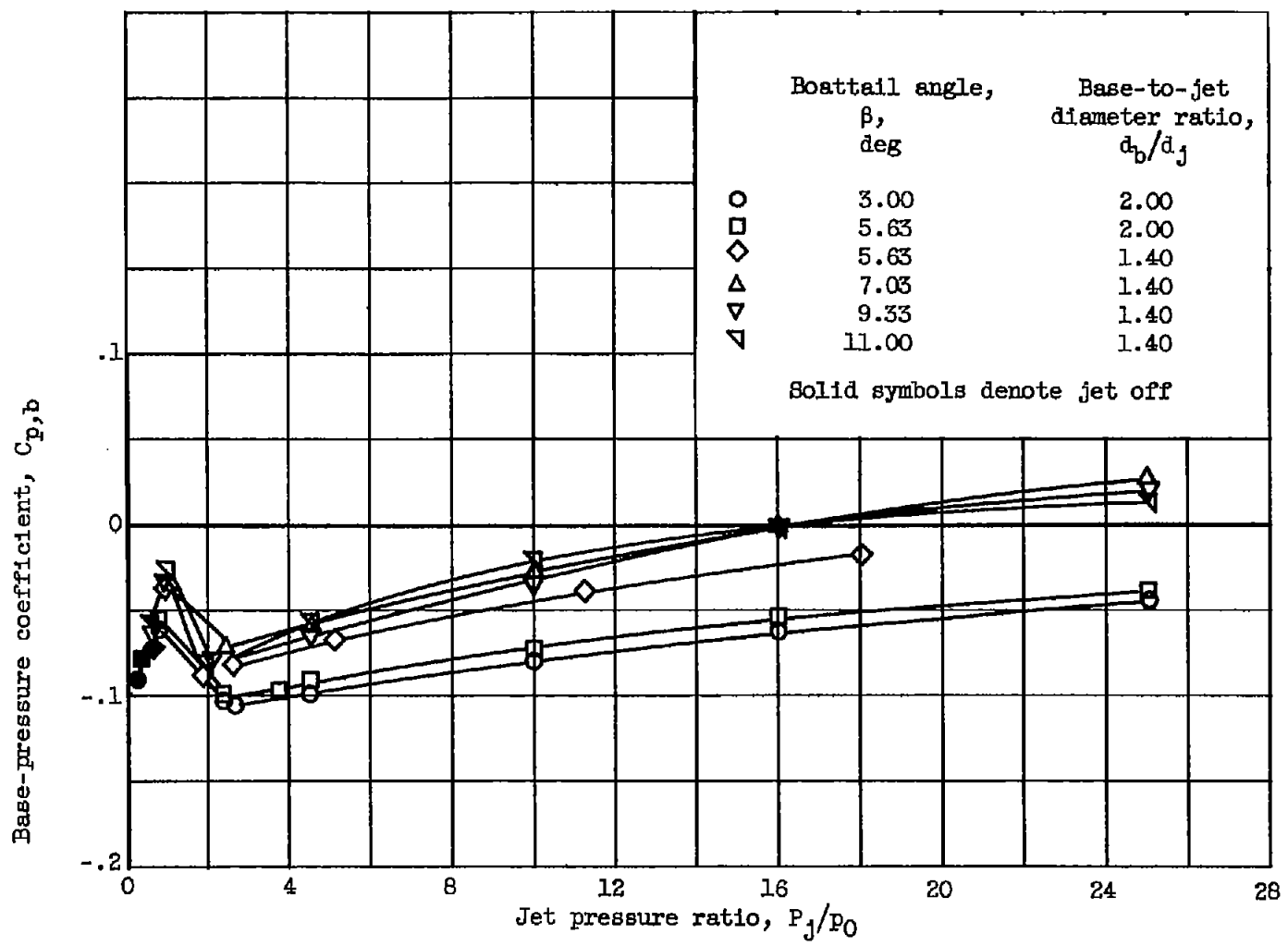
(a) Jet Mach number, 1.00.

Figure 23. - Effect of boattail angle on base-pressure coefficient at free-stream Mach number of 1.91. Nozzle angle, 0°.



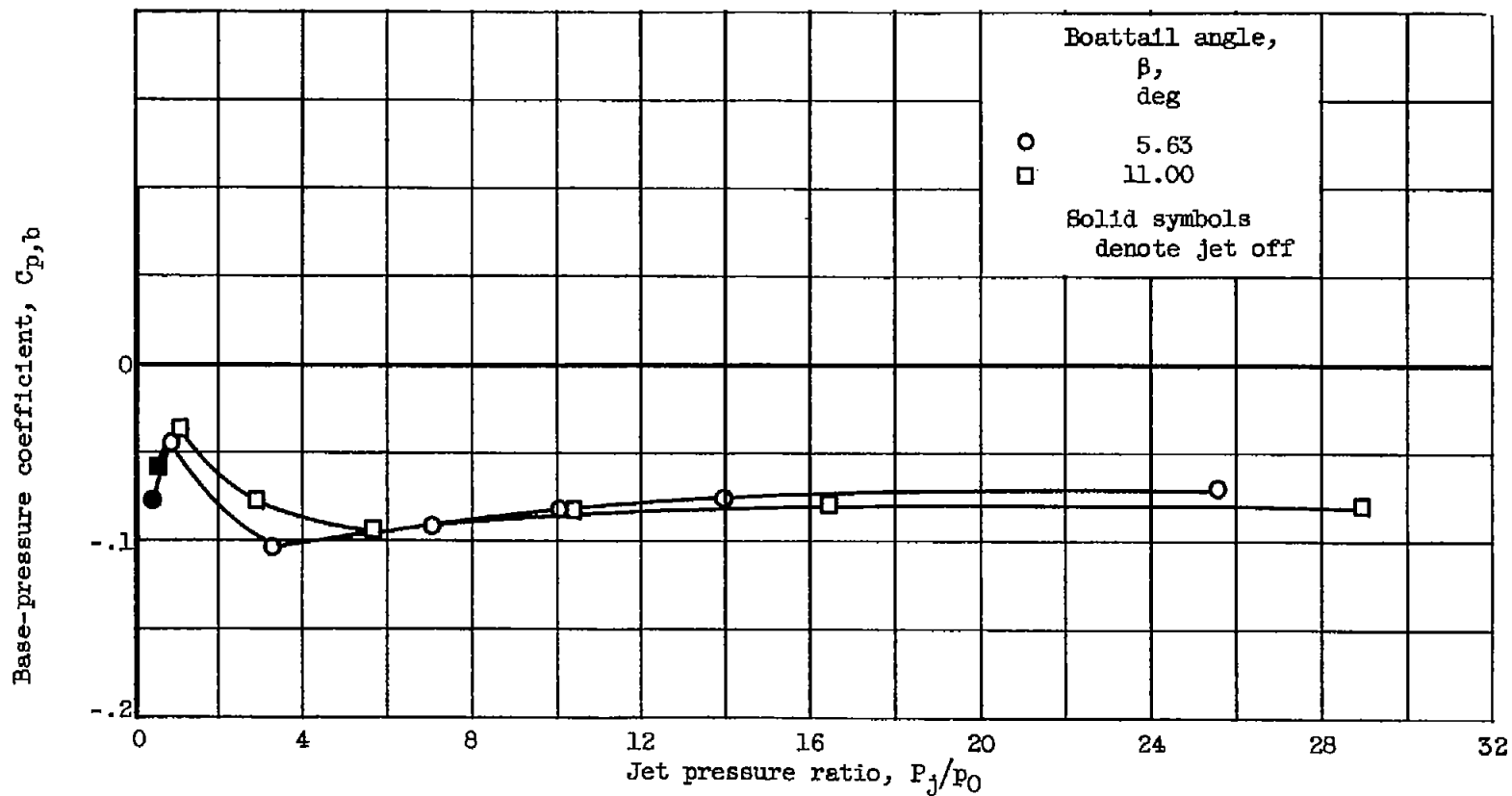
(b) Jet Mach number, 2.19; base-to-jet diameter ratio, 1.40.

Figure 23. - Concluded. Effect of boattail angle on base-pressure coefficient at free-stream Mach number of 1.91. Nozzle angle,  $0^\circ$ .



(a) Convergent nozzle; jet Mach number, 1.00.

Figure 24. - Effect of boattail angle on base-pressure coefficient at free-stream Mach number of 3.12. Nozzle angle, 0°.



(b) Jet Mach number, 2.19; base-to-jet diameter ratio, 1.40.

Figure 24. - Concluded. Effect of boattail angle on base-pressure coefficient at free-stream Mach number of 3.12. Nozzle angle,  $0^\circ$ .

3808

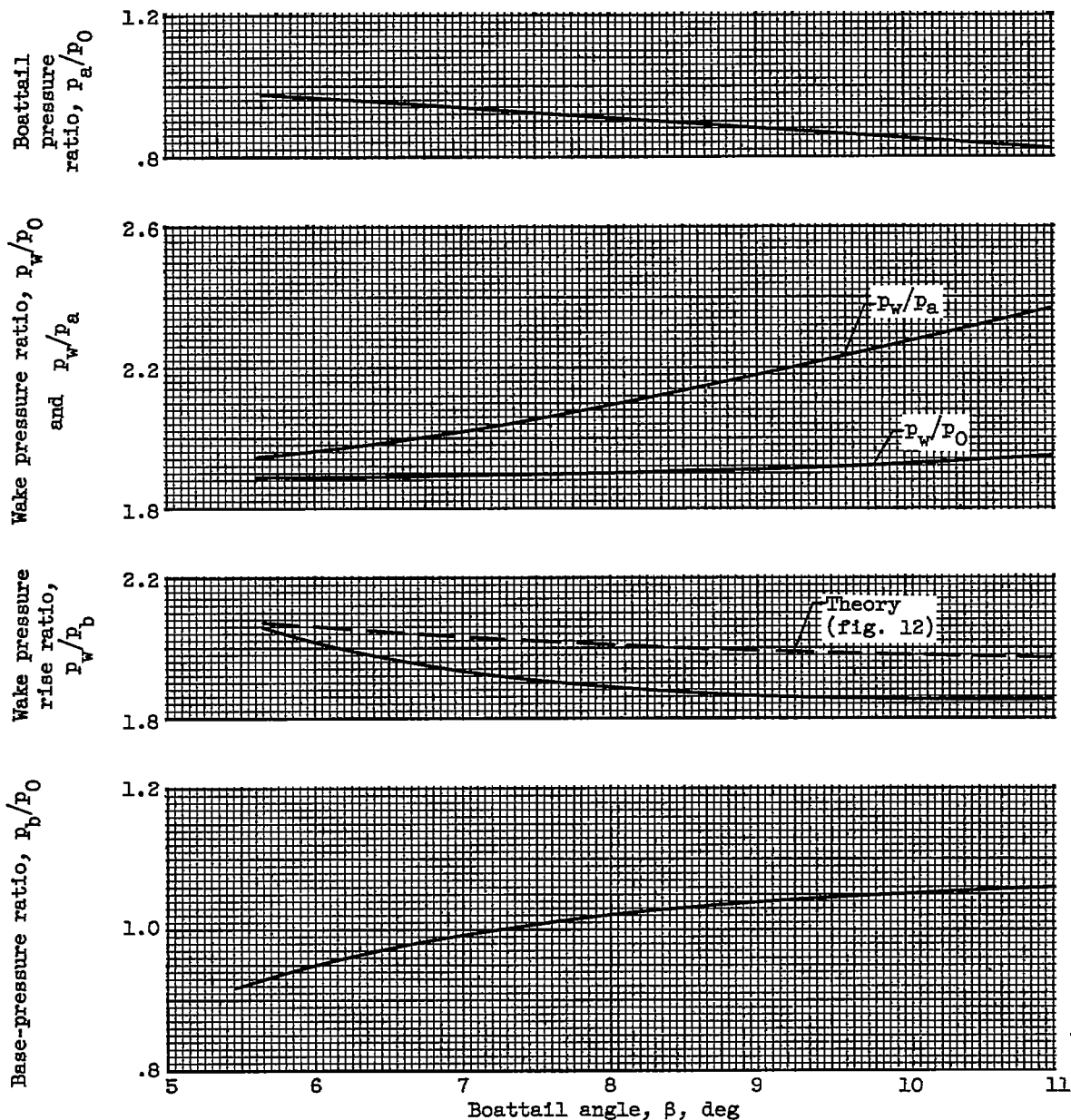
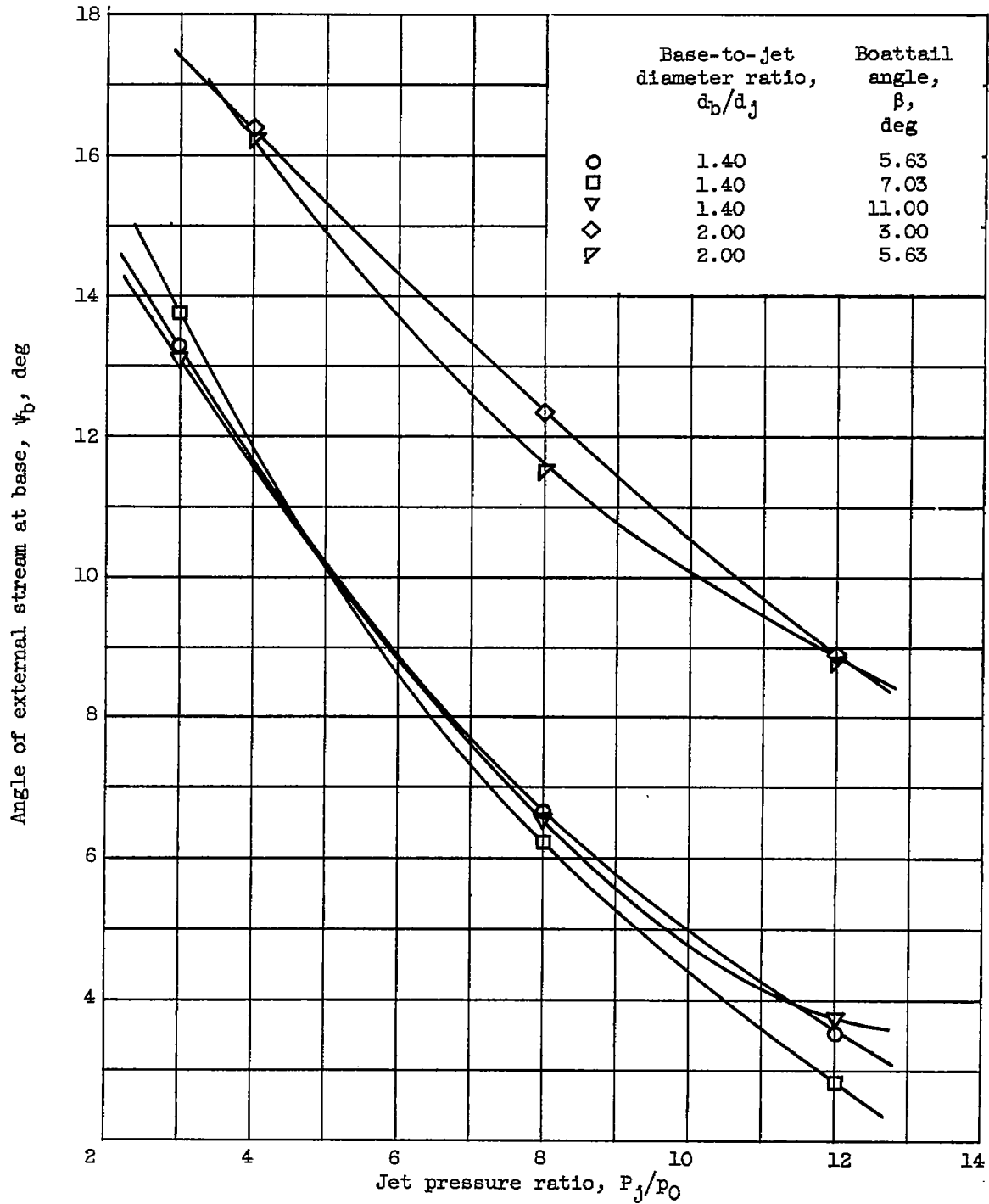


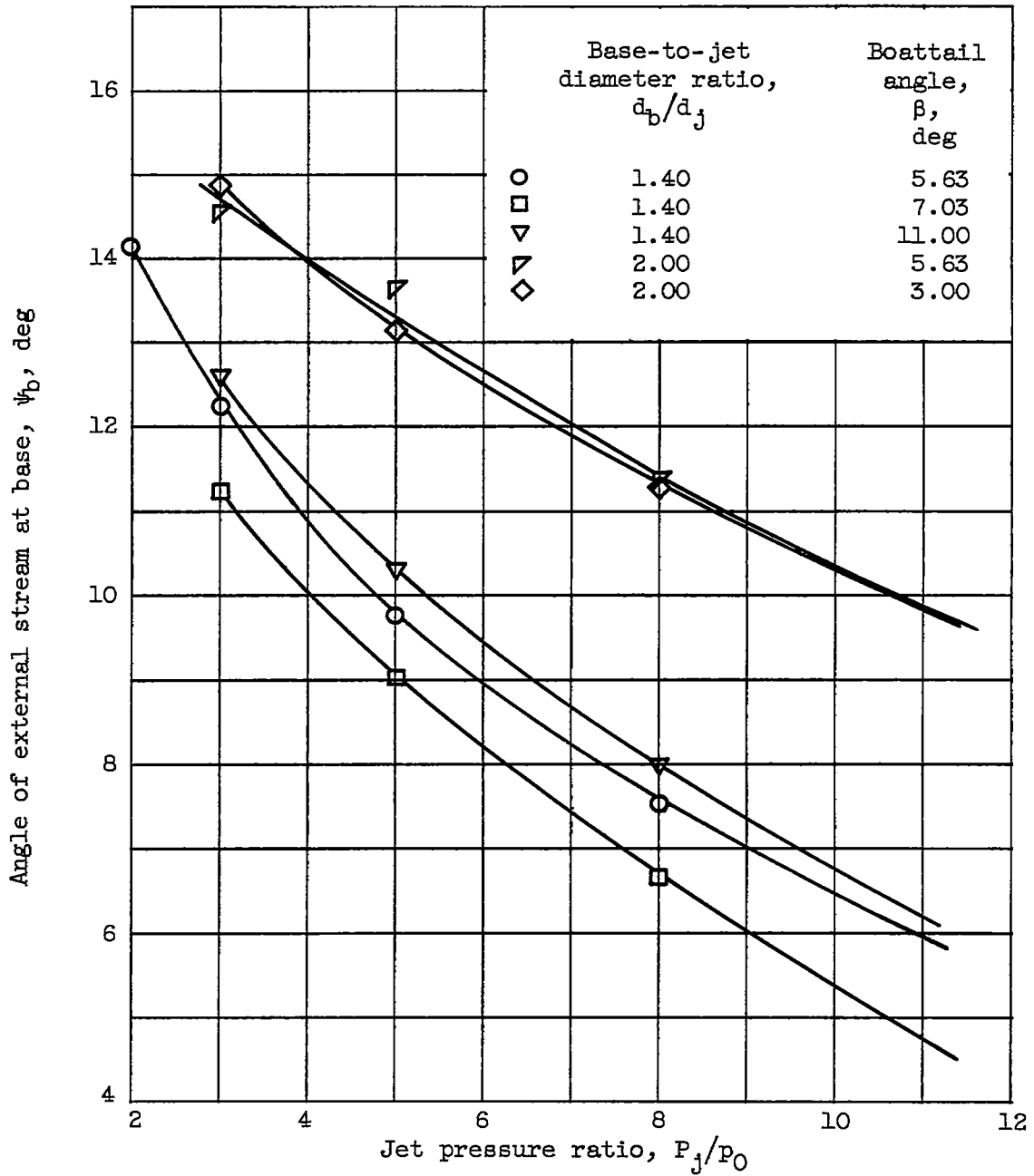
Figure 25. - Variation of component pressure ratios with boattail angle. Base-to-jet diameter ratio, 1.40; jet Mach number, 1.00; free-stream Mach number, 1.91; jet pressure ratio, 8.



(a) Free-stream Mach number, 1.91.

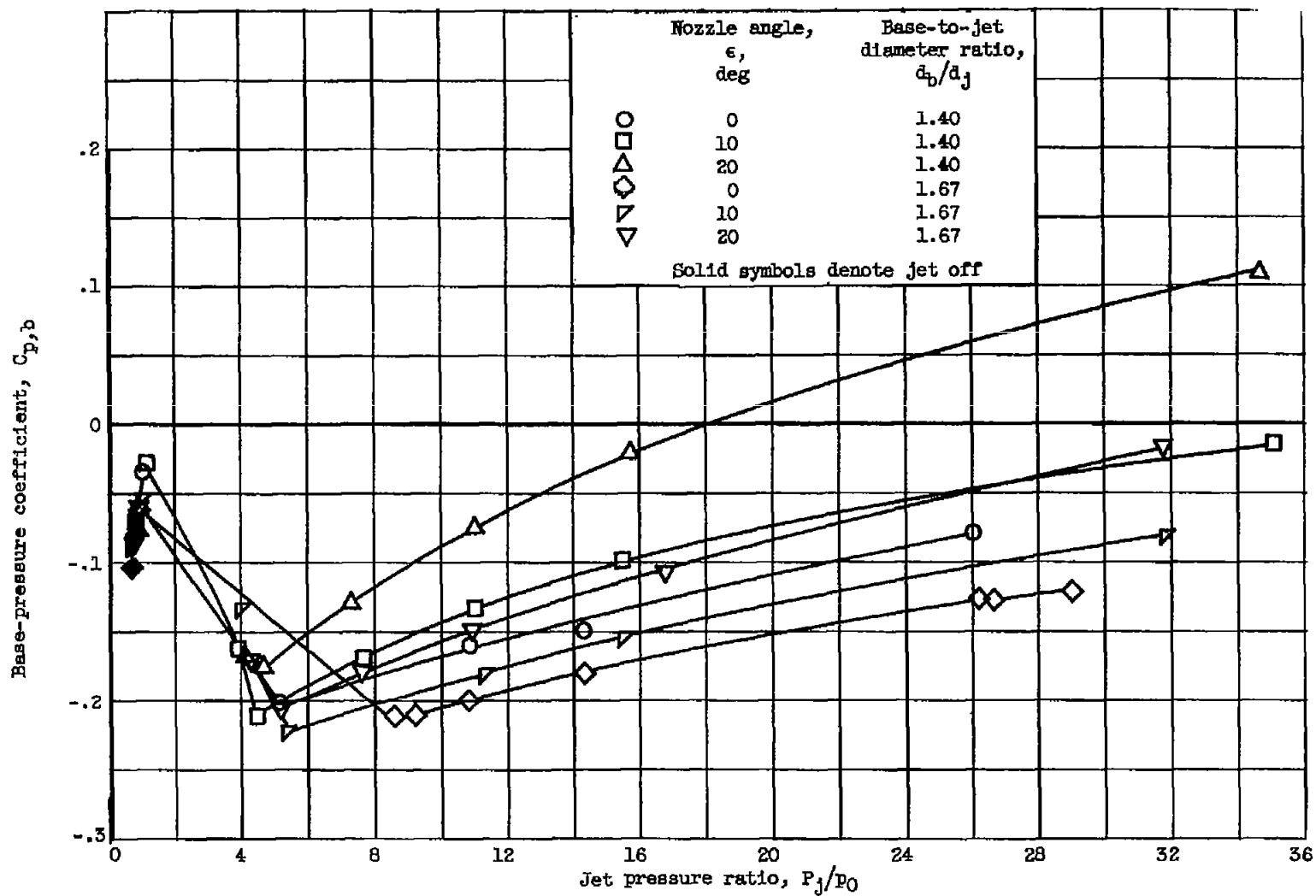
Figure 26. - Boattail angle correlation. Convergent nozzle.

3808



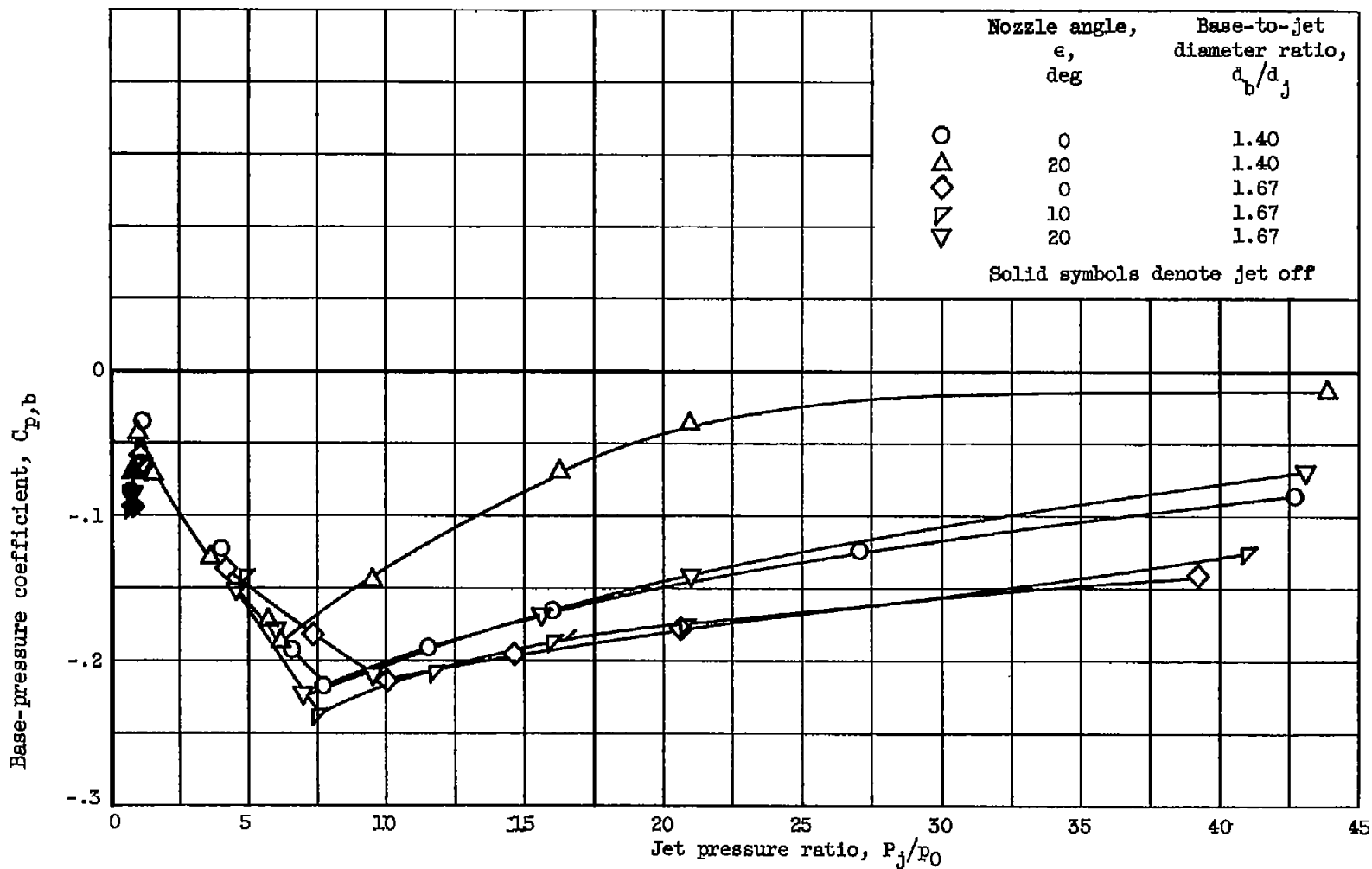
(b) Free-stream Mach number, 3.12.

Figure 26. - Concluded. Boattail angle correlation. Convergent nozzle.



(a) Jet Mach number, 2.19.

Figure 27. - Effect of nozzle angle on base-pressure coefficient at free-stream Mach number of 1.91. Boat-tail angle,  $5.63^\circ$ .



(b) Jet Mach number, 2.60.

Figure 27. - Concluded. Effect of nozzle angle on base-pressure coefficient at free-stream Mach number of 1.91. Boattail angle,  $5.63^\circ$ .

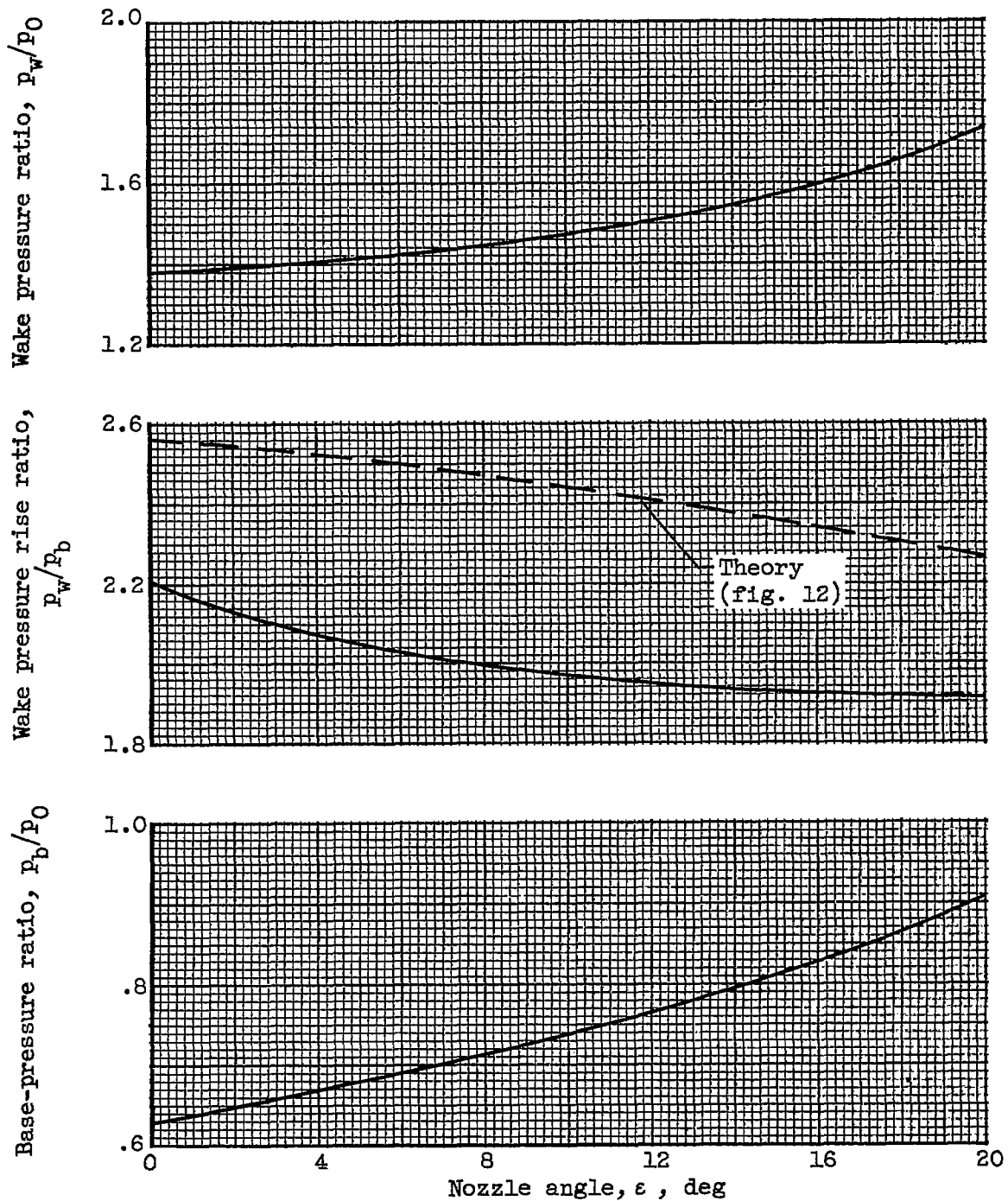
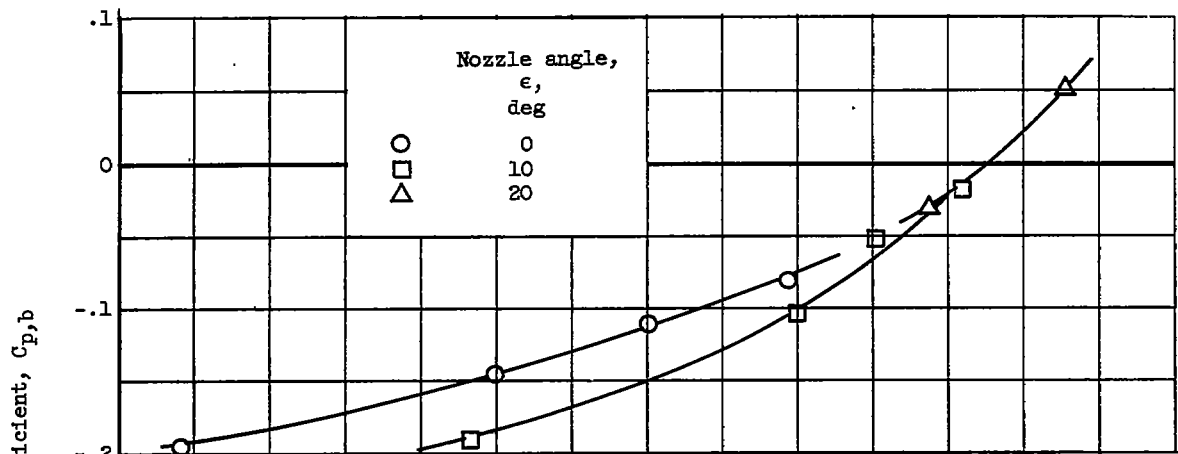
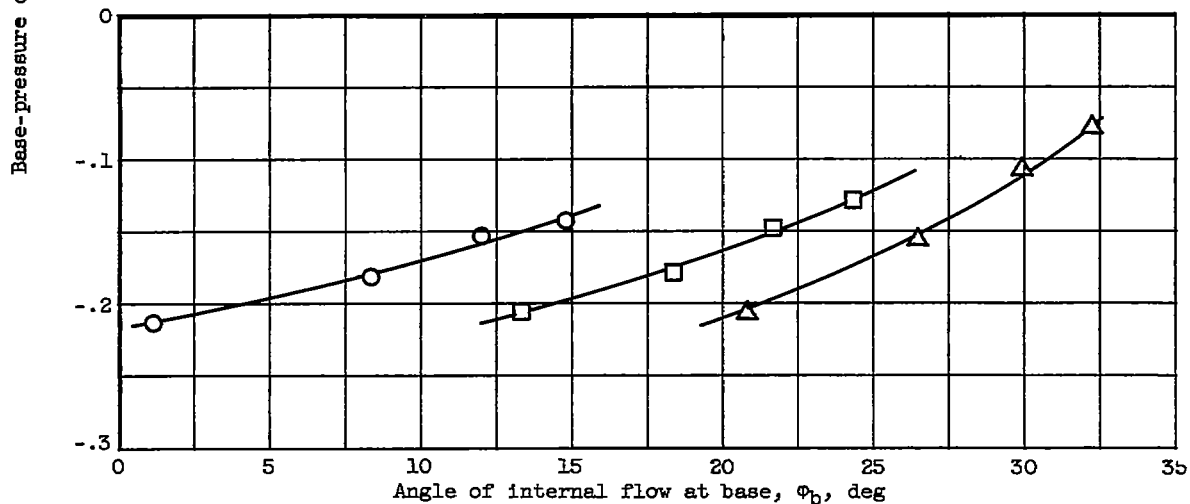


Figure 28. - Variation of base-pressure components with nozzle angle. Base-to-jet diameter ratio, 1.40; boattail angle,  $5.63^\circ$ ; jet Mach number, 2.19; free-stream Mach number, 1.91; jet pressure ratio, 15.



(a) Base-to-jet diameter ratio, 1.40; jet Mach number, 2.19.



(b) Base-to-jet diameter ratio, 1.67; jet Mach number, 2.60.

Figure 29. - Nozzle angle correlation. Free-stream Mach number, 1.91; boattail angle,  $5.63^\circ$ .

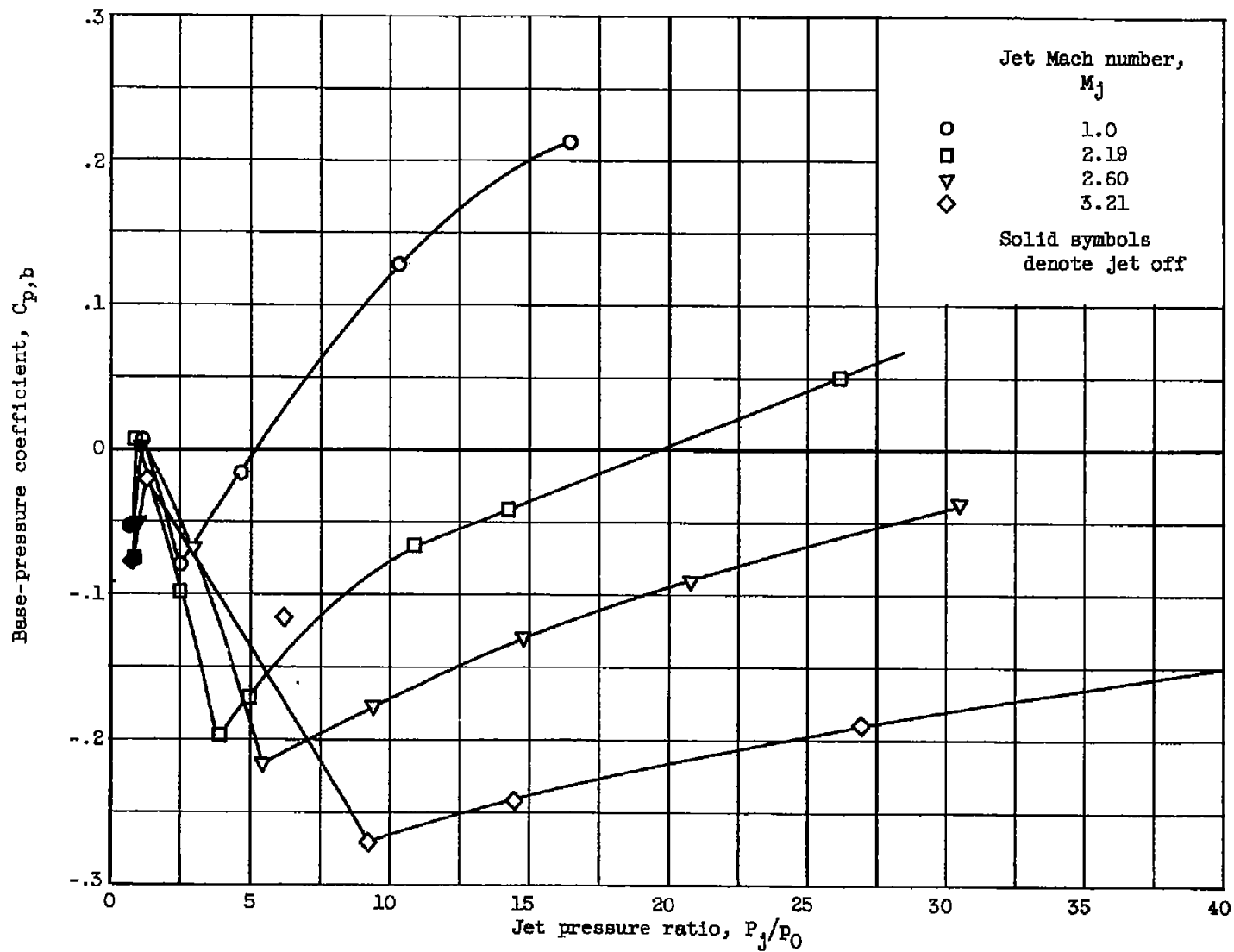
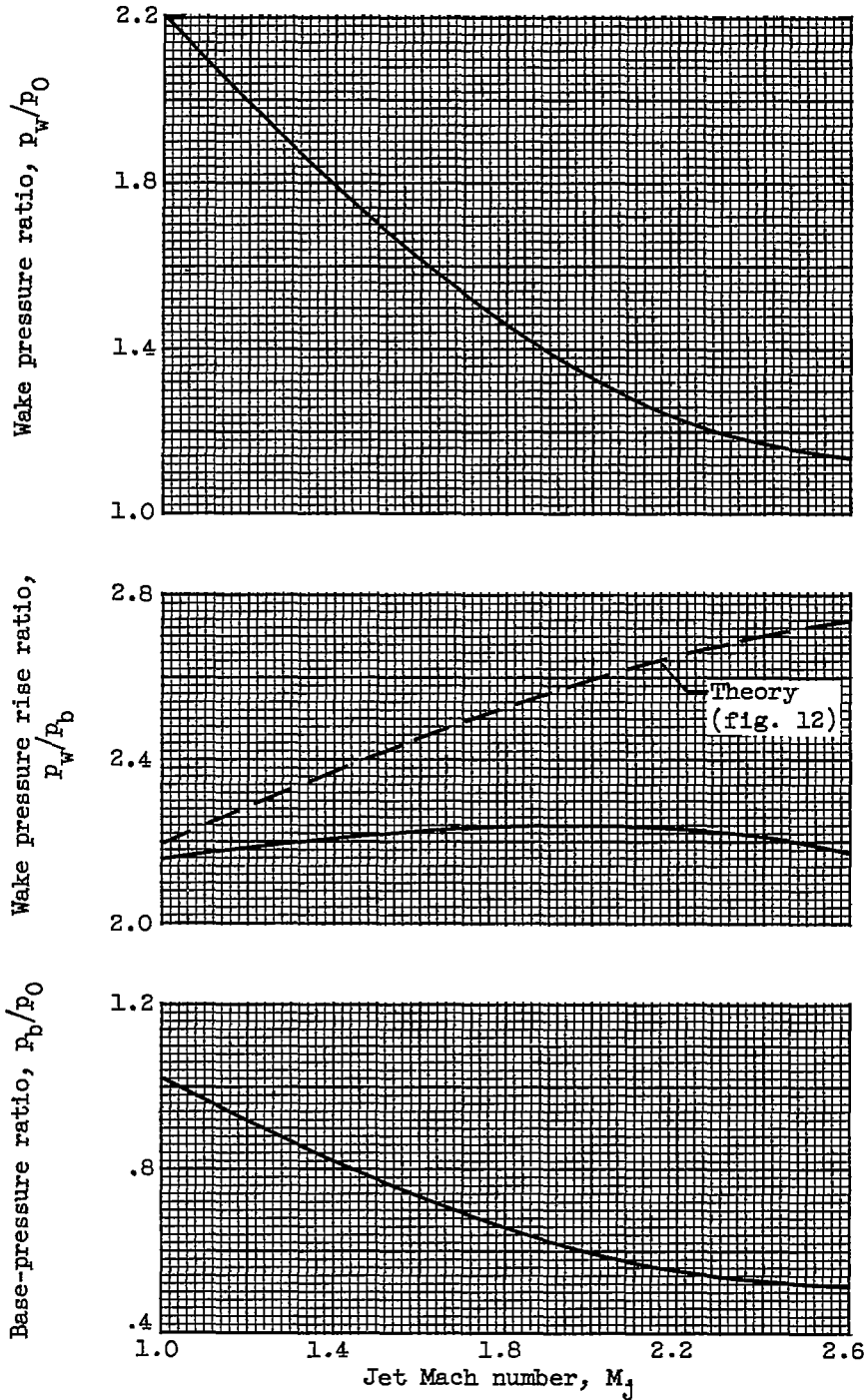


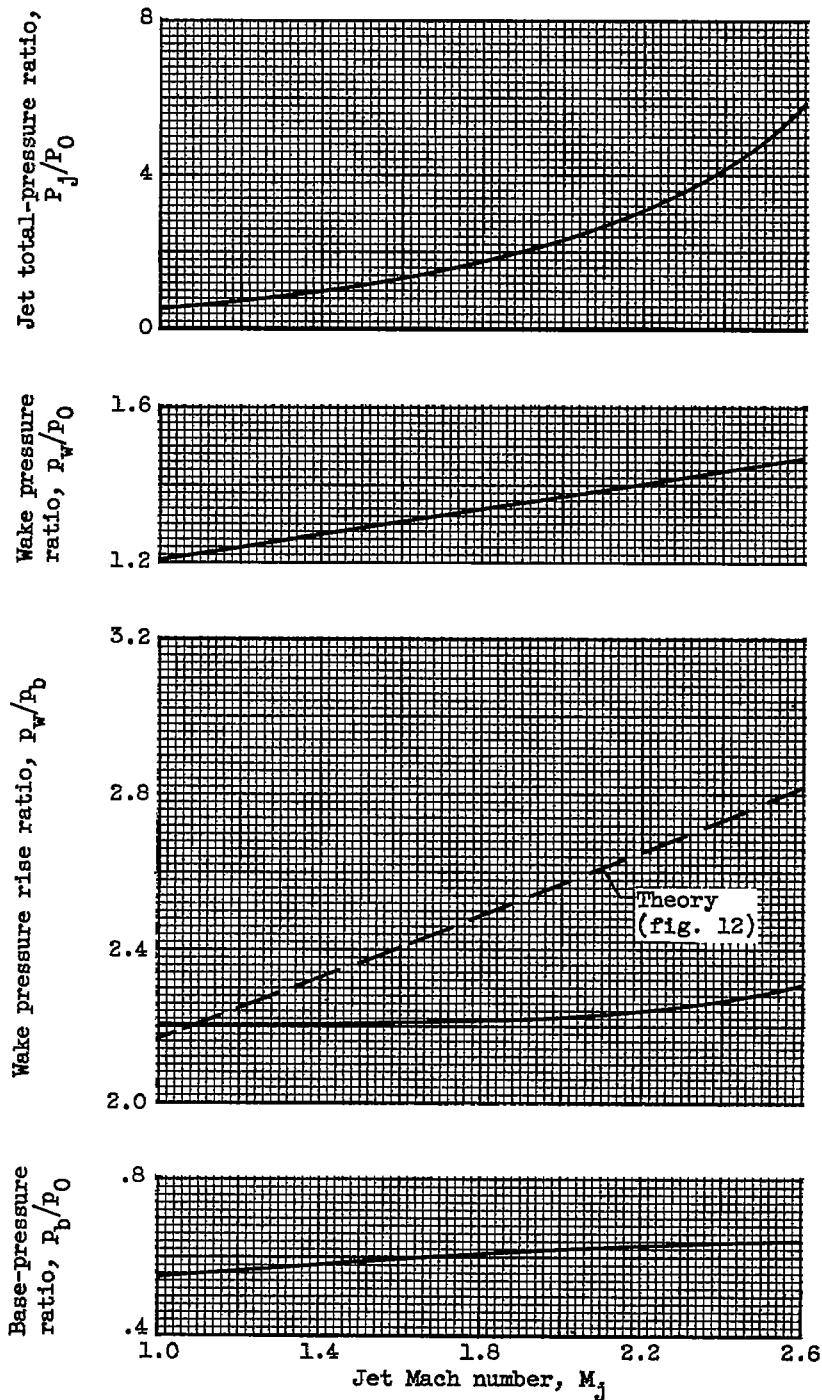
Figure 30. - Effect of jet Mach number on base pressure. Base-to-jet diameter ratio, 1.11; boat-tail angle,  $5.63^\circ$ ; free-stream Mach number, 1.91.

3808



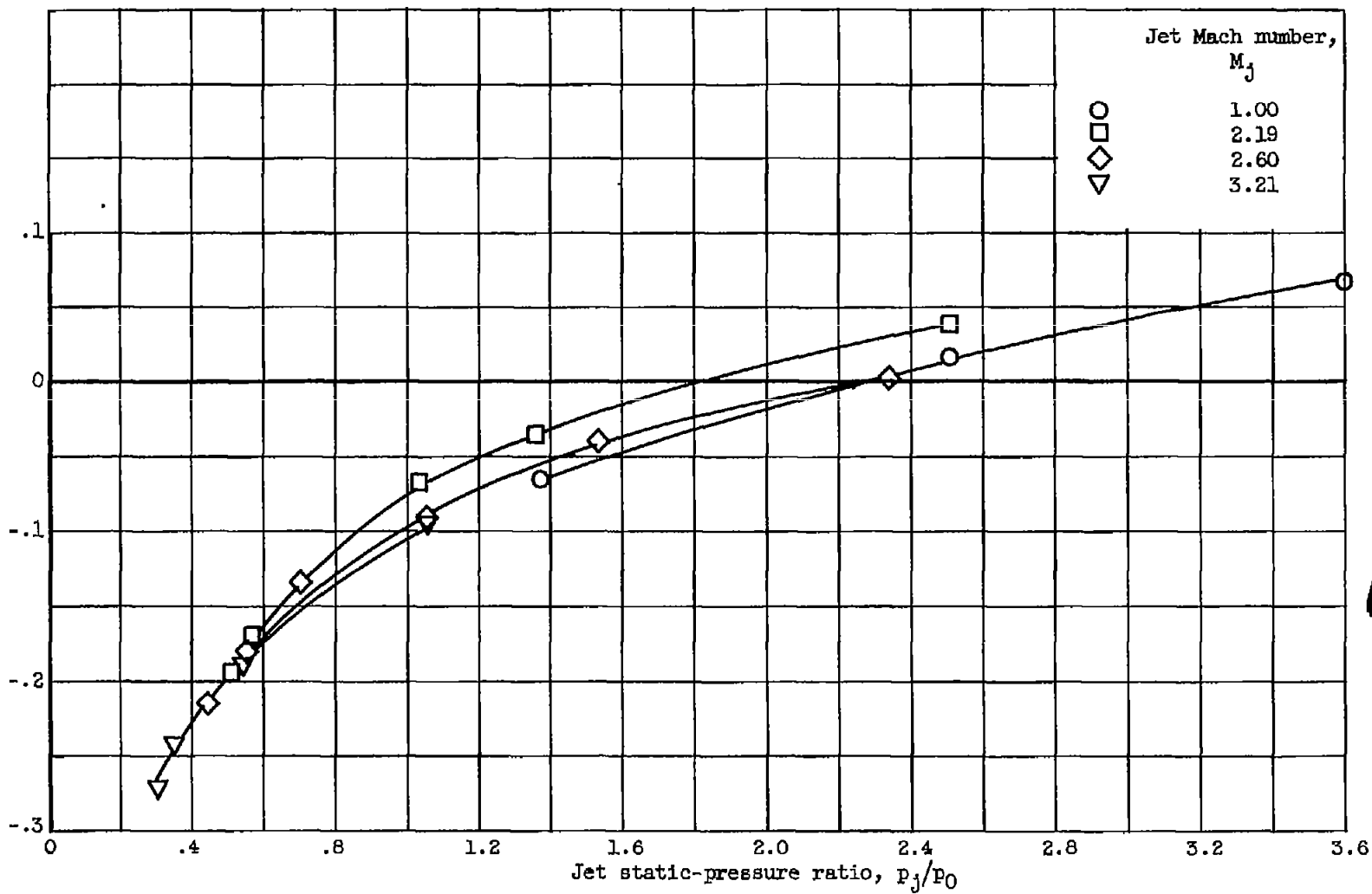
(a) Constant jet pressure ratio, 15.

Figure 31. - Variation of base-pressure components with jet Mach number. Base-to-jet diameter ratio, 1.67; boattail angle,  $5.63^\circ$ ; nozzle angle,  $0^\circ$ ; free-stream Mach number, 1.91.



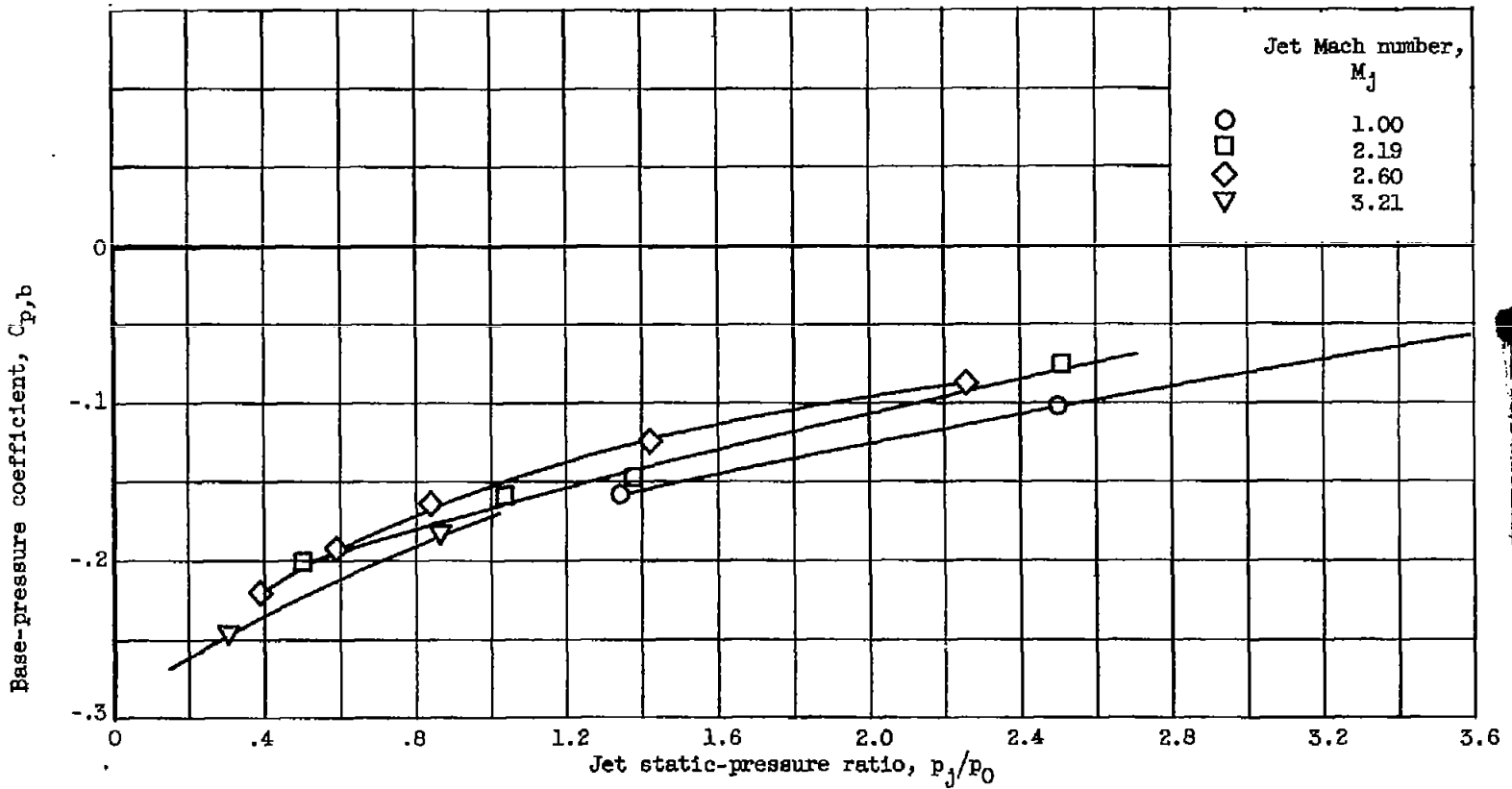
(b) Constant jet static-pressure ratio, 2.0.

Figure 31. - Concluded. Variation of base-pressure components with jet Mach number. Base-to-jet diameter ratio, 1.67; boattail angle,  $5.63^\circ$ ; nozzle angle,  $0^\circ$ ; free-stream Mach number, 1.91.



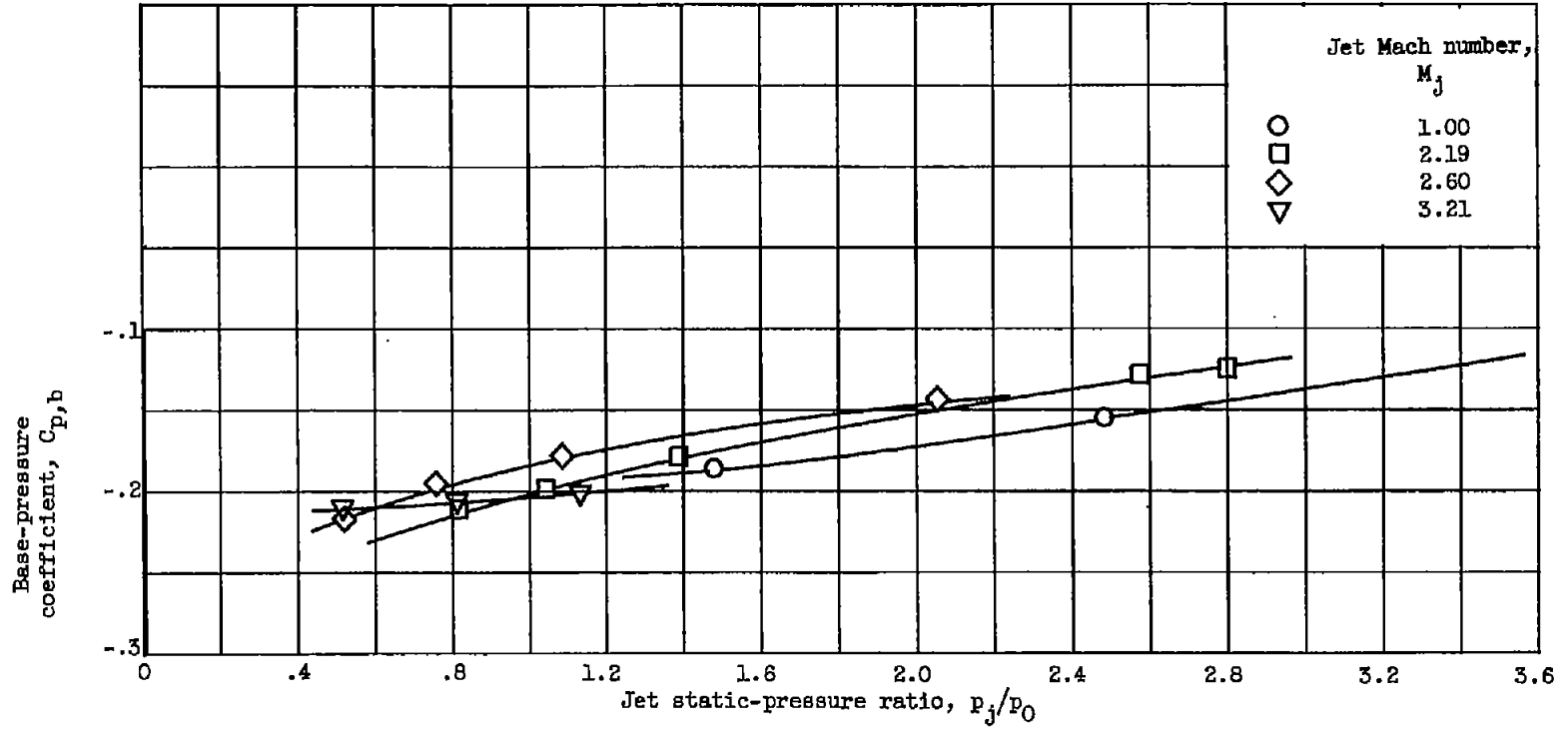
(a) Base-to-jet diameter ratio, 1.11.

Figure 32. - Correlation of jet Mach number effects by means of jet static-pressure ratio at free-stream Mach number of 1.91. Boattail angle,  $5.63^\circ$ ; nozzle angle,  $0^\circ$ .



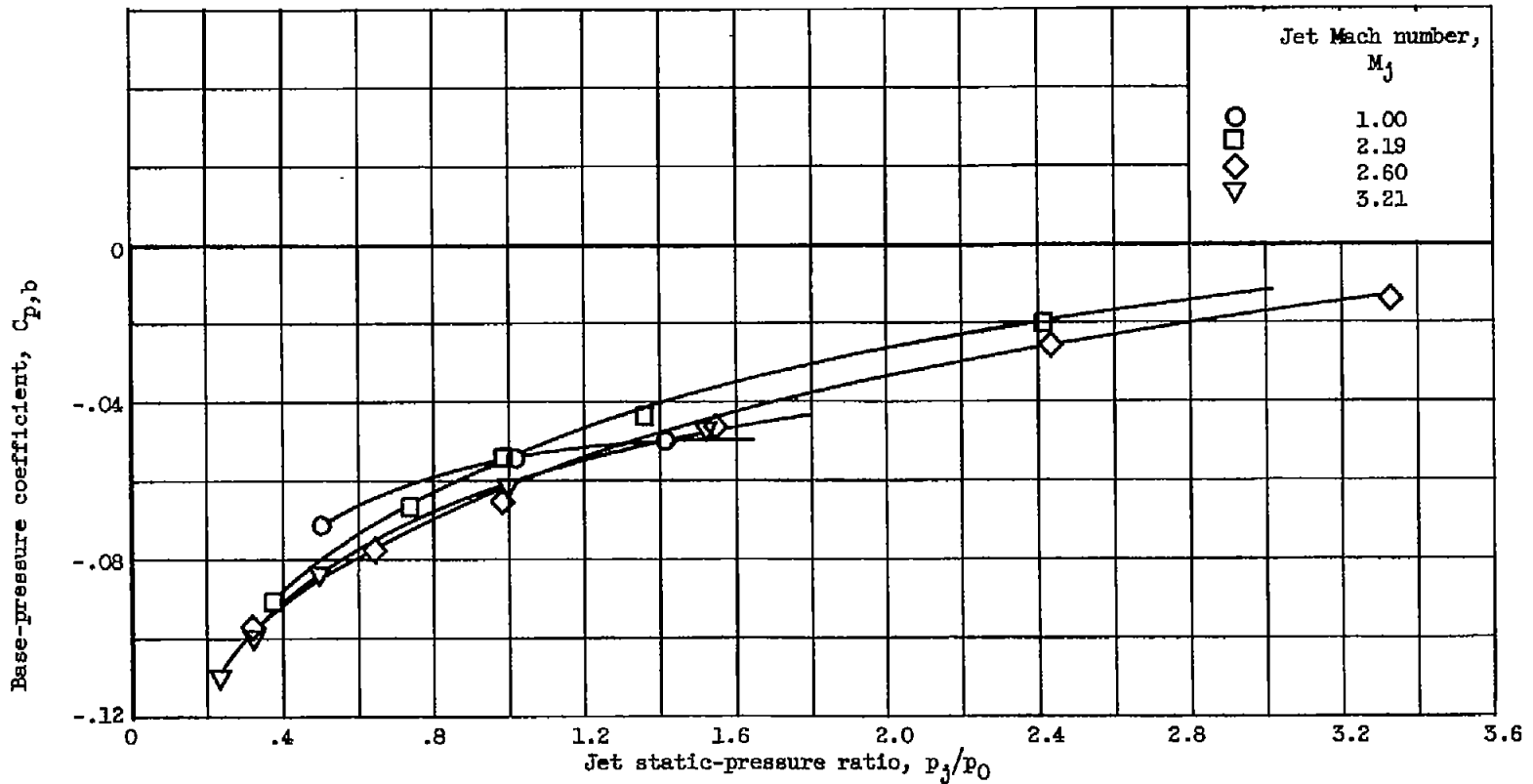
(b) Base-to-jet diameter ratio, 1.40.

Figure 32. - Continued. Correlation of jet Mach number effects by means of jet static-pressure ratio at free-stream Mach number of 1.91. Boattail angle,  $5.63^\circ$ ; nozzle angle,  $0^\circ$ .



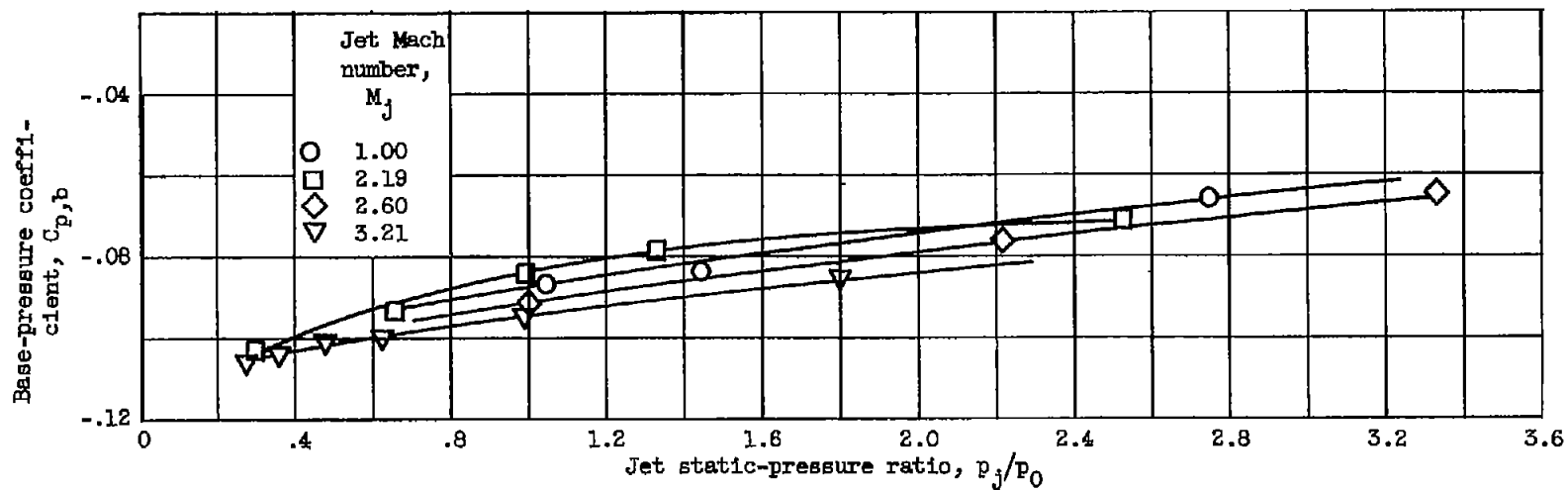
(c) Base-to-jet diameter ratio, 1.67.

Figure 32. - Concluded. Correlation of jet Mach number effects by means of jet static-pressure ratio at free-stream Mach number of 1.91. Boattail angle,  $5.63^\circ$ ; nozzle angle,  $0^\circ$ .



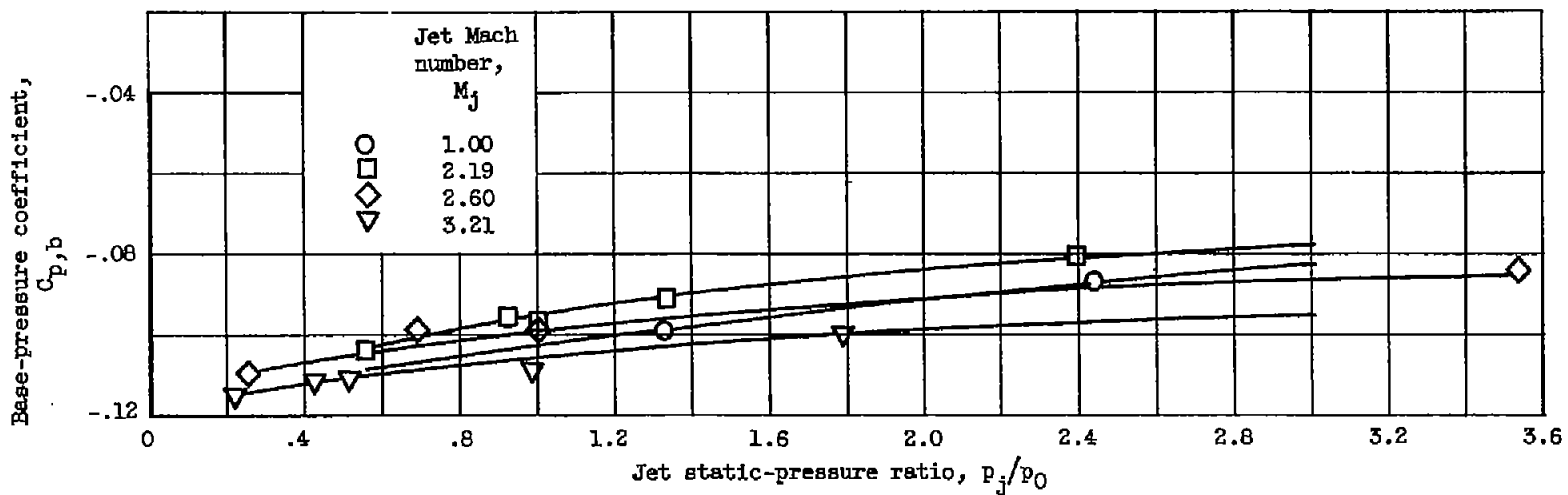
(a) Base-to-jet diameter ratio, 1.11.

Figure 33. - Correlation of jet Mach number effects by means of jet static-pressure ratio at free-stream Mach number of 3.12. Boattail angle,  $5.63^\circ$ ; nozzle angle,  $0^\circ$ .



(b) Base-to-jet diameter ratio, 1.40.

Figure 33. - Continued. Correlation of jet Mach number effects by means of jet static-pressure ratio at free-stream Mach number of 3.12. Boattail angle,  $5.63^\circ$ ; nozzle angle,  $0^\circ$ .



(c) Base-to-jet diameter ratio, 1.67.

Figure 33. - Concluded. Correlation of jet Mach number effects by means of jet static-pressure ratio at free-stream Mach number of 3.12. Boattail angle,  $5.63^\circ$ ; nozzle angle,  $0^\circ$ .

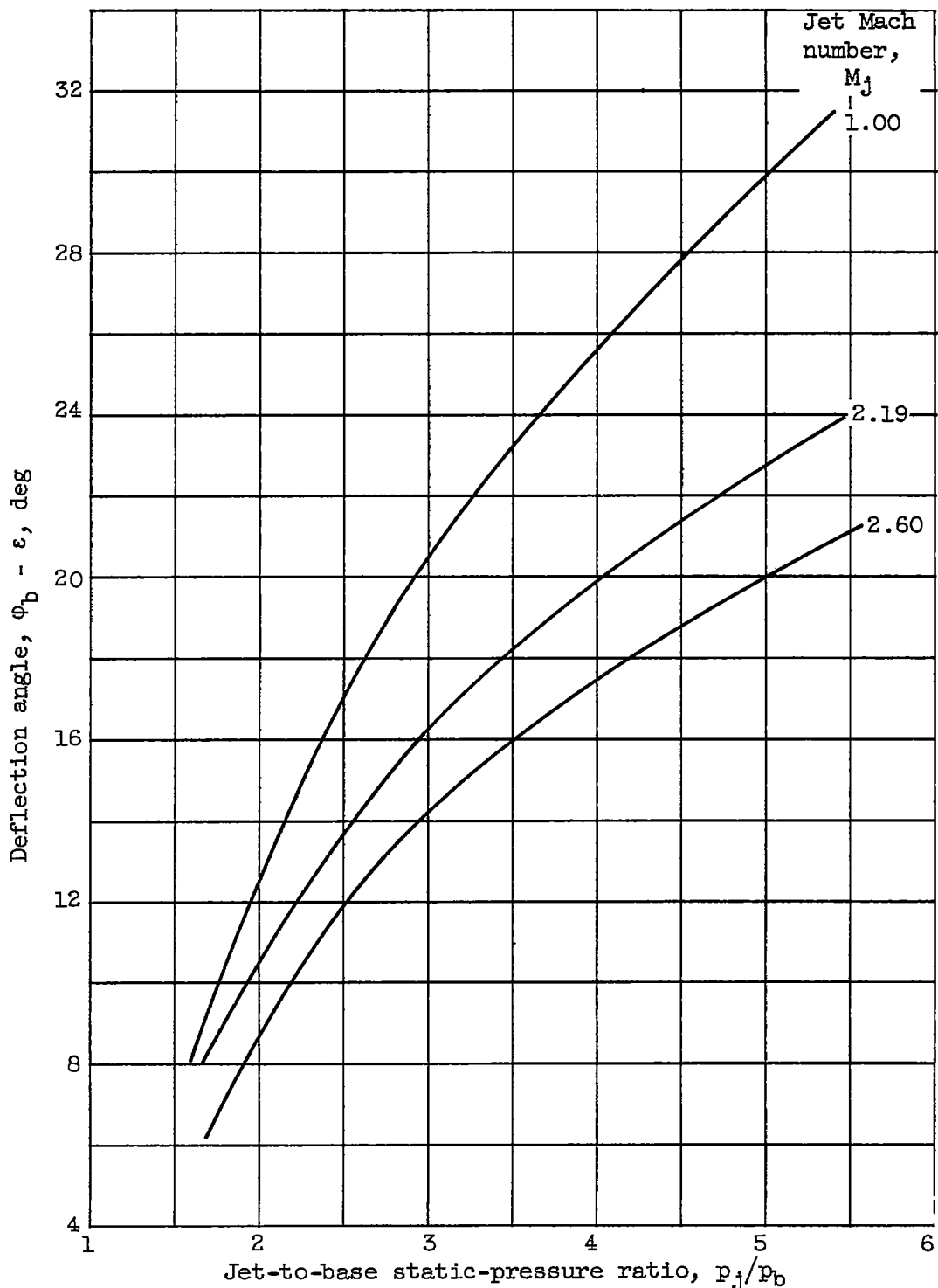


Figure 34. - Variation of deflection angle at base with jet to base static-pressure ratio for several values of jet Mach number. Ratio of specific heats, 1.4.

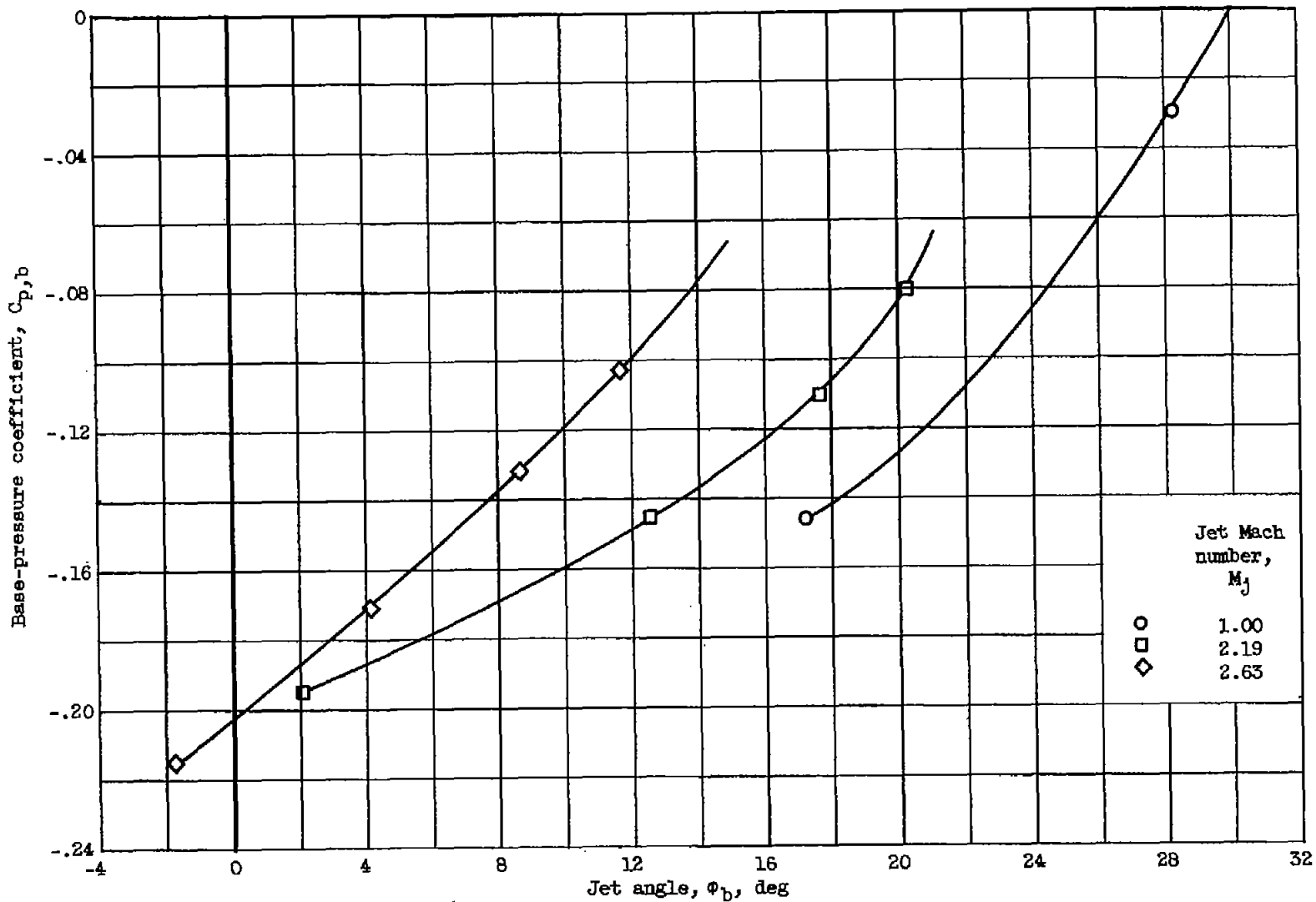


Figure 35. - Correlation of jet Mach number effects by means of jet angle at base. Base-to-jet diameter ratio, 1.40; boattail angle,  $5.63^\circ$ ; free-stream Mach number, 1.91.

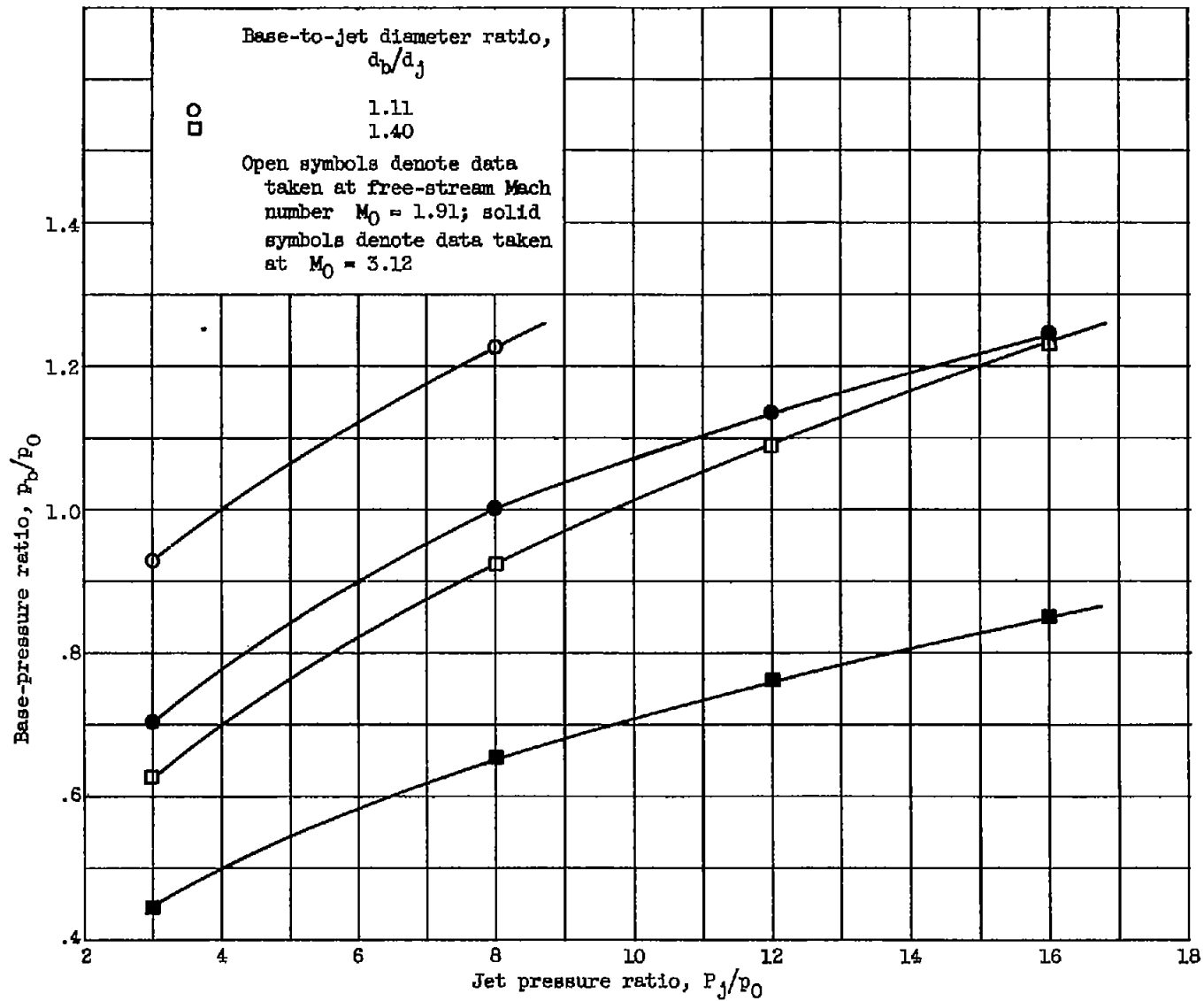


Figure 36. - Effect of free-stream Mach number on base pressure. Boattail angle,  $5.63^\circ$ .

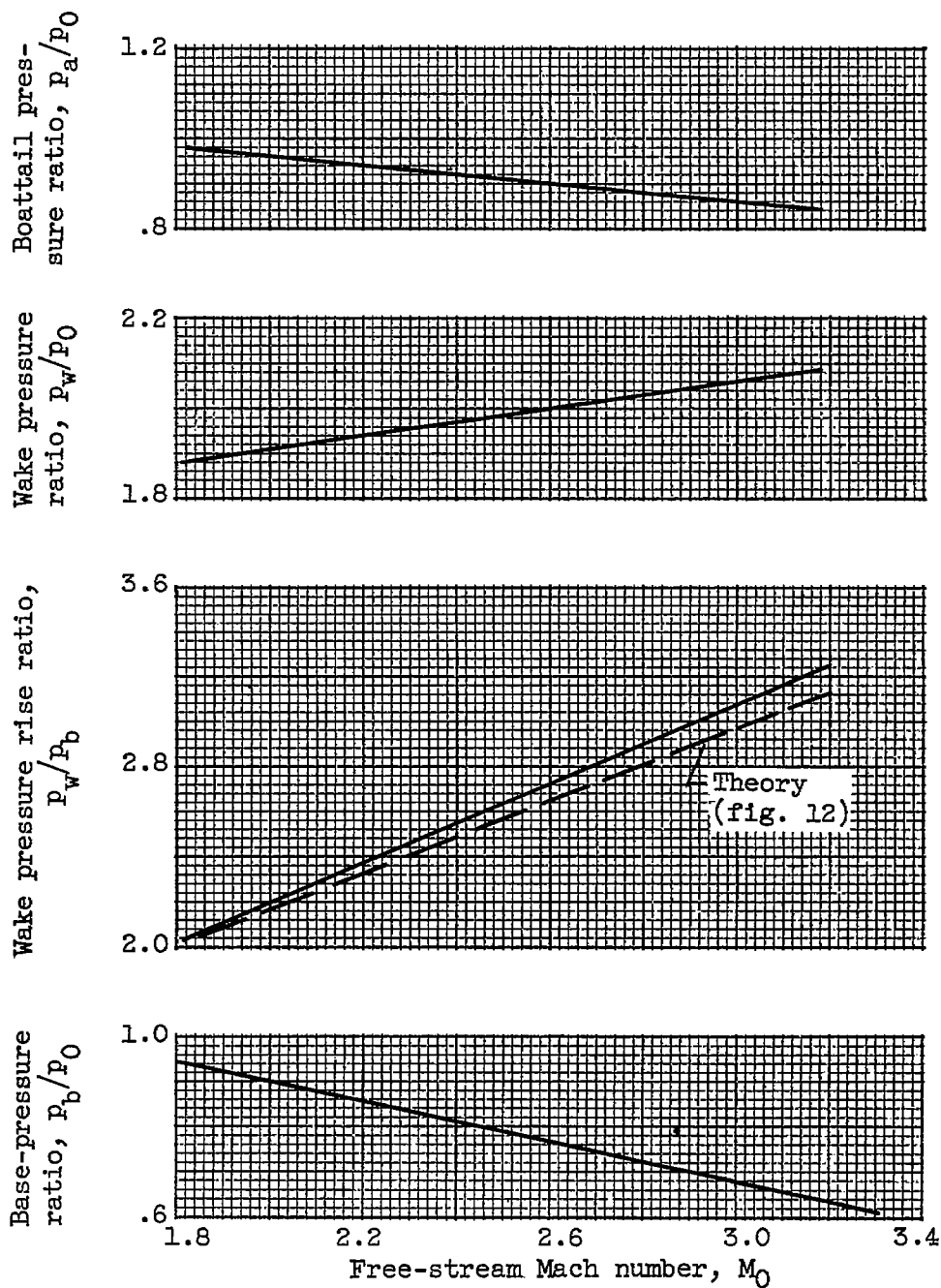


Figure 37. - Variation of component pressures with free-stream Mach number. Base-to-jet diameter ratio, 1.40; boattail angle,  $5.63^\circ$ ; jet Mach number, 1.0; jet pressure ratio, 8.

38408  
CW-13

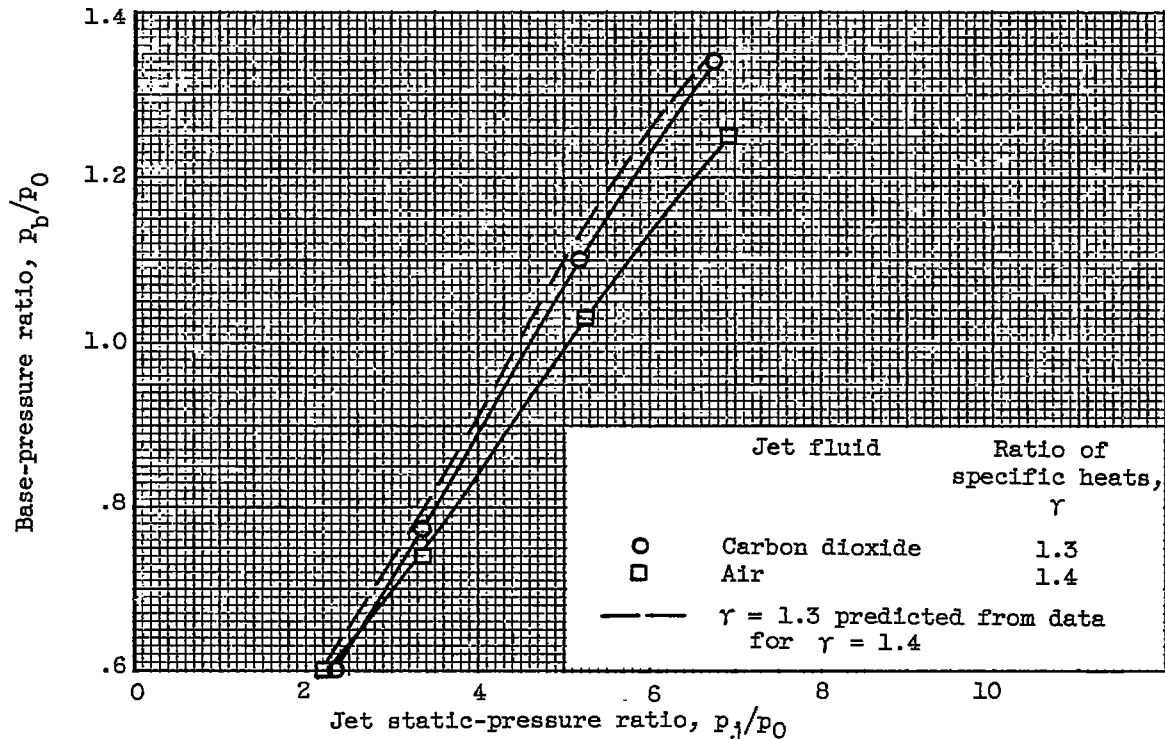


Figure 38. - Effect of ratio of specific heats on base pressure. Base-to-jet diameter ratio, 1.40; boattail angle,  $5.63^\circ$ ; free-stream Mach number, 1.91.

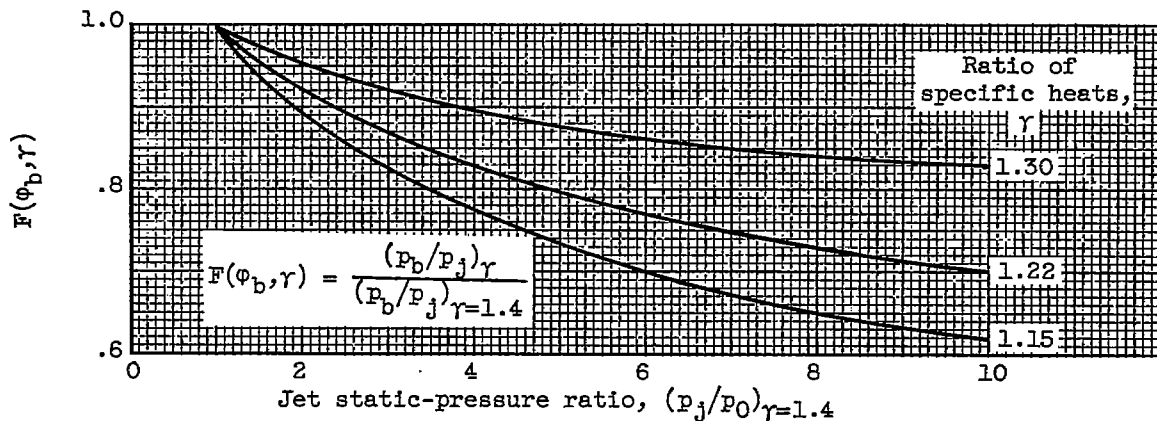
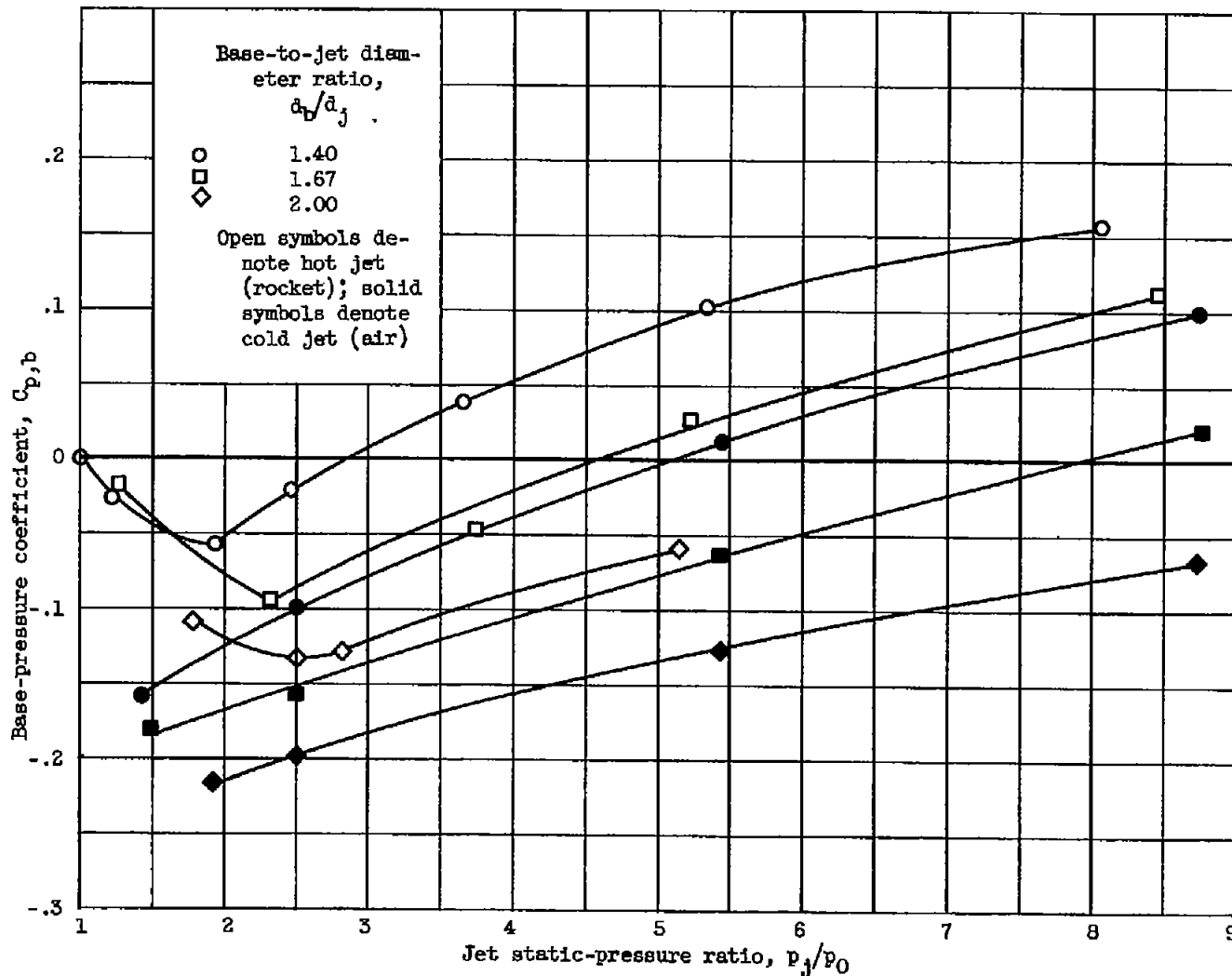


Figure 39. - Gamma correction function. Jet Mach number, 1.0; nozzle angle,  $0^\circ$ .

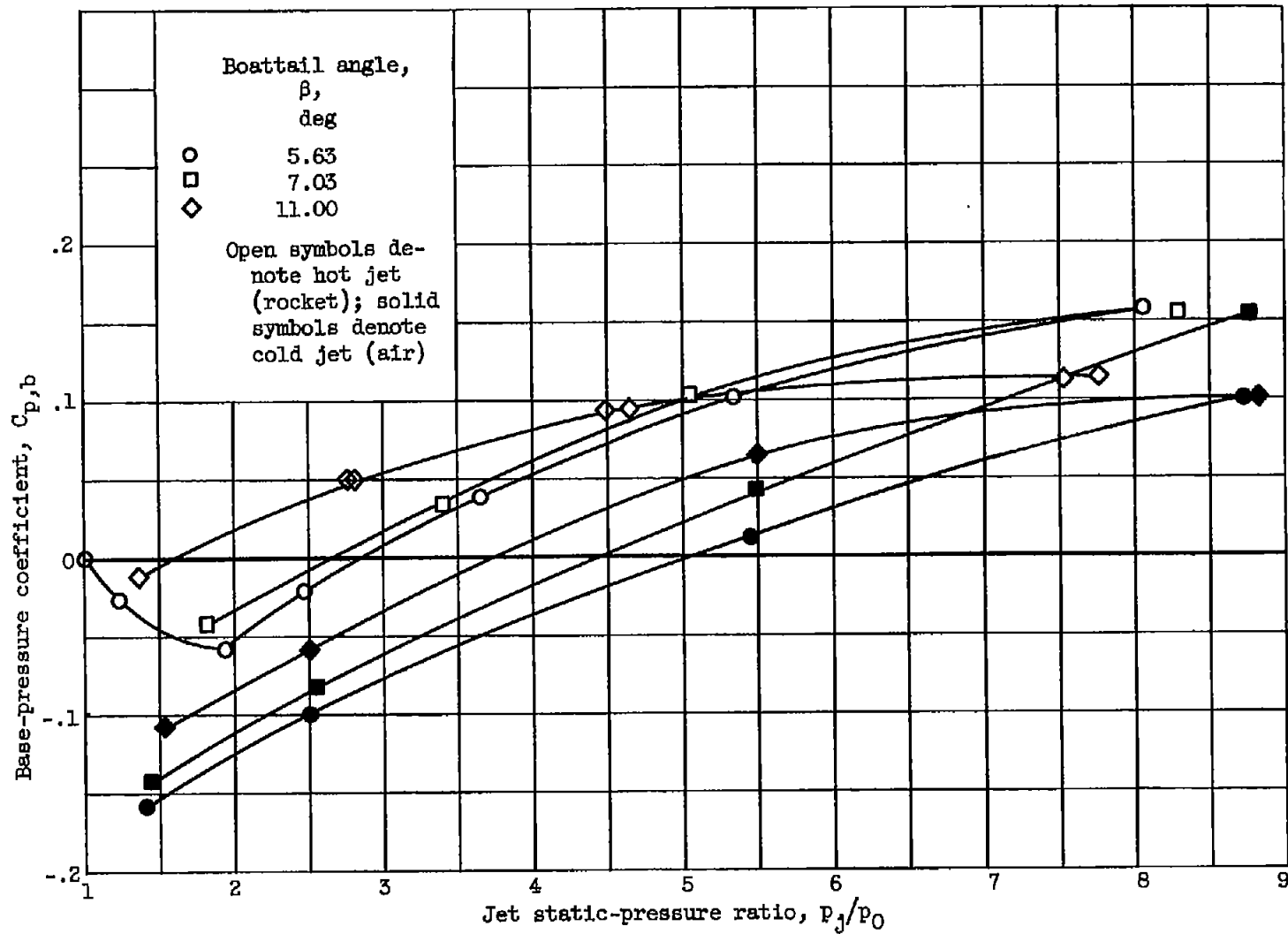
CONFIDENTIAL



(a) Jet Mach number, 1.0; boattail angle,  $5.63^\circ$ .

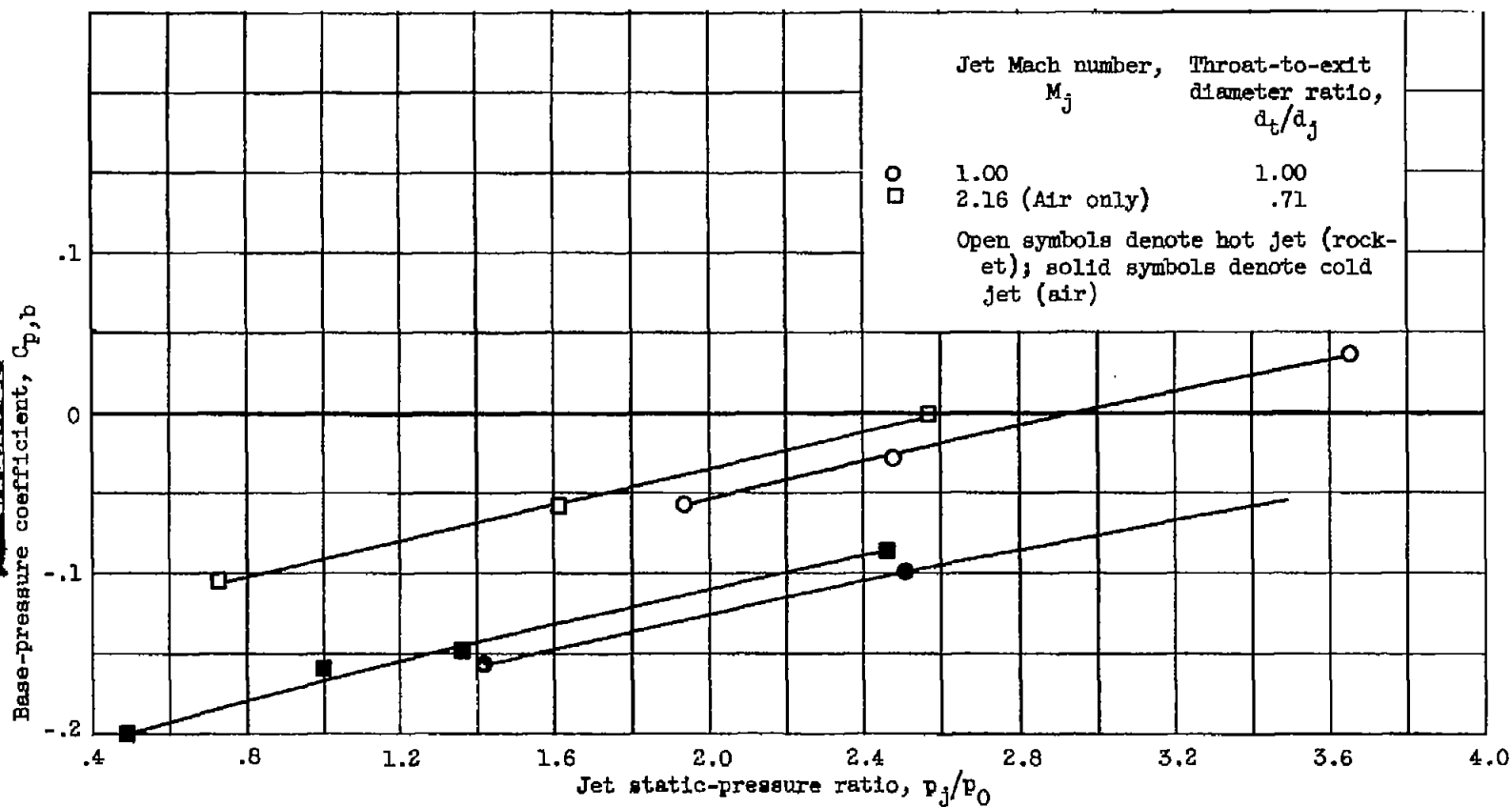
Figure 40. - Effect of hot jet on base pressure. Free-stream Mach number, 1.91.

CONFIDENTIAL



(b) Jet Mach number, 1.0; base-to-jet diameter ratio, 1.40.

Figure 40. - Continued. Effect of hot jet on base pressure. Free-stream Mach number, 1.91.



(c) Boattail angle,  $5.63^\circ$ ; base-to-jet diameter ratio, 1.40.

Figure 40. - Concluded. Effect of hot jet on base pressure. Free-stream Mach number, 1.91.

CONFIDENTIAL

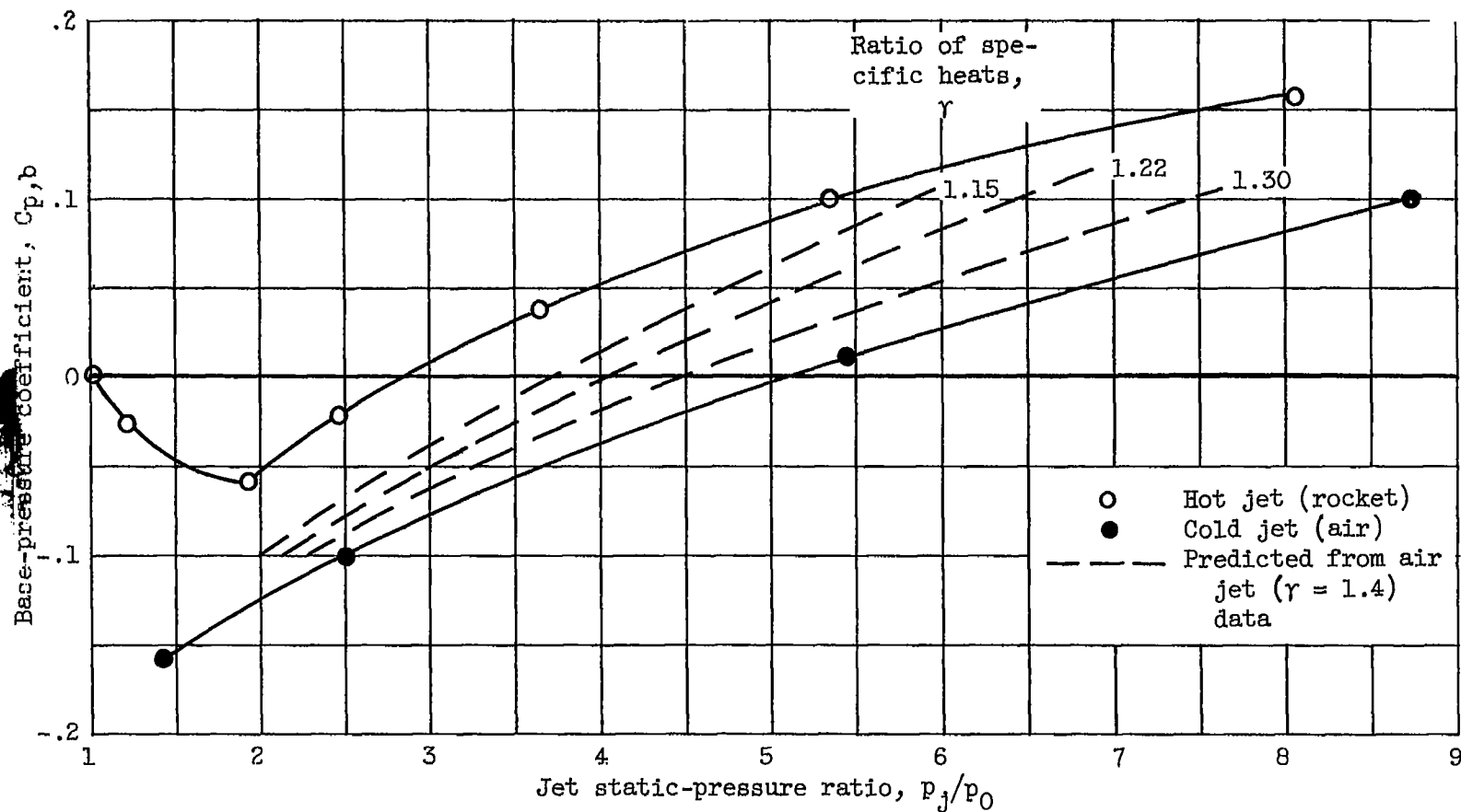
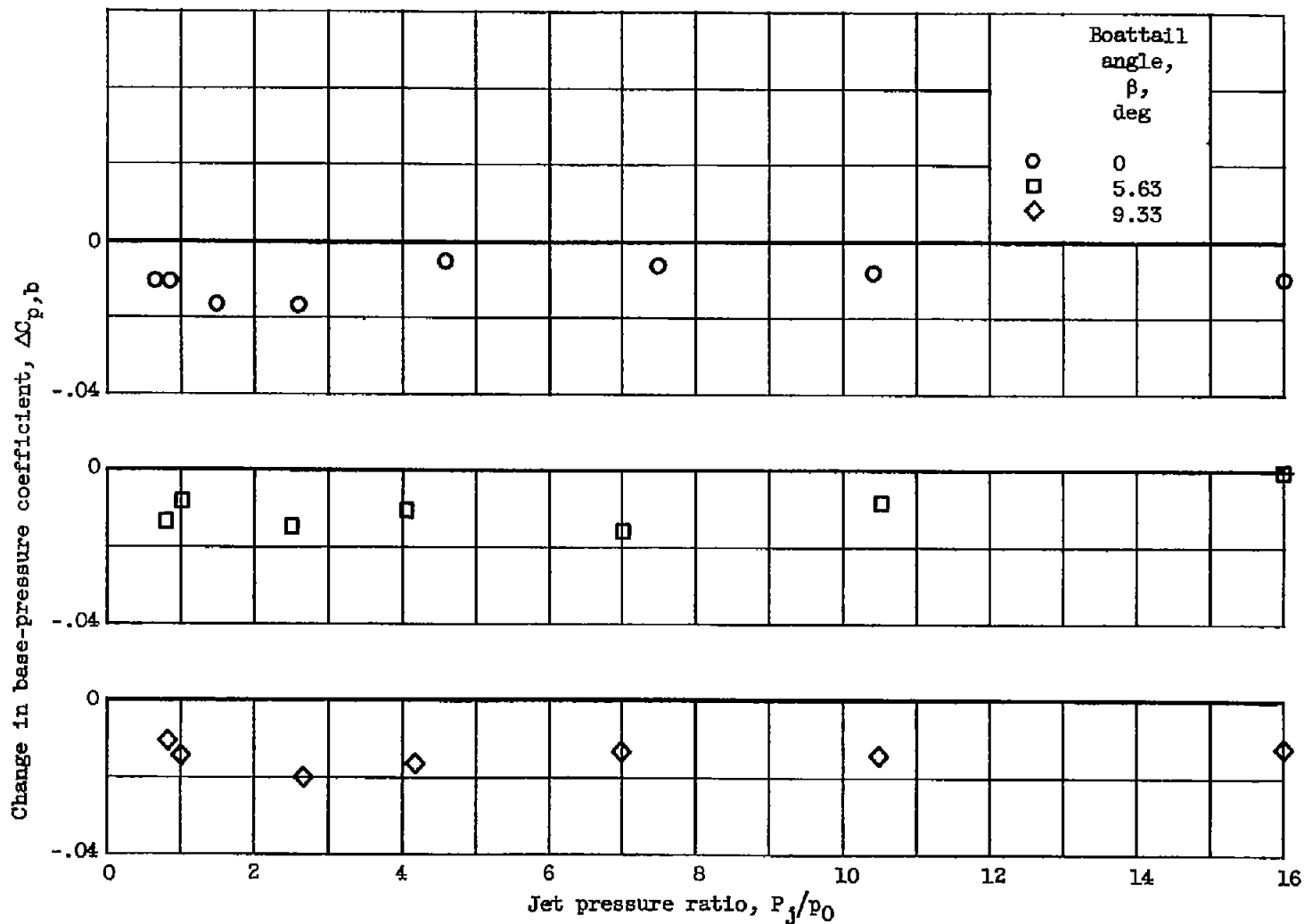
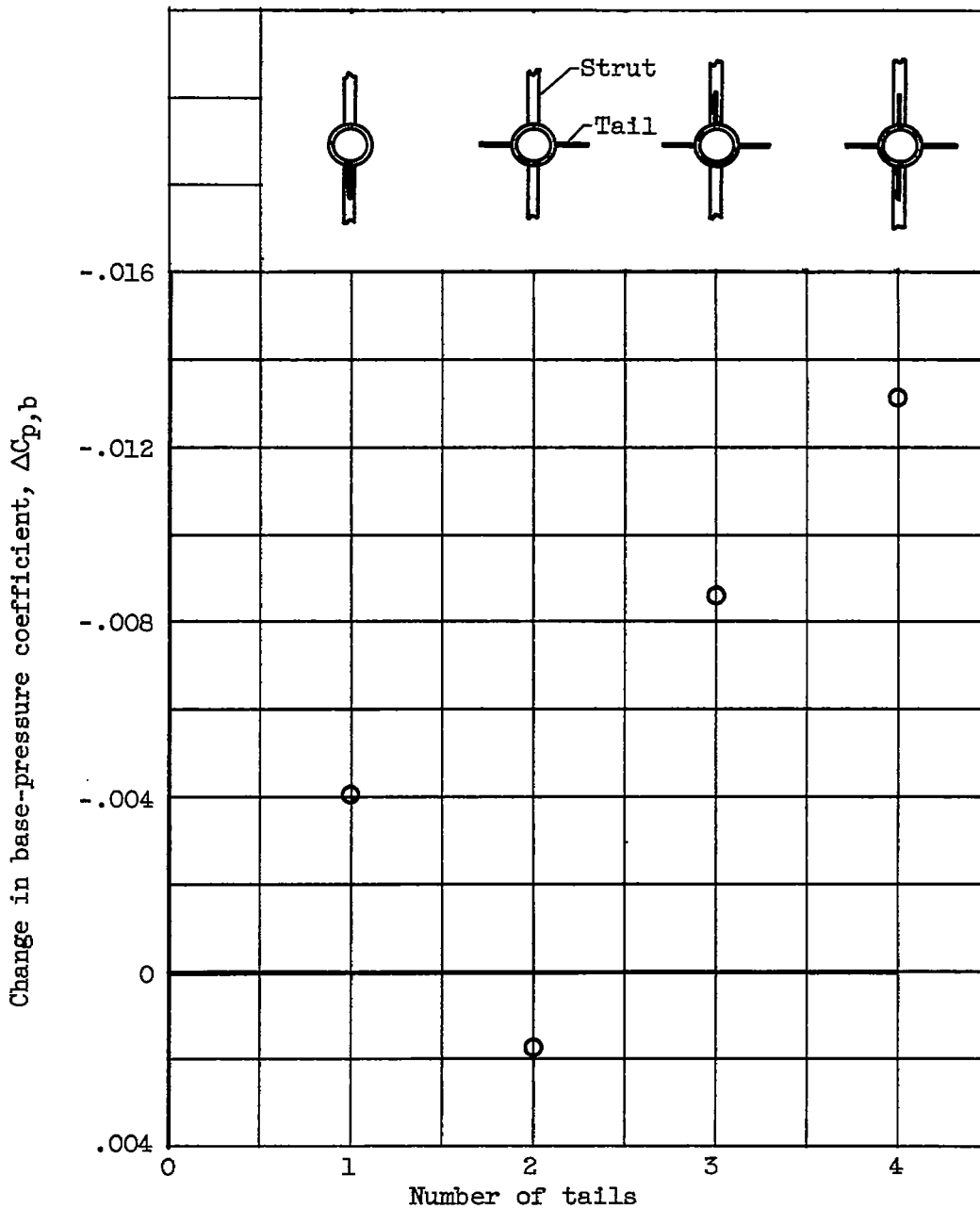


Figure 41. - Utility of correction of ratio of specific heats in predicting hot-jet base pressures. Base-to-jet diameter ratio, 1.40; boattail angle,  $5.63^\circ$ ; free-stream Mach number, 1.91; jet Mach number, 1.0.



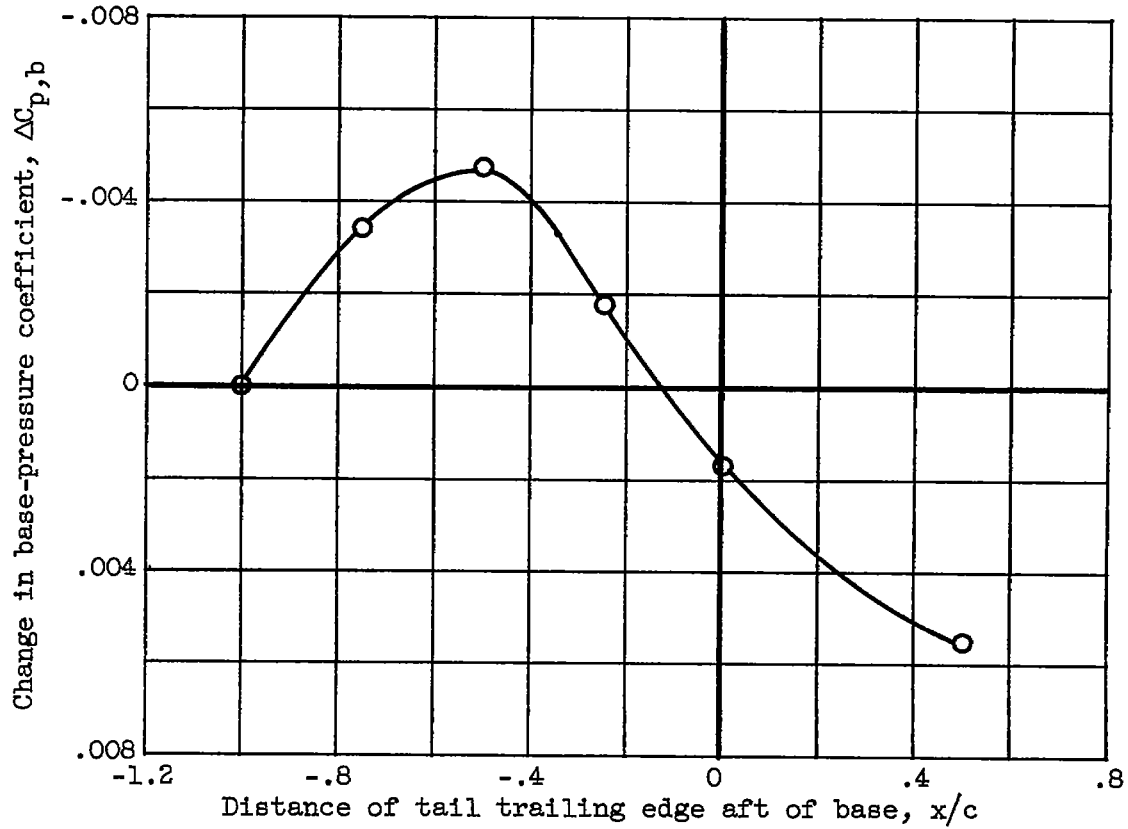
(a) Effect of jet pressure ratio and boattail angle. Cruciform tail; distance from base, 0.

Figure 42. - Interference effect of a 5-percent-thick rectangular tail. Aspect ratio, 3; free-stream Mach number, 1.91.



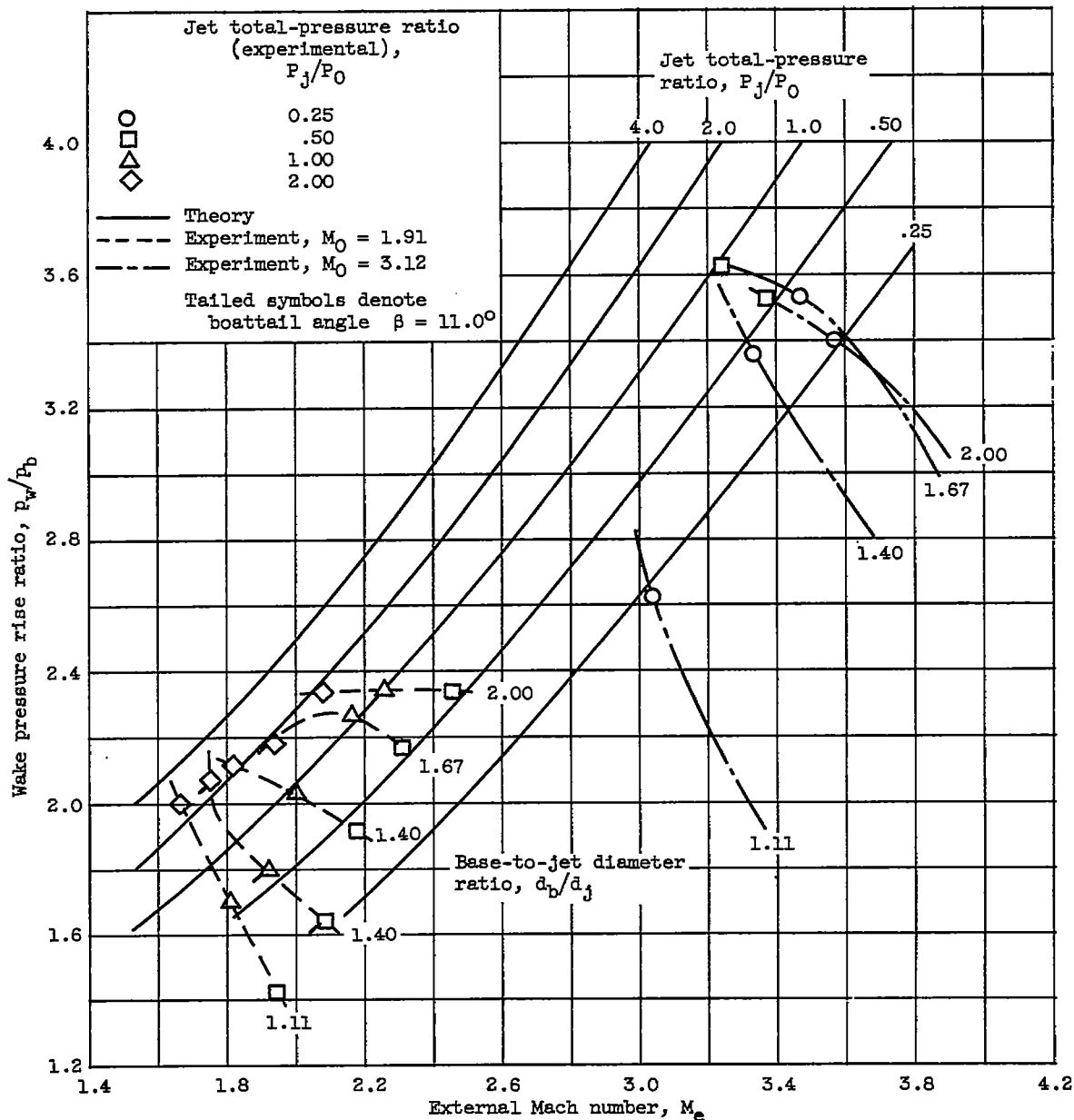
(b) Effect of number of tail surfaces. Distance from base, 0; no jet flow.

Figure 42. - Continued. Interference effect of a 5-percent-thick rectangular tail. Aspect ratio, 3; free-stream Mach number, 1.91.



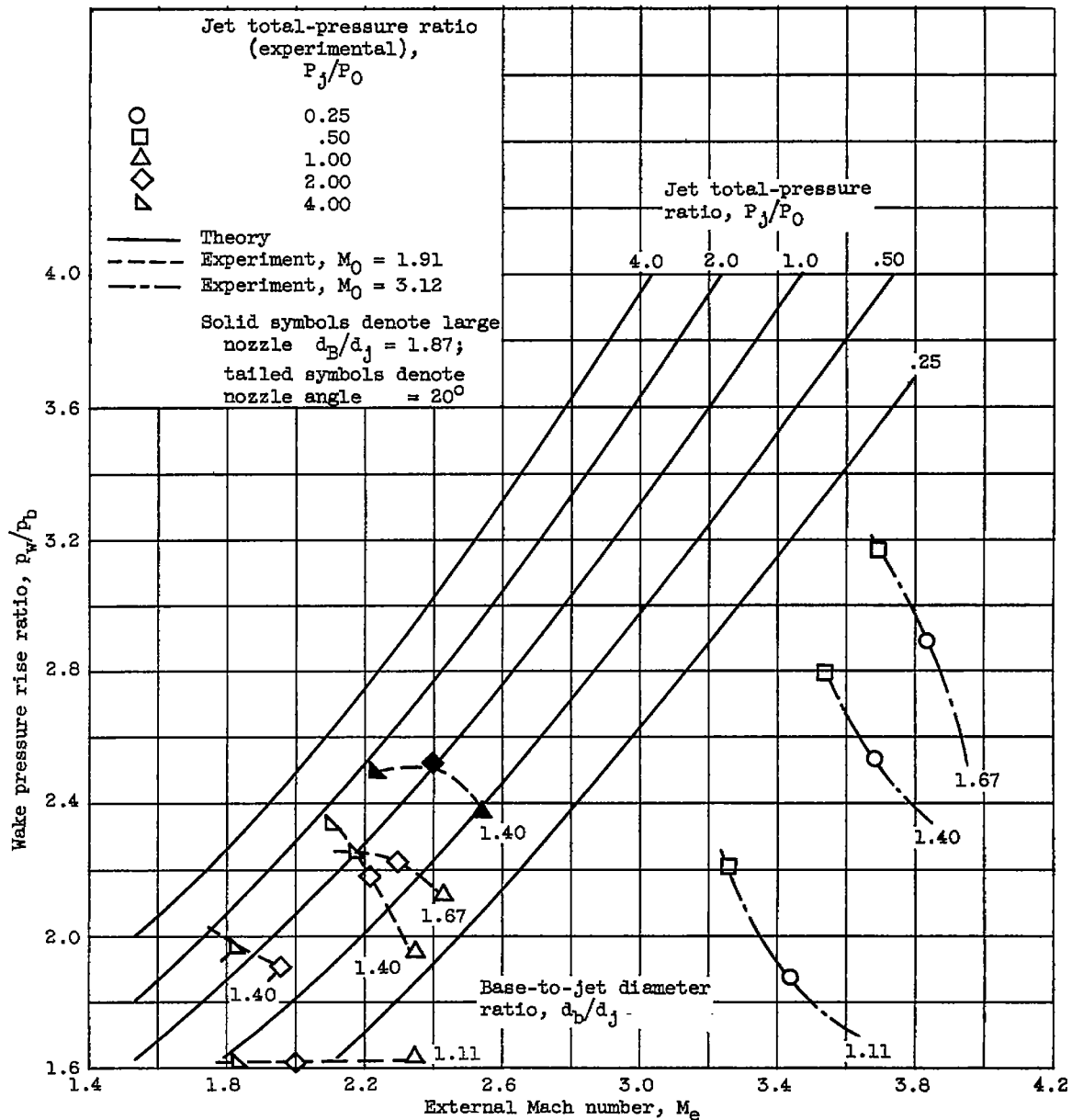
(c) Effect of axial position of plane tail. Boattail angle,  $5.63^\circ$ ; no jet flow.

Figure 42. - Concluded. Interference effect of a 5-percent-thick rectangular tail. Aspect ratio, 3; free-stream Mach number, 1.91.



(a) Convergent nozzle; jet Mach number, 1.0; body-to-jet diameter ratio, 2.67.

Figure 43. - Summary of wake pressure rise ratio data. Boattail angle,  $5.63^\circ$ ; nozzle angle,  $0^\circ$ .



(b) Convergent-divergent nozzle; jet Mach number, 2.16; body-to-jet diameter ratio, 2.67 (except as noted).

Figure 43. - Concluded. Summary of wake pressure ratio data. Boattail angle,  $5.63^\circ$ ; nozzle angle,  $0^\circ$ .

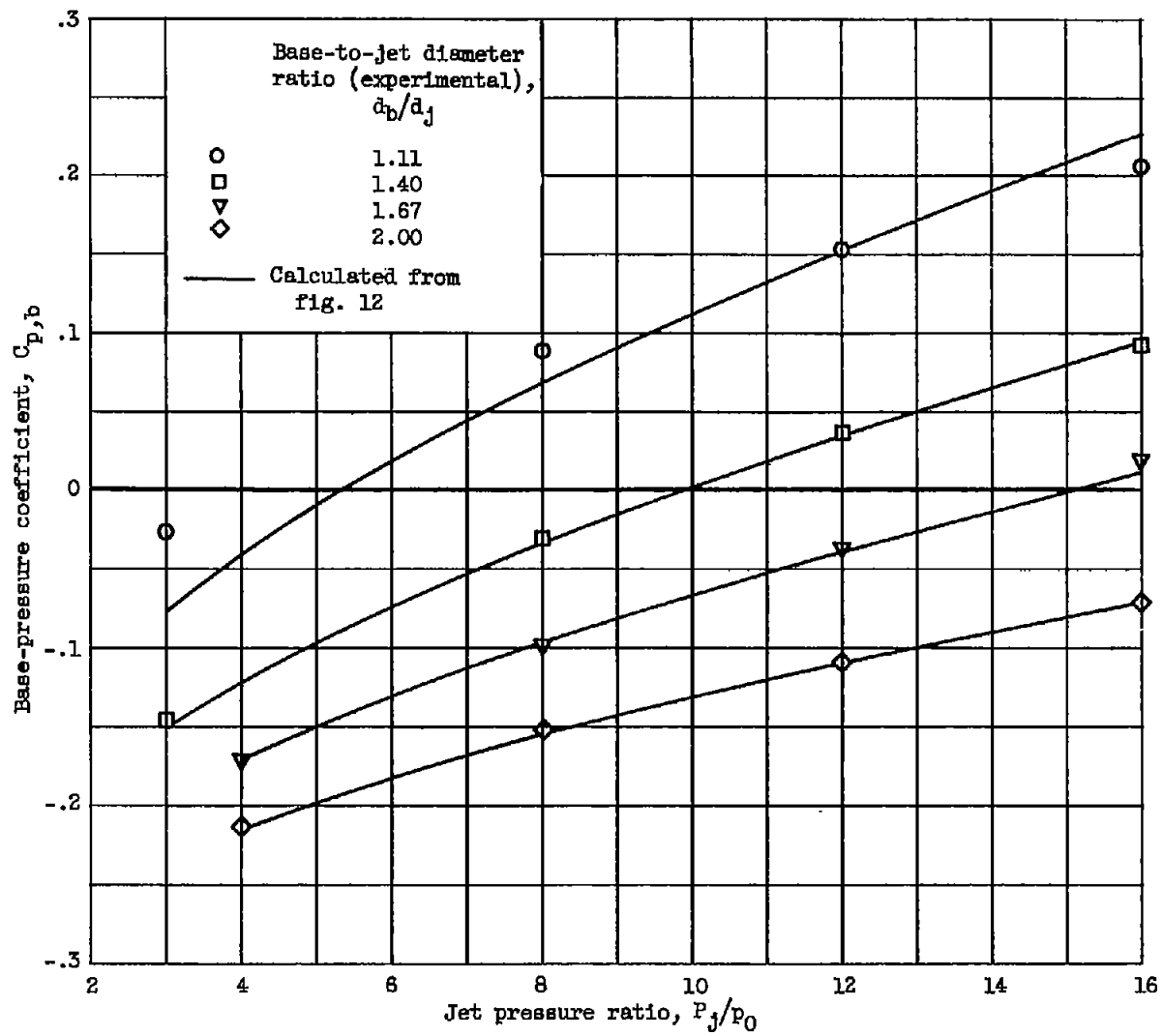


Figure 44. - Comparison of experimental and calculated base-pressure coefficients. Free-stream Mach number, 1.91; convergent nozzle (jet Mach number, 1.0); boat-tail angle, 5.63°.

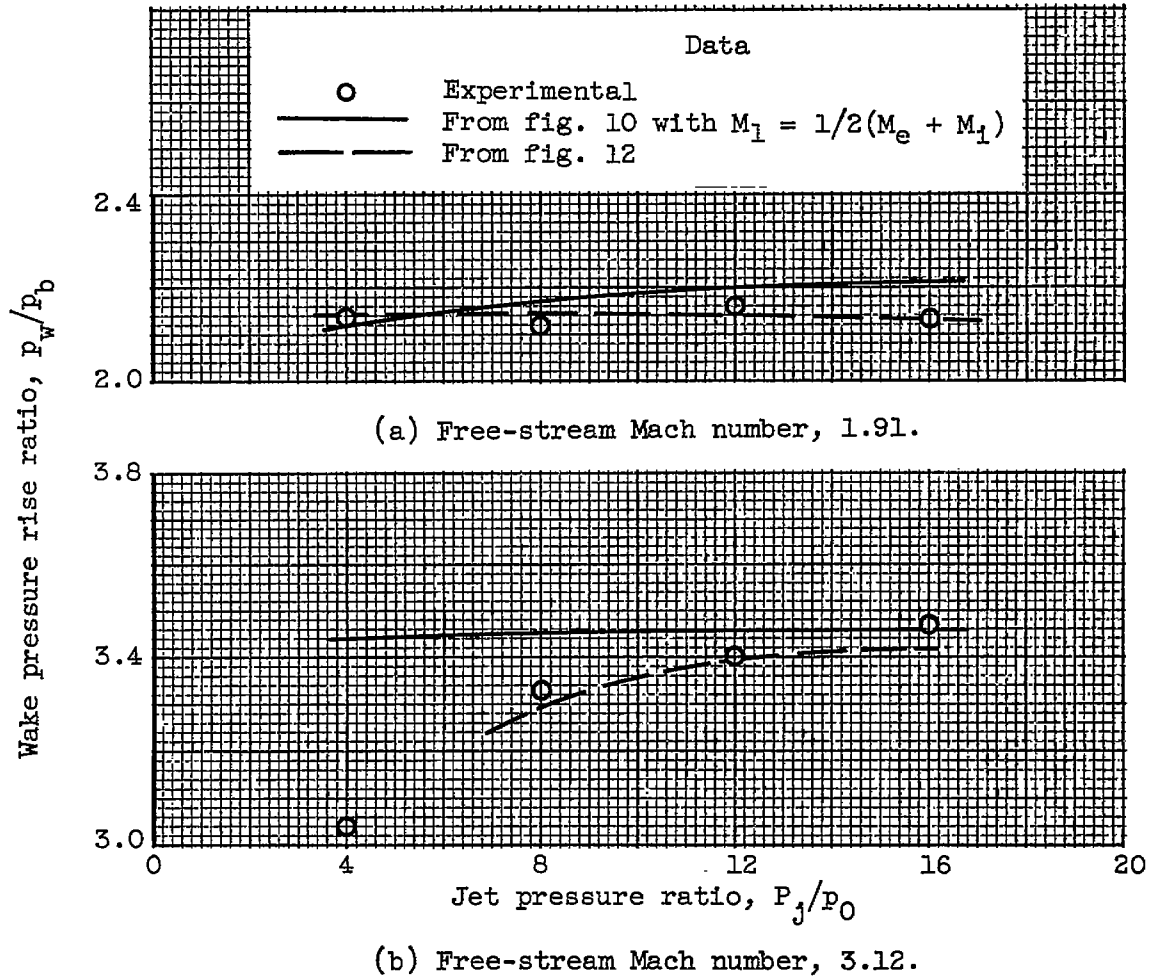
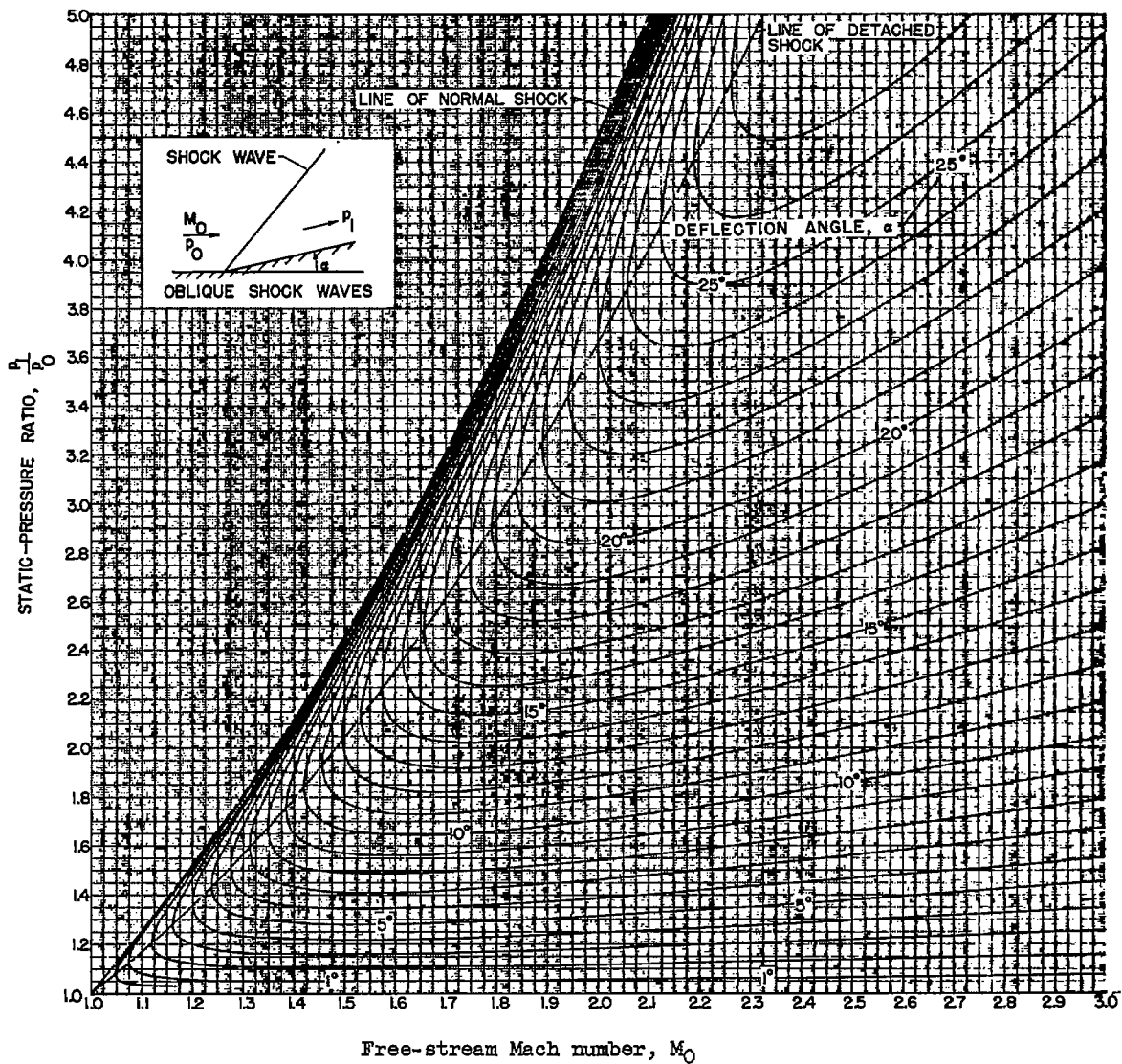
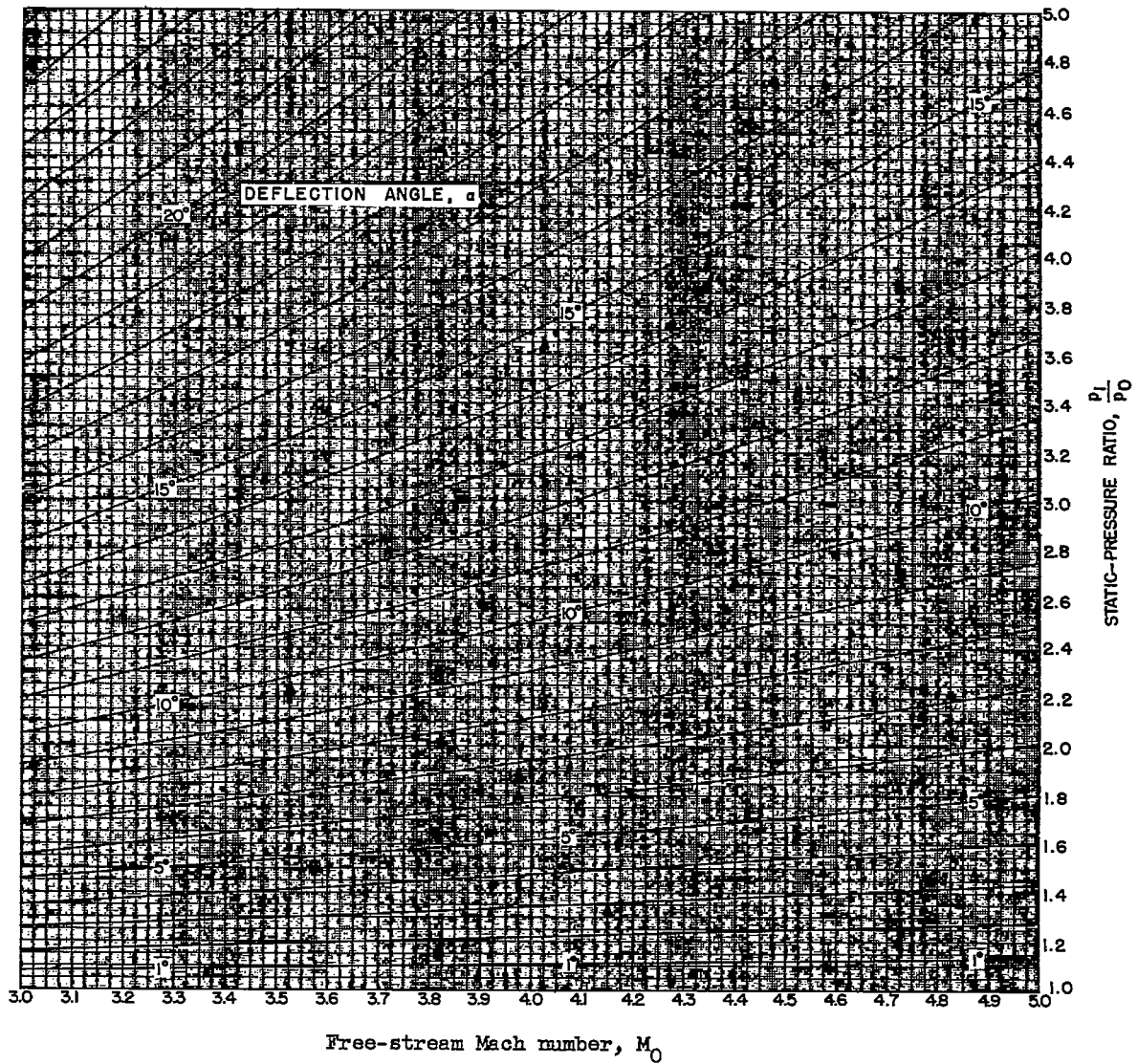


Figure 45. - Wake pressure rise ratio approximated by method of reference 4. Base-to-jet diameter ratio, 2.00; boattail angle,  $5.63^\circ$ ; jet Mach number, 1.0.



(a) Free-stream Mach number, 1.0 to 3.0.

Figure 46. - Variation of static-pressure ratio across shock waves with flow-deflection angle for various upstream Mach numbers. Perfect gas; ratio of specific heats, 1.4. (A large working copy of this fig. may be obtained by using the request card bound in the back of the report.)



(b) Free-stream Mach number, 3.0 to 5.0.

Figure 46. - Concluded. Variation of static-pressure ratio across shock waves with flow-deflection angle for various upstream Mach numbers. Perfect gas; ratio of specific heats, 1.4. (A large working copy of this fig. may be obtained by using the request card bound in the back of the report.)